



Swansea University
Prifysgol Abertawe



Swansea University E-Theses

Parameterising and developing models for the use of microalgae as a feedstock for biofuels and valuable chemicals production.

Sui, Jiyuan

How to cite:

Sui, Jiyuan (2013) *Parameterising and developing models for the use of microalgae as a feedstock for biofuels and valuable chemicals production..* thesis, Swansea University.

<http://cronfa.swan.ac.uk/Record/cronfa42610>

Use policy:

This item is brought to you by Swansea University. Any person downloading material is agreeing to abide by the terms of the repository licence: copies of full text items may be used or reproduced in any format or medium, without prior permission for personal research or study, educational or non-commercial purposes only. The copyright for any work remains with the original author unless otherwise specified. The full-text must not be sold in any format or medium without the formal permission of the copyright holder. Permission for multiple reproductions should be obtained from the original author.

Authors are personally responsible for adhering to copyright and publisher restrictions when uploading content to the repository.

Please link to the metadata record in the Swansea University repository, Cronfa (link given in the citation reference above.)

<http://www.swansea.ac.uk/library/researchsupport/ris-support/>

Parameterising and developing models for the use
of microalgae as a feedstock for biofuels and
valuable chemicals production

Jiyuan Sui

Submitted to the University of Wales in fulfillment of the
requirements for the Degree of Doctor of Philosophy of
Biological Science

Swansea University

Submitted in 2013



ProQuest Number: 10805368

All rights reserved

INFORMATION TO ALL USERS

The quality of this reproduction is dependent upon the quality of the copy submitted.

In the unlikely event that the author did not send a complete manuscript and there are missing pages, these will be noted. Also, if material had to be removed, a note will indicate the deletion.



ProQuest 10805368

Published by ProQuest LLC (2018). Copyright of the Dissertation is held by the Author.

All rights reserved.

This work is protected against unauthorized copying under Title 17, United States Code
Microform Edition © ProQuest LLC.

ProQuest LLC.
789 East Eisenhower Parkway
P.O. Box 1346
Ann Arbor, MI 48106 – 1346

Abstract:

With the development of photobioreactor technology, microalgal culture has been proposed for various purposes in the past decades. However, primarily due to the low productivity, challenge remains to scale up from laboratory studies to mass cultivation. The increasing interest of using microalgae for biodiesel production has put this challenge back on the priority list. In this investigation, fatty acid composition of *Nannochloropsis oculata* (Droop) (CCAP 849/1) in relation to elemental stoichiometry has been studied and used to inform the development of algal growth models. Through tuning C:N and Chl:C ratios, a model description can be made regulating total fatty acid content and polyunsaturated fatty acid content respectively. This quota-based model also mechanistically describes the dynamics of nutrient (nitrate and phosphate) uptake and depth integrated photosynthesis with growth. When used in a generic descriptive mode, with a bulk description of energy reserve (excess-C), the model was used to evaluate the potential biomass and biofuels production and used to explore the options of optimization of biomass and biofuel productivity from a “typical” microalga under various operational scenarios in a bioreactor. Data from experiments using *Nannochloropsis oculata* (Droop) (CCAP 849/1) were used to parameterize this bioreactor model. The model fits the data in general terms except for phosphate uptake, probably due to the phosphate precipitation in seawater. While the development of a fully functional model of microalgae growth capable of describing biochemical stoichiometry is still in its infancy. The work described here indicates the potential value and scope of developing the functional model of microalgae growth for biofuels and valuable chemicals production

Acknowledgment

Many thanks for the friendly people in Centre of Sustainable Aquatic Research (CSAR) providing help and support for all my experiments. My deeply gratitude gives to my respectful supervisor Kevin J. Flynn, who always there to help me and guide me. Thank to everyone providing help and support during my PhD years. Most importantly, thanks to my parents and my lovely lady to support me to complete this short journey.

Table of contents

List of abbreviations

Chapter 1: Introduction	1.1
1.1 Types of models	1.2
1.2 The monod model	1.3
1.3 The quota model	1.5
1.4 The mechanistic model	1.6
1.5 photosynthetic simulations	1.7
1.6 Elemental and biochemical composition of microalgae	1.10
1.7 Microalgal cultivation	1.12
Chapter 2: Methods and Materials	2.1
2.1 Experimental set-up	2.1
2.1 Model development	2.11
2.2 Data transformation	2.13
Chapter 3: Growth and biochemical composition of <i>Nannochloropsis</i>	
<i>oculata</i> (Droop) in a tubular photobioreactor; an experimental	
study	3.1
3.1 Introduction	3.1
3.2 Methods	3.2
3.3. Results	3.3
3.4 Discussion	3.8
3.5 Conclusion	3.13
Chapter 4: Fatty acid composition in relation to elemental	
stoichiometry (C: N: P: Chl) of <i>Nannochloropsis oculata</i> (Droop)	
in a photobioreactor.	4.1
4.1 Introduction	4.1
4.2 Methods	4.3
4.3. Results	4.5
4.4 Discussion	4.8

Chapter 5: Development of a mathematical model of microalgal growth in photobioreactors and simulation of the accumulation

of energy reserves for biofuel production 5.1

5.1 Introduction	5.1
5.2 Model development and scenarios	5.3
5.3 Results and Discussion	5.15
5.4 Conclusion	5.21

Chapter 6: Application of the mathematical model of microalgal growth in photobioreactors: simulating growth of

***Nannochloropsis oculata* in a tubular photobioreactor 6.1**

6.1 Introduction	6.1
6.2 Methods	6.3
6.3. Results	6.3
6.4 Discussion	6.6

Chapter 7 Conclusion 7.1

References

- Appendix A**
- Appendix B**
- Appendix C**
- Appendix D**

List of abbreviations

ATP: Adenosine-5'-triphosphate

MUFA: Monounsaturated fatty acid

AP: areal productivity

NADPH: Nicotinamide adenine
dinucleotide phosphate

Chl: Chlorophyll

PBR: Photobioreactor

CCAP: Culture Collection of Algae and
Protozoa

PFD: Photon flux density

DIC: Dissolved inorganic carbon

PS: Photosynthesis

DIN: Dissolved inorganic nitrogen

PUFA: Polyunsaturated fatty acid

DIP: Dissolved inorganic phosphors

SFA: Saturated fatty acid

DHA: Docosahexaenoic acid

v/v: volume per volume

EPA: Eicosapentaenoic acid

VP: volumetric productivity

MAP: Model of algal physiology

1. Introduction

Microalgae represent the largest group of oxygen producer in the world (Williams and Laurens 2010). As primary producers, microalgae play a significant role in the ecosystem. Most microalgae are autotrophic organisms, which can convert sunlight and CO₂ into biomass, although some are heterotrophic or mixotrophic. Most of the microalgae belong to the group of phytoplankton but some algae living in freshwater stream is attaching to the bed, which does not meet the definition of phytoplankton. As phototrophic eukaryotic organisms, microalgae photosynthetically capture sunlight (400-700nm) to obtain energy to complete carbon fixation. The growth of microalgae strongly depends on the cultivation conditions. Various factors such as nutrients, temperature, pH, CO₂ and illumination have been linked to the biomass composition and biochemical products formation in the microalgae (Sánchez et al. 2000, Renaud et al. 2002, Solovchenko et al. 2008). The utilization of microalgal biomass has not yet been fully exploited, although its carbohydrate can be used for producing H₂ and ethanol, its lipid can be used for biodiesel generation (Amin 2009) and its protein can be used to feed stock as food. The remarkable potential capabilities of microalgae producing highly valuable lipid, which can be used for converting as biofuel or body health ingredients like polyunsaturated fatty acid (e.g. EPA and DHA) (Adarme-vega et al., 2012) and CO₂ removal from the waste produced by the industrial factory have raised global attention recently (Chiu et al. 2008). The debate for biofuel finally appears to have conversed on microalgae because of its numerous advantages in farming and attractive potential ability of producing oily biomass (Li et al. 2008). However, the challenge of mass cultivation remains although the massive effort and investment have been done during the last couple decades (Ugwu, 2008). The complex interactions between the physical, chemical and biological components during the cultivation of microalgae are still unclear. A large amount of fundamental research enable us to focus separately on one or two even three factors which will affect the algal growth (Zhu et al. 1997; Bouterfas et al. 2002; Solovchenko et al. 2008; Pruvost and Legrand 2008), but there

is lack of research concentrating on the interactions between or among the factors from the natural environment. There is a need to develop a technique which can simultaneously simulate all the factors existing in the culture system and thereby understand the interaction between or among these factors to provide a guideline for production. Modeling techniques using mathematical equations to describe the dynamic overview of the function of biology could be the solution to investigate the interaction of parameters of microalgal growth.

1.1 The type of models

Models may be empirical or mechanistic depend on the purposes of simulation. Empirical model provides a quantitative description of the available data but lack of the insights of the mechanism of the system. The advantage of using empirical model can be mainly summarized into two points: 1) the degree of complexity is low, so they are relatively easy to construct and use. 2) The parameters of the model are easier to collect in comparison with mechanistic models. However, the risk of using empirical models for prediction is problematic. The prediction restricted to the particulate experimental settings when using empirical models. Mechanistic models on the other hand are attempted to describe the fundamental rules of the functional processes, but it is more difficult to obtain suitable, sufficient parameters and usually more complicated than empirical models. It can provide more insights to the complex biological processes once a functional mechanistic model has been constructed. The models using in the following chapters are the hybrid of both (e.g., the equation describes photosynthesis P-E curve), functionally mechanistic with empirical description for certain functions where there is a lack of suitable datasets to support development of a mechanistic model.

Models can be simulated in steady-state or dynamic mode. Steady-state is a special condition where the rates of changes are constant (e.g. a chemostat). This condition is often employed in the experimental set-up of phytoplankton growth (Laws and

Bannister, 1980; Sukenik *et al.*, 1993; Leonardos and Geider, 2004) to control the assigned element limitation. It is important to note that steady-state can occur in a dynamic system. For example, the rate of biomass increase for an organism in exponential growth is constant with the time. The rate of biomass increase is the slope of the linear equation when plot the data only in exponential growth against time. The models were operated in a dynamic mode with changing into steady-state mode (i.e. semi-continues culture) when the culture was entering stationery phase.

1.2 The Monod model

The original Monod model was developed to describe the growth of micro organisms, mainly bacteria, in steady-state culture where growth rate equals dilution rate (Monod 1942). The Monod equation (Eq.1) defined the growth rate (μ) as the product of limiting nutrient quotient (U_{X_i}) and maximum growth rate (μ_{max}). The nutrient quotient is a rectangular hyperbolic function of the concentration of substrate nutrient (X_i) (Eq.2). This equation links the concentration of external nutrient and a half saturation constant (K_{g_i}) to the growth. Multiple nutrient simulation using the Monod model is simply adding a fixed ratio of other nutrients (typically Redfield ratio, Redfield 1958)

$$\mu = \mu_{max} \cdot \min U_{X_i} \quad (1)$$

$$U_{X_i} = \frac{X_i}{X_i + K_{g_i}} \quad (2)$$

The implication of the equation above can be understood as the specific growth rate is controlled by the external nutrient. When the nutrient is depleted, the growth will be halted because the equation fails to simulate the internal nutrient pool of the cell. Using a fixed ratio to simulate the multi-nutrient condition is seriously dangerous (Flynn 2002). Nutrient ratios can change related to different nutrient status and

growth conditions. Although the Monod model has been widely used in present microalgae growth simulations, it fails in giving the reliable data for multi-nutrient simulations (Flynn 2003).

When Monod model is inadequate in describing the relationship of growth rate and nutrient concentration, Quota model, the most cited model, based on Droop's (1968) or Caperon and Meyer's (1972) has been developed.

The original two equations Droop's (1968) (Eq.3) and Caperon and Meyer's (1972) (Eq.4) are stated below.

$$C_u = \mu_{m_x} \cdot \frac{XC - XC_0}{XC} \quad (3)$$

$$C_u = \mu_{m_x} \cdot \frac{XC - XC_0}{(XC - XC_0) + K_{q_x}} \quad (4)$$

In both equations, C_u is the carbon specific growth rate. μ_{m_x} is the theoretical maximum growth rate under specific nutrient cultivation. XC is the nutrient : C quota. XC_0 is the minimum quota when there is no growth (growth rate is zero). K_{q_x} is the half saturation constants of nutrient uptake. Both of the models relate the specific growth rate to the inner nutrient quota which enables the growth in the absence of the external nutrient. The Quota model also enables the simulation of C-biomass changing with nutrients while the Monod type equation can only use a fixed ratio with C. However, the parameter used in the quota model are specifics for the assigned nutrient (i.e. μ_{m_x} , K_{q_x}). Despite of the limitation of specific parameters, the quota model is designed for steady-state simulation. Lack of the ability to simulate the dynamic growth situation of the Quota model therefore cannot provide detail of the experiment (Flynn 2008).

The change of nutrient quota can be stated as follows (Eq.5)

$$\frac{d}{dt} \cdot XC = \mu_{\max} \cdot XC_m \cdot \frac{X}{X + K_{u_x}} - C_u \cdot XC \quad (5)$$

Note that use of $\mu_{\max} \cdot XC_m$ as maximum uptake rate is not determinate. The maximum uptake rate can be replaced by other value or a function of nutrient status (Flynn et al. 1997). The K_{u_x} , which is the half saturation constant of nutrient:C specific growth rate, cannot describe the half saturation of nutrient concentration of maximum growth of the organisms.

1.3 The Quota model

The original quota model includes a theoretical maximum growth rate (μ_{\max}) at an infinite nutrient quota, which is different from the traditional μ_{\max} growth rate of organisms (i.e. C-specific). To solve this problem, another version based on Droop's equation has been develop by Burmaster (1979) (Eq.6). In this equation, μ_{mx} act as the same as μ_{\max} .

$$C_u = \mu_{mx} \cdot \frac{XC - XC_0}{XC_m - XC_0} \quad (6)$$

There is a more convenient version of the quota type model based on the original Caperon and Meyer (1972) structure. Flynn (2001) normalized the equation to give a quotient using a dimensionless constant (KQX) to control the curve shape (Eq.7). in this equation, XC_0 and XC_m can be altered without changing the form of curve, which Eq.6 cannot achieve.

$$XCu = \frac{(1 + KQX) \cdot (XC - XC_0)}{(XC - XC_0) + KQX \cdot (XC_m - XC_0)} \quad (7)$$

The most common way to combine nutrient limitation is to apply the threshold control, which the growth limits by the most limiting nutrient. The μ thus can be stated as the maximum growth rate of organism (μ_{\max}) combining with the minimum nutrient quotient ($\min X_i/Cu$) (Eq.8).

$$\mu = \mu_{\max} \cdot \min X_i/Cu$$

(8)

1.4 The mechanistic model

Although the Monod model and Quota model more or less include mechanistic descriptions, the mechanistic model is more accurate in providing biological meaningful details. Mechanistic model based on the knowledge of biochemical reactions of the cell has been employed to simulate the growth of microorganisms. The mechanism of active feedback control plays an important and essential role in nutrient uptake of controlling the growth of living organisms. Nonetheless, lack of knowledge of the full biochemical reactions of the organism slows the construction of mechanistic models. It is difficult to construct a detail mechanistic model to appear fully functional. Furthermore, it is unnecessary to construct a model of each single detail, which would bring along a heavy cost in processing. Building a cost-effective model with significant components describing the critical physicochemical reactions would be the principle in developing a mechanistic model. There is a mechanistic model coupled with Quota like components, developed by Flynn et al. (1997) using detailed mechanistic function for controlling ammonium-nitrate interactions. Followed by other detailed mechanistic models (Flynn & Hipkins 1999, Flynn 2001), mechanistic model has been widely accepted as a useful tool to study the critical biochemical interactions.

In the mechanistic model, active feedback control can be described as a hyperbolic function (Eq.5) in terms of terminating the uptake of non-limiting nutrient (Geider et

al. 1998), or use a sigmoid function (Eq.6) which can gradually terminate the uptake (Flynn 2001).

$$\frac{d}{dt} \cdot X_i C = \mu_{\max} \cdot X_i C_m \cdot \frac{X_i}{X_i + K_{u_{x_i}}} \cdot \frac{\left(1 - \frac{X_i C}{X_i C_m}\right)}{\left(1 - \frac{X_i C}{X_i C_m}\right) + K_{x_i}} - C_{u_i} \cdot X_i C \quad (9)$$

$$\frac{d}{dt} \cdot X_i C = \mu_{\max} \cdot X C \cdot \text{surge} \cdot \left\{ (X_i C_{u_i} > X C_{u_{\min}}) \cdot \theta^\beta + (X_i C_{u_i} = X C_{u_{\min}}) \right\} \cdot \frac{X_i}{X_i + K_{u_{x_i}}} \cdot \frac{\left(1 - \frac{X_i C}{X_i C_{\text{abs}}}\right)^H}{\left(1 - \frac{X_i C}{X_i C_{\text{abs}}}\right)^H + K_{x_i}} \quad (10)$$

Although Eq.9 and Eq.10 seem a little complicated, the extra parameters can be altered to suit the specific situation. For example, with the surge function can give a better explain that organism growth more faster when first come into a rich nutrient environment and then slow down by feedback control.

1.5 Photosynthetic simulation

Photosynthesis (PS) as a form of metabolism consists of a coupling of light and dark reactions. During the light reaction, photons are converted into electrons which will fall into the electron transport system with the results being ATP and NADPH in the Z scheme pathway (Richardson et al., 1983), providing energy for organic compound synthesis and growth. The Dark reactions use ATP and NADPH generated from light reaction fixes CO₂ to form carbohydrate and then cell carbon (Albert 1994). Hence, the rate of photosynthesis is the key to algal growth and product formation. Under the “optimal” cultivation of microalgae (i.e. no nutrient limiting), the photosynthetic rate depends on the availability of light energy. Light limitation becomes the ultimate factor that limits the growth, although CO₂, which is the raw material for the dark reaction, cannot play a neglectable role in growth. The relationship between light and PS under various culture conditions are primarily

important for research into algal cultivation. The relationship between the rate of PS and irradiance can be expressed as PI curve (or PE curve) (Figure 1.1).

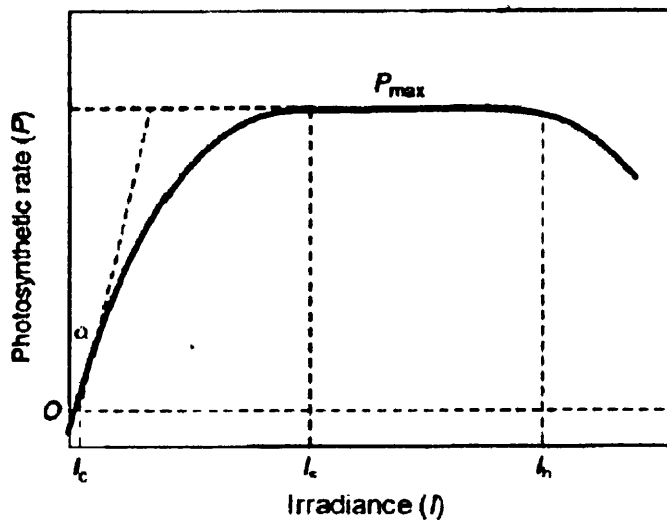


Figure 1.1. the relationship between photosynthesis and irradiance. Pmax is the maximum PS rate, α =initial slope, I_c =light compensation point, I_s =light saturation point, I_h =light inhibition point. Goldman (1980)

Below zero of the PS rate, there is an intercept, where the rate of respiration against over the rate of photosynthesis. At the point where the rate of respiration equals the rate of PS, is defined as compensation point (I_c). above the I_c growth may begin. PS rate slow down and maintain at a relatively high value when the irradiance increase to I_s indicating the absorbing of light tends to saturation and hence reach the maximum rate of PS. After the increasing of irradiance, PS starts to decrease at I_h due to the photo- inhibition. Several mathematical equations describing the relationship of irradiance and PS have been used for examining datasets (Jassby and Platt, 1976), but the one that is most commonly used (Platt et al. 1980) is:

$$P^B = P_S^B \cdot \left[1 - \exp\left(-\alpha^B \cdot \frac{E}{P_S^B}\right) \cdot \exp\left(-\beta^B \cdot \frac{E}{P_S^B}\right) \right] \quad (11)$$

In Eq.11, P^B is the PS rate at irradiance E . P_s^B is the PS rate at light-saturation point. It is equal to the maximum PS rate (P_{qm}). The α^B here is the initial slop at light limitation. The β^B is a parameter describing the light inhibition at high irradiance. If the light inhibition can be ignored ($\beta=0$), the equation can be rewritten as:

$$PS = P_{qm} \cdot \left[1 - \exp\left(-\alpha \cdot \frac{E}{P_{qm}}\right) \right] \quad (12)$$

Photoacclimation is a significant activity of phototrophic organisms. Review implies that phototrophic organisms can modify the photosynthetic pigment contents (generally Chla) to change the appearance of PE curve due to the changes in growth irradiance (MacIntyre et al. 2002). Therefore, the equation should include Chl:C quota to normalize the growth as C-specific, not Chl a specific, as original equation. The photoacclimation function has been used into mechanistic model which is able to describe the decrease of Chla quota with increasing irradiance (Flynn 2001). The equation thereby can be written as:

$$PS = P_{qm} \cdot \left[1 - \exp\left(-\alpha \cdot ChlC \cdot \frac{E}{P_{qm}}\right) \right] \quad (13)$$

During the microalgae cultivation, light distribution in a bioreactor is various. Irradiance decrease with the depth increase (Figure 1.2)

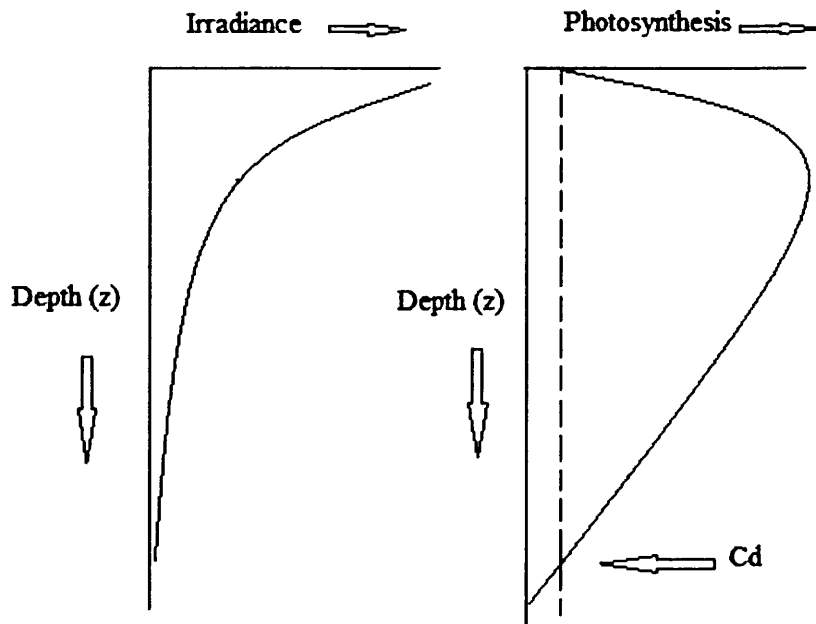


Figure 1.2. Irradiance and photosynthesis change with depth. C_d is the critical depth where PS equals to respiration.

Photosynthesis (PS) at the surface of water column is very low due to the photoinhibition then increases and finally down regulated with the depth increases. The regulation with depth suggests an active progress in microalgae. Above critical depth, the gross PS rate of microalgae is positive indicating the continuous growth. On the contrary, there is no growth when depth is deeper than the critical depth.

1.6 Elemental and biochemical composition of microalgae

Microalgae display wide variability in their elemental composition, rarely conforming to the Redfield C:N:P ratio of 106:16:1 (by mole) (Redfield, 1958; Geider and La Roche, 2002). This variability largely reflects interactions with their physico-chemical environment, and specifically with the balance of light versus nutrient (i.e., nitrogen (N) and/or phosphorous (P)) supply. Under N and P limiting conditions these organisms continue to assimilate CO_2 , until they attain a

species-specific maximum C:N or C:P value (attaining the so-called subsistence quota). While doing so they lay down the surplus carbon (hereafter termed excess-C) as combinations of carbohydrate and/or lipid; the form of excess-C varies with taxonomy and species. The elevation of cellular C:(N:P) has well known implications for microalgal growth (Flynn, 2008a; Flynn, 2008b) as well as for trophic dynamics, through various manifestations of stoichiometric ecology (Sterner and Elser 2002; Anderson *et al.*, 2004; Vrede *et al.*, 2004; Mitra and Flynn, 2006). In addition, with increasing interest in the commercial exploitation of microalgae for biofuel production (Chisti, 2007; Greenwell *et al.*, 2010), a more detailed knowledge of the dynamics of the accumulation of excess-C is needed. More importantly, data suitable for supporting the development of models for commercial applications are essential.

Microalgal biochemical composition can usefully be partitioned into nucleic acid (i.e., DNA and RNA), protein, lipids (i.e., phosphoglycerides and neutral lipid), carbohydrate, pigments (chlorophyll, carotenoids and xanthophylls, etc.) and low molecular metabolites (e.g. free amino acids, ATP) (Geider and La Roche, 2002). Nitrogen is mainly distributed into nucleic and amino acids, protein, chlorophyll, phosphoglycerides and ATP. Phosphorous is associated with nucleic acids, phosphoglycerides and ATP, NADP(H) and other metabolic mediators, plus, if applicable, into polyphosphate granules (John and Flynn, 2000). Under nutrient replete conditions, protein is a major component, which can achieve 50% of cell mass; under such conditions the contribution to “storage” (i.e. neutral lipid and/or carbohydrate) is minor. In comparison with cells in nutrient replete conditions, cells in nutrient deplete conditions have more “storage” which can typically be obtained over 50% of cell mass (see schematic Figure 1.3). The accumulation of “storage” and partition within the “storage” is expected to depend on the selected species and culture conditions, especially nutrient conditions (Shifrin and Chisholm, 1981; Reitan *et al.*, 1994). This may explain the variations of lipid content reported from the same genus of microalgae (see review Chen *et al.*, 2011); unless there is a

rigorous control (and documentation) of the nutrient history then it is difficult to isolate differences attributed to species or clones from nutrient stress effects.

Cellular C:N:P ratios are the deprivations of cellular biochemical composition (Geider and La Roche, 2002). Changing the cellular C:(N:P) ratios is a reflection of interactions between light and nutrient availability (i.e., nitrogen (N) and phosphorous (P)). Under nutrient limitation or deprivation (especially N), newly fixed carbon (C) is diverted from the structure material which rich in N and P into accumulation of storage C pool (i.e. starch or lipid, upon the species). Various experiments of microalgal cultivation have shown the decrease of nitrogenous components such as nucleic acid and protein while increase of the total lipid and/or carbohydrates under N limitation growth (Fernandez *et al* 1989; Sukenik *et al.*, 1991; Sukenik *et al.*, 1993; Berdalet *et al.*, 1994; Fabregas *et al.*, 1995; Fermindez *et al.*, 1996; Larson and Rees 1996; Otero *et al.*, 1997; Fidalgo *et al.*, 1998). For biofuel production, biomass with high C:N ratio indicating high accumulation of storage C is desired. However, high C:N ratio under N limitation depress the growth rate and hence biomass productivity. The trade-off between storage C content and growth rate is needed to be evaluated for commercial production of microalgae (Williams and Laurens, 2010). Models with the capability to describe the change of cellular C:N may have potential to extend the description into biochemical composition and evaluate biofuel productivity.

1.7 Microalgal cultivation

Microalgal cultivation can be conducted either in closed photobioreactor (PBR) or open pond (e.g. raceway-type) system (see review Ugwu *et al.*, 2008). Open pond or raceway systems are easier to construct and relatively low cost in construction and operation than closed PBR system. However, poor productivity and quality control subject to light utilization, evaporation and contamination are limiting the use of open pond system to several fast growing species (e.g. *Nannochloropsis sp.*)

(Anderson 2005 book) Closed PBR system which usually has shallower optical depth provides better biomass productivity and both quality and operational control but higher costs in comparison with open pond system (see review Xu *et al.*, 2009). Large scale open ponds may be suitable for the relatively low value biofuel production while PBRs may be more viable for high value chemical products at current production (e.g. polyunsaturated fatty acids). Increasing the productivity and minimising the cost are the two main factors to consider in PBR system design in order to realise the cost-effective production in mass cultivation.

Various types of PBR, commonly including tubular PBRs, flat-panel PBRs and vertical column PBRs, have been manufactured to evaluate productivity in mass cultivation. The principle for designing the PBR is maximising the light utilisation inside the PBR units (Richmond, 1992). For tubular PBRs, increasing tube diameter has been found to decrease the volumetric productivity of biomass (Jimenez *et al.*, 2003). A decrease in light path from 17 to 1.3cm in a flat-panel PBR results in an increase of volumetric productivity for *Nannochloropsis sp.* over 7 fold (Richmond and Cheng-Wu, 2001). Therefore, light attenuation passing the optical depth (i.e. light path) is a crucial characteristic for optimization of biomass productivity for the PBR. If all the nutrients are in excess, the growth of microalgae is expected to be ultimately limited by the availability of light inside the PBR due to the effect of self-shading from the increasing pigmentation with cell growth. To scale up the culture, increase of the optical depth is likely to decrease the potential productivity of reactor unit. Realization of large scale cultivation using these PBRs can be achieved by placing an assemblage of modular reactor units (Eriksen, 2008).

2. Materials and Methods

2.1 Experimental setup.

2.1.1 Organism and Stock Culture

Nannochloropsis oculata (Droop) (strain CCAP849/1) was used. Stock cultures were maintained in 100 ml volumetric flask with 25 ml sterilized natural seawater enriched with f/2 nutrient medium. Natural seawater was collected from the open area of Swansea bay and treated by O₃ and/or UV treatment in a processing tank in the Centre of Sustainable Aquaculture Research (CSAR). Residue nutrient (mainly DIN and DIP) was checked regularly by using the spectrophotometer DR/2500, HACH (Loveland, U.S.A) to ensure the residue nutrient was little for algal culture. Seawater collected from CSAR was then filtered by 0.22 Durapore (Millipore) filter and sterilized by autoclaving at 121°C for 20min. Enrichment was 1× strength f/2 medium (Guillard and Ryther, 1962) as described (Table 2.1).

Stock cultures were grown at 18°C with 16h light and 8h dark (16:8 light-dark cycles) in a constant temperature room. Cool white fluorescent light (400nm-700nm as the wavelengths) was provided at a photon flux density (PFD) of 75 $\mu\text{mol m}^{-2} \text{s}^{-1}$ measured by a Biospherical QSL-100 light meter (Biospherical Instruments Inc, San Diego, U.S.A) on the culture surface. Sub-culturing was conducted weekly by a CSAR technician.

Table 2.1 Guillard medium (usually call *f/2* medium, Guillard and Ryther, 1962) composition. The final concentration list below represents one strength (1×) of *f/2* concentration. *indicates nutrient added only for diatom cultures.

f/2 medium				
Components	Chemicals	Final Concentration (g L⁻¹)	Final Concentration (μM)	Molar
	NaNO ₃	0.075	882	
	NaH ₂ PO ₄ ·2H ₂ O	0.00565	36.2	
	*Na ₂ SiO ₃ ·9H ₂ O	0.03	106	
Trace elements				
	Na ₂ EDTA	4.16	11.7	
	FeCl ₃ ·6H ₂ O	3.15	11.7	
	CuSO ₄ ·5H ₂ O	0.01	0.0393	
	ZnSO ₄ ·7H ₂ O	0.022	0.0765	
	CoCl ₂ ·6H ₂ O	0.01	0.042	
	MnCl ₂ ·4H ₂ O	0.18	0.91	
	Na ₂ MoO ₄ ·2H ₂ O	0.006	0.026	
Vitamin mix				
	Cyanocobalamin (Vitamin B ₁₂)	0.0005	3.69x10 ⁻⁴	
	Thiamine HCl (Vitamin B ₁)	0.1	0.296	
	Biotin	0.0005	2.05x10 ⁻³	

2.1.2 Scaling-up cultures

Cultures were scaled up through 3 steps in the algal growth room (C4) in CSAR before inoculating to bioreactor experiment (Figure 2.1). All cultures in C4 were grown in batch mode with a 16:8h light:dark cycles at a room temperature of 22±2 °C. Cool white fluorescent light (400-700nm) was applied to provide a PFD of 125 μmol m⁻² s⁻¹ at the side of the culture surface. The *f/2* medium base was supplied using the “Cell-hi F2P” all-in-one powder provided by Varicon (Varicon Aqua Solution Ltd, U.K.). To make one strength of *f/2* nutrient medium, 1g of all in one powder is needed to dissolve into 10 l deionized water. This was prepared to give a

1000 fold of *f/2* medium followed by the manufactures instructions. Axenic cultures were grown in duplicate for each species.

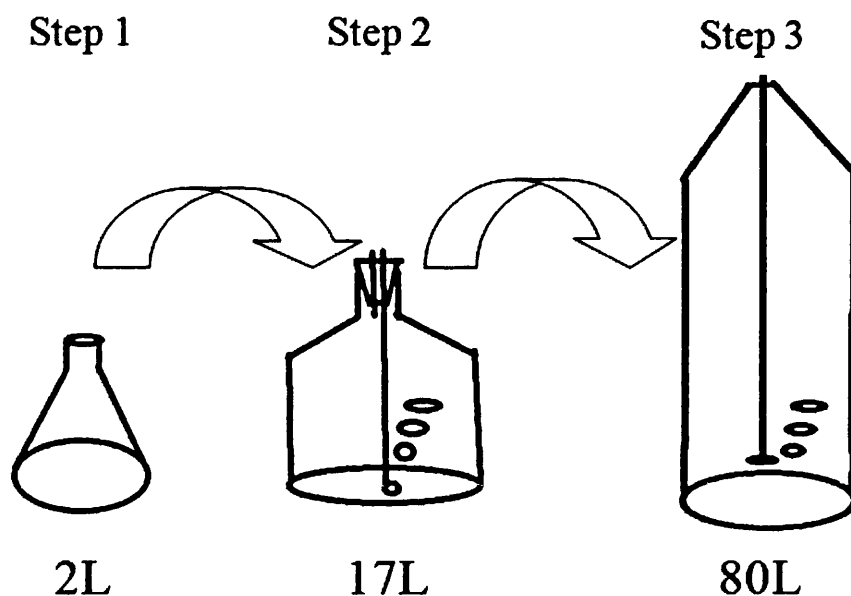


Figure 2.1 Schematic figure showing the process of scaling up culture for PBR experiment

Initial, first stage, cultures were inoculated with 2% (v/v) inoculums from stock cultures into 1L sterilized seawater within 2L flasks. Nutrients were added to provide $1 \times f/2$ concentration (i.e. $882 \mu\text{M NO}_3^-$ and $36 \mu\text{M PO}_4^-$). Cells were grown in static, un-aerated, batch culture for 7 days.

For the second stage, the 1L cultures from stage 1 were used to inoculated into 20L transparent polyethylene carboys (diameter of 0.24m), with a 2% (v/v) inocula. The bulk water in these carboys was seawater sterilized by using 10 ml commercial bleach (sodium hypochloride) per carboy (about 20L) and mutualised (removed the bleach) with 3g of sodium thiosulfate ($\text{Na}_2\text{S}_2\text{O}_3 \cdot 5\text{H}_2\text{O}$) per carboy before the inoculation (Anderson, 2005). Nutrients were added in equate to $1.5 \times f/2$ concentration (i.e. $1323 \mu\text{M NO}_3^-$ and $54 \mu\text{M PO}_4^-$). Cultures were bubbled with CO_2 mixed with air at 5% (v/v). Vigorous bubbling from the bottom enabled sufficient dissolution of CO_2

(pH<8.5) and fully mixed the culture. Water temperature, salinity and pH of the culture were monitored daily by portable pH meter (Multi 340i, WTW, Weilheim, Germany) to ensure conditions remained within the ranges of 18-22°C, salinity 28-30‰ and pH 8-9. Cells were grown for 7 days before being used for stage three.

For stage three, the 17 L cultures were used to inoculate 80 L polyethylene bags which have a diameter as 0.27m. The inoculum level was <10% inocula (v/v). Again the bulk water had been chemically sterilized, using the same method as described in stage two, with nutrient added at 1.5× f/2 concentrations, as described above. Cultures were bubbled vigorously with 5% CO₂ (v/v) with air mixture, as for stage two. Cultures were normally grown for a week before being used to commence a bioreactor experiment.

2.1.3 Photobioreactor (PBR)

Two tubular bioreactors of nominal volume 600L (Fig. 2.2), were provided by Varicon (Varicon Aqua Solutions Ltd, Malvern, U.K.). The cell suspension was driven through the biofence by a Rotary-type mechanical pump from the dark tank to 48 transparent plastic tubes with an internal diameter of 0.03m. Organisms were exposed to light for 2min before returning to the dark tank. The volume of the illuminated plastic tubes was the same as in the dark tank; the time spent in the dark tank was thus expected to be (on average) the same as light illumination.

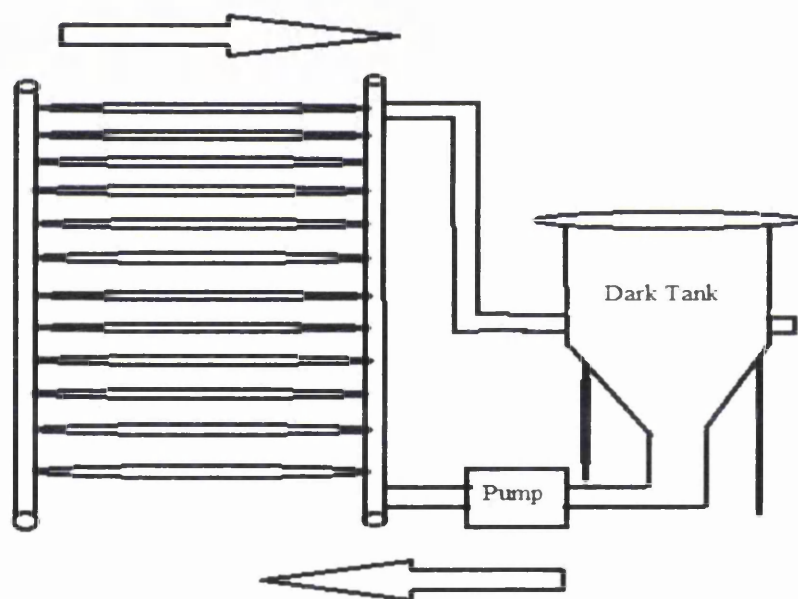
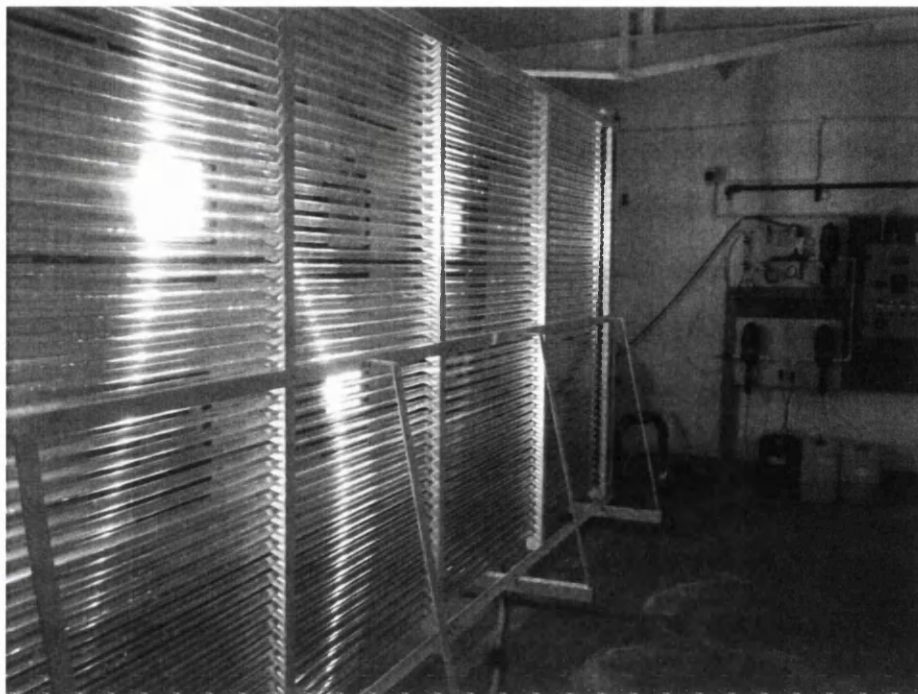


Figure 2.2 Illustration of the construction of tubular PBR used in the experiment.

Tubular photobioreactors were installed in an outdoor greenhouse. Artificial lightings (400-700nm Metal halide lamp, OSRAM, Germany) were applied continuously at around $250 \mu\text{mol m}^{-2} \text{s}^{-1}$. Artificial lightings are able to compensate

for the low sunlight in winter time. These incandescent lamps also helped to compensate for the low temperature in the greenhouse.

Temperature and pH of the culture were recorded automatically by the incorporated electric pole inside the dark tank. The pH was regulated by pure CO₂ gas injection, triggering injection when pH >8 and halting when pH < 8. Cells from the bag culture (see stage 3 in section 2.1.2) were inoculated into the PBRs with 10-20% inocula (v/v) to ensure a substantial rapid growth of cells. The f/2 based nutrient, as used in scaling up cultures, was added and final concentration after inoculation equals 4.5 × f/2 concentration (i.e. 3969 μM. NO₃⁻ and 162 μM PO₄⁻). Cells were grown in a batch culture and switched to semi-continues culture. In this setup a certain volume of culture was removed and replaced each day with fresh nutrient medium; this type of culture method has been named “stretch-batch” culture (Page *et al.*, 1999)

2.1.4 Sampling technique.

Cells were collected using gravity filtration with low vacuum pressure (< 100mm Hg) onto 13mm diameter pre-combusted (500°C for 12h) Gelman Pall glass fibre A/E type filters. The minimum amount of cells (i.e. 2.5-5 μL biovolume of cells on the filters) was determined by the biovolume (BV) concentration of the culture using the approximation 1L BV = 200g C (Wood and Flynn 1998). Filters were frozen (-20°C) immediately in 1.5ml microtubes awaiting for particulate organic C, N, P, pigments and cellular fatty-acid analysis. The filtrate was collected into 6mL polyethylene (PE) scintillation vials and frozen (-20°C) for dissolved inorganic nutrient, including nitrate (NO₃⁻), nitrite (NO₂⁻) and ammonia (NH₄⁺), and DIP, analysis. Samples were collected in duplicate for each analysis (Note: particulate C and N can be analyzed from the same filter)

2.1.5 Analytical techniques

2.1.5.1 Cell numbers and biovolume analysis

Cell counts were performed on live samples with a Beckman Coulter Counter (Multisizer 4, Beckman Ltd, U.K.) running with a 50 μ m aperture tube, with occasional verification by microscopic counting using haemocytometer. Dilution was applied depending on the cell concentration of the culture. Biovolume was obtained along with the measurement of cell density from Coulter Counter by computing the equivalent spherical diameter (ESD) of particles passing through the aperture tube. The peak of the algal cells was identified for each species and the start and end points selected manually to obtain the total cell concentration and total biovolume (BV) concentration. Cell specific growth rates were calculated by using this equation (Eq 2.1).

$$\ln(\text{CD}_{t_1}) - \ln(\text{CD}_{t_0}) / (t_1 - t_0) \quad (2.1)$$

Where CD = cell density (cells mL⁻¹), and its value at time t_0 and t_1 (day).

2.1.5.2 Dissolved inorganic nutrient analysis

The concentrations of dissolved inorganic nitrogen and phosphate (DIN & DIP) in the medium were measured using segment flow nutrient analyser (AutoAnalyser 3, Seal Analytical, U.K.). Calibrated with series of nutrient standards for DIN (120, 80, 40, 20 and 10 μ mol L⁻¹) and DIP (60, 40, 20, 10 and 5 μ mol L⁻¹), the concentration of in the nutrient samples were measured by colorimetry after chemical reactions with reagents (detail reagents and wavelengths used, see Table 2.2). Because of the high concentration of nutrients applied in the experiment, dilutions were conducted with de-ionized water to obtain the nutrient concentration measured within the range of calibration. (Note: High concentration standards were not used since the strong colour after the chemical reaction exceeded the linearity of the measurements.)

2.1.5.3 Particulate Organic Carbon (POC) and Nitrogen (PON) analysis

Frozen filter samples were incubated overnight at 70°C until the samples were completely dehydrated. Filters with cells were wrapped with acetone pre-washed (to remove potential organic contaminations) 16mm diameter tin foil discs (Elemental Microanalysis Ltd, U.K.). All wrapping processes were conducted within a clean bench to minimise carbon contamination from the surrounding environment. Samples then were combusted using a 20:20 Stable Isotope & Elemental Analyser (PDZ Europa, Crewe, U.K.) with isoleucine wrapped in 4×6 mm tin capsules (PDZ Europa Ltd, U.K.) as standard (standard concentration used 100, 80, 60, 50, 40, 30, 20, 10 and 5 µg of N; C was calculated according to the chemical formula of isoleucine). Samples were fully combusted at 1000°C. The elements C and N in the samples were oxidised completely into CO₂ and NO₂ with oxygen supplied. Carried by Helium gas, NO₂ was converted into N₂ gas in a reduction column and measured along with CO₂ using the incorporated mass spectrometer where the elements were separated in a magnetic field to perform a peak area of the elements. Air blanks were used to monitor and calibrate the drift of the machine.

Data for the amount of C and N in the samples from the elemental analysis were calculated by relating the correspondence peak area with known standards after the air drift correction where the drift of the air assumed to be evenly distributed into each sample. A linear regression is expected to obtain between drift corrected total peak area and standard amount of elements. The intercept should be forced to zero when the correlation equations are obtained. Polynomial level two fittings were applied for the calibration curve.

2.1.5.4 Particulate organic phosphorus (POP) analysis.

Cellular phosphorus was determined using an alkaline persulphate oxidation to convert organic P to phosphate, followed by a colorimetric determination. A solution of 25g potassium peroxodisulphate ($K_2S_2O_8$, Sigma-Aldrich Co. LLC. U.K.) and 15g boric acid in 500mL of 0.375M sodium hydroxide ($15g L^{-1}$) was made and stored away from sunlight in a sealed polythene bottle. Frozen filters, dried overnight at $70^\circ C$, were folded and placed into a 5mL glass ampoule (Sigma-Aldrich Co. LLC. U.K.) and flame sealed after adding 1.5mL of the oxidising solution. The sealed glass ampoules were autoclaved for 20min at $121^\circ C$ to ensure full digestion (no colors remain on the filter). Digestions were pipette into 1.5mL eppendorf tubes and spin for 5min using a Beckman benchtop E1 microfuge to remove all the particles. The supernatant was collected and frozen into 1.5mL microtubes prior to DIP analysis (see section 2.1.5.2).

2.1.5.5 Pigments analysis

Chlorophyll a, b, c and carotenoids were extracted using N,N-Dimethylformamide (DMF) according to the methods by Inskeep and Bloom (1985). DMF (1.2mL) was added to the frozen filters in 1.5mL Eppendorf tubes, and placed in the dark at $4^\circ C$ for at least 4h until the pigments were fully extracted. The samples were then centrifuged for 5mins to remove all the particles and measured with dual beam UV spectrophotometer (UV-2550, Shimadzu Ltd, U.K.) in a 1cm path length quartz cuvette to obtain the absorbance at wavelengths 480, 510, 630, 647 and 664nm. The background was calibrated simultaneously with DMF at the wavelengths employed. The concentrations of the pigments were then calculated according to the equations (see below) determined by Jeffery and Humphery (1975).

$$\text{Carotenoids } (\mu g mL^{-1}) = v/V \times 7.6 \times (A_{480} - 1.49 \times A_{510}) \quad (2.2)$$

$$\text{Chl a } (\mu g mL^{-1}) = v/V \times ((11.85 \times A_{664}) - (1.54 \times A_{647}) - (0.08 \times A_{630})) \quad (2.3)$$

$$\text{Chl b } (\mu\text{g mL}^{-1}) = v/V \times ((21.03 \times A_{647}) - (5.43 \times A_{664}) - (2.66 \times A_{630})) \quad (2.4)$$

$$\text{Chl c } (\mu\text{g mL}^{-1}) = v/V \times ((24.52 \times A_{630}) - (1.67 \times A_{664}) - (7.6 \times A_{630})) \quad (2.5)$$

Where, v = volume of DMF added (mL), V = the volume of sample filtered on the filters (mL), A_n = the absorbance of wavelength over a 1 cm light path.

2.1.5.6 Cellular lipid extraction and fatty-acid analysis

Total lipids were analysed according to the method of Folch *et al.* (1957). This method employed an extraction using 2:1 chloroform:methanol solution and non-lipid impurities were removed by washing with 0.88% (w/v) KCl. The weight of lipids was determined gravimetrically after evaporation of solvent and overnight desiccation under vacuum with N_2 gas. (Note: procedure of Folch method is given as the following: Weigh between 0.5 g and 1.0 g of sample into the tube and record the weight to 4 decimal places. Add chloroform/methanol (C:M) (2:1, v/v) (20 to 40 ml, approx. 40 fold excess by volume) to the weighed samples in the tubes. Keep the tubes on ice. Record the volume. Homogenise the samples using the Ultra TurraxTM in the fume cupboard, remembering to rinse the probe in C:M (2:1) between samples. Stopper the tubes and leave on ice for a minimum of 1 hour. Add 0.25 volumes of 0.88% (w/v) KCl to the homogenised sample, i.e. 5 ml per 20 ml 2:1. Whirlimix vigorously for at least 5 seconds and stand on ice for at least 5 minutes. Centrifuge at 400g (1500 rpm Jouan C 412 bench centrifuge) for at least 5 minutes. Remove the top (aqueous) layer by aspiration. Weigh 15 ml quickfit tubes to 4 decimal places and record weight. Transfer the bottom layer of the centrifuged sample to the weighed tubes through prewashed (with C:M 2:1) Whatman no. 1 filter papers. Evaporate the solvent to dryness under a stream of oxygen-free nitrogen (OFN) on a nitrogen evaporator and desiccate the tube in vacuo overnight. Reweigh tubes to 4 decimal places and redissolve the total lipid in C:M (2:1) + 0.01% (w/v) BHT at a concentration of 10 mg/ml and transfer to labelled 2 ml glass vials. Store under nitrogen or argon in a freezer at -18°C or less)

Fatty acid methyl esters (FAME) were prepared by acid-catalysed transesterification of total lipids according to the method of Christie *et al.* (2003). Extraction and purification of FAME was performed as described by Ghioni *et al.* (1996). FAME were separated by gas-liquid chromatography using a ThermoFisher Trace GC 2000 (ThermoFisher, Hemel Hempstead, U.K.) equipped with a fused silica capillary column (ZBWax, 60m x 0.32 x 0.25 mm i.d.; Phenomenex, Macclesfield, U.K.) with hydrogen as carrier gas and using on-column injection. The temperature gradient was from 50 to 150°C at 40°C min⁻¹ and then to 195°C at 1.5°C/min and finally to 220°C at 2°C/min. Individual methyl esters were identified by reference to published data (Ackman, 1980). Data were collected and processed using the Chromcard for Windows (version 2.00) computer package (Thermoquest Italia S.p.A., Milan, Italy).

2.2 Model development

2.2.1 Modelling Platform

Models presented in the following chapters were constructed using Powersim Constructor version 2.5 (Isdalsto, Norway), which is a modelling package running under the 16 bit MS Windows operational system. The advantage of using Powersim constructor is that this package is operated with “Forrester diagrams”, which is typically employed to describe dynamic interaction systems (Haefner 1996). The graphic user interface encoded within Powersim constructor enables the user to easily note the interaction between the components (see Table 2.3 for symbols used in Powersim Constructor). The algorithm structure and syntax of Powersim constructor is similar (e.g., power, multiplication, square root, and, if, etc.) to that in MS Excel, though with some additional descriptors (e.g., time, timestep etc.).

Models constructed by Powersim Constructor are described with ordinary differential equations with Boolean logic statements and drive the simulations using integration of equations with the chosen timestep (minimum unit of step that simulation time is running). For the biological systems considered here, the integration timestep is

critically important for describing the rate changes with time. Some reactions happen in under seconds (e.g. electron transport and photodamage), where smaller timestep is needed to catch the sensible changes of the rate. However, some datasets use time in terms of days or even longer (e.g. seasonal growth of phytoplankton).

Data generated from a model in a simulation can be transferred into MS Excel using the Dynamic Data Exchange function (DDE). By using DDE, data in Excel can also be transferred back into Powersim Constructor, replacing the settings of constants at specific time points in simulations.

Mathematical traps are employed in the algorithm for some equations to prevent nonsense data generation (e.g., preventing uptake of DIN when the concentration had (just) become negative). These traps are not supposed to change the outputs of models but to ensure that the sensible mathematical calculations can be performed.

System mass balance was checked after the model was constructed. The total amount of elements should remain constant in the system. This can be easily achieved by adding up the elements distributed within the system in Powersim Constructor. For example, the cellular N is assembly from the extracellular DIN (assume there is no organic N source available in the medium) and thereby N in cell plus the N in water should give a constant value, which is the amount of N added initially. In reality, the mass balance rule also applied to the experimental data. The unbalance elements usually indicate a coding error.

2.2.4 The Model of Algal Physiology (MAP)

Model of Algal Physiology version 2 (MAP2, Flynn 2003) was selected to develop the PBR model for the purpose of this thesis. The MAP2 is a quota based mechanistic model driven by elemental stoichiometry (e.g., C: N: P: Si: Fe) (Flynn 2001; Flynn 2003), associated with Chl.a synthesis to describe the C-specific photosynthesis rate with empirical equation (Jassby and Platt, 1976). With the control of internal nutrient quota, specific nutrient transporters are uptaking the external

nutrient (mainly consider dissolve inorganic nutrients. e.g., DIN & DIP) into cells to finish the assembly of biochemical components (e.g., DNA, RNA and protein) and eventually cell growth. Details of the equations and constants enclosed in the MAP2 are discussed in Chapter 5. Since the model species chosen by this thesis are not diatoms, the Si sub-model was not used. The Fe sub-model was also not used because the nutrient medium applied in the experiment has excess Fe (i.e., Fe did not limit the growth.). The parameters required to drive the MAP2 model are listed in Table 2.4.

2.2.5 Model Validation and Optimisation

PBR models (see Chapter 5) were simulated under the same conditions as the experimental setups described in PBR section (see. Chapter 2.2.3) and validated against the datasets obtained from the experiment. Tuning of these models to experimental data was performed with Powersim Solver version 2 (Isdalsto, Norway). Solver uses an evolutionary algorithm to search the combination of constant parameters giving the best fit to the present datasets. The degree of fitting is determined by the least squares method, in terms of deviation. The best fit usually has a lowest deviation. The ranges of the constants that usually can be found in the literatures if the constants have been defined can be computed and set in the Solver. If the constants are original, a range is assigned initially and gradually narrows it down to obtain best fit to the dataset during the tuning.

2.3 Data transformation

Growth of phytoplankton has been studied for many decades. Data generated are used with different methods in various forms. It has been raised a concern for the modeller attempting to construct a mechanistic model to describe the dynamic growth of phytoplankton since the data available in the literature (e.g. dry weight or per cell based) are not functionally suitable for the mechanistic model applied here. Therefore, the datasets express in this thesis either measured in cellular C based (e.g.

gram X per gram cell-C, where X represent elements) or transformed to cellular C based from other units based (e.g., per dry weight, ash-free dry weight, cell and calorific value etc.). The data transformation here not only enables the available data to transform into suitable dataset for the models presented in this thesis but also interpreted the data from a mechanistic point of view.

2.3.1 C-based biochemical transformation

To achieve the C-based transformation, C and N contributions of the cellular biochemical compositions (i.e., protein-C, protein-N, carbohydrate-C and lipid-C) and cellular C:N ratio of the culture are calculated by using the converting values from various units listed in Table 2.5. Therefore, the correspondence chemical C per cell-C (i.e. carbohydrate-C per cell-C and lipid-C per cell-C etc.) can be derived.

2.3.2 C-based fatty acid transformation

Fatty acids (FA) differ from one another in length of the hydrocarbon tails, degree of unsaturation (double bond), position of the double bonds in the chain. For example, the nomenclature of oleic acid (C18:1(n-9)) can be interpreted as length of 18 carbon chain with 1 double bond in position 9 from the carbon head.

Fatty acid data can be normalised to Fatty-acid-C per cell-C (FACC) using a general chemical formula of fatty acid $C_nH_{2(n-x)}O_2$, proportion of C in specific fatty acid can be calculated using following equation:

$$C\% = \frac{12n}{(12n + 2(n - x) + 32)} \times 100$$

In the equation, n is the number of C, x is the number of double bond. Fatty acid-C now can be calculated by its amount times the percentage of C in specific fatty acid. Total fatty acid-C of each group (e.g. saturated fatty acid) was calculated by adding up all the detected fatty acid-C. Total cellular fatty acid was determined by adding up

the detected saturated, monounsaturated and polyunsaturated fatty acid (i.e., SFA, MUFA & PUFA).

Table 2.2 Chemicals and wavelengths used for colormetric analysis of dissolve inorganic nutrients.

Parameters	Reagents	Chemicals	Concentration	Wavelength
Nitrate and Nitrite	Ammonium chloride reagent	Ammonium chloride	10g L ⁻¹	550nm
		Brij-35 30% solution	0.5ml L ⁻¹	
		Ammonia solution, 25%	6 ml L ⁻¹	
	Colour reagent	Sulfanilamide	10g L ⁻¹	
		Concentrated Phosphoric acid	100ml L ⁻¹	
		N-1-Naphthylethylene diamine dihydrochloride	0.5 g L ⁻¹	
	Copper sulphate solution	Copper sulphate	2.5g L ⁻¹	
Hydrochloric acid solution	Hydrochloric acid	495ml L ⁻¹		
Ammonia	Complexing reagent	EDTA	30g L ⁻¹	660nm
		Tri-Sodium citrate dihydrate	120g L ⁻¹	
		Sodium nitroprusside	0.5g L ⁻¹	
		Brij-35	3ml L ⁻¹	
	Dichloroisocyanuric acid (DCI)	Dichloroisocyanuric acid sodium salt dihydrate	0.2g L ⁻¹	
		Sodium hydroxide	3.5g L ⁻¹	
Salicylate	Sodium salicylate	300g L ⁻¹		
Phosphate	Stock antimony potassium tartrate	Antimony potassium tartrate	23g L ⁻¹	880nm
	Ammonium molybdate reagent	Ammonium molybdate	6g L ⁻¹	
		Concentrated Sulfuric acid	64ml L ⁻¹	
		Stock antimony potassium tartrate	22ml L ⁻¹	
	Ascorbic acid reagent	Ascorbic acid	8g L ⁻¹	
		Acetone	45ml L ⁻¹	
		Sodium dodecyl sulphate (SDS)	8g L ⁻¹	

Table 2.3 Descriptions of symbols in the modelling platform Powersim Constructor version 2.5.





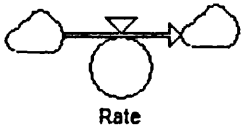
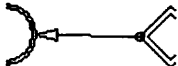


Name	Symbols	Descriptions
Level		A state variable of a system with a description of historical changes with time (e.g. C-biomass and nutrient concentrations in the medium etc.).
Auxiliary		A variable with description of instant changes of the parameters (e.g. growth rate and the rate of nutrient uptake etc.).
Constant		a function maintain the value with no change during the simulation. It can be used as conditional inputs (e.g. maximum growth rate and half saturation constant etc.).
Flow		Flow function describing energy flow from one level into another level or air where the energy lost.
Flow with rate		Flow with a control of rate changing with time (e.g. the rate of nutrient uptake and the rate of chemical synthesis etc.).
Link		Link function connects the constant to variables and/or variables to variables to describe the interaction between the parameters
Arrayed parameters		Overlapped population of parameters. This function enables the simulation running with different conditions at one time.
Snapshot parameters		A copy of the original parameters. It can use to link to other parameters but cannot be active by others.

Table 2.4. Primary experimental parameters measured for entry to the MAP2 model.

Parameters	Descriptions	Units	Methods
Light intensity	Light intensity on the surface of culture	$\mu\text{mol photons.m}^{-2}.\text{s}^{-1}$	See section 2.1.1
Optical depth	Diameter of the culture vessel facing to light source	Meter (m)	
*Temperature	Temperature in the medium	$^{\circ}\text{C}$	-
*pH	pH in the medium	-	-
DIN	Dissolve Inorganic Nitrogen in the medium	$\mu\text{mol.L}^{-1}$	See section 2.1.5.2
DIP	Dissolve Inorganic Phosphorus in the medium	$\mu\text{mol.L}^{-1}$	See section 2.1.5.2
POC	Cellular Particulate Organic Carbon	mg.L^{-1}	See section 2.1.5.3
PON	Cellular Particulate Organic Nitrogen	mg.L^{-1}	See section 2.1.5.3
POP	Cellular Particulate Organic Phosphorus	mg.L^{-1}	See section 2.1.5.4
Chl a	Cellular Chlorophyll a	$\mu\text{g.L}^{-1}$	See section 2.1.5.5

*Temperature and pH are maintained relatively constant by the system in this study. Therefore, they are treated as a reference but not viable parameters.

Table 2.5. Equations and conversion factors used in cell-C based data transformation.

Species	Data transformation	References
<i>Heterosigma carterae</i>	$\mu\text{gC L}^{-1} = 0.278 \times \text{nL BV L}^{-1}$	Wood and Flynn, 1995
Diatoms and flagellates	$\text{pgC cell}^{-1} = 0.109 \times \text{BV}(\mu\text{m}^3)^{0.991}$	Montagnes <i>et al.</i> , 1994
Phytoplankton	1mgC = 11.40 calories	Platt and Irwin 1972
Phytoplankton	1g Cellular C = 2g ash free dry weight	Geider and Roche, 2002
Organic matter	1g Crude protein = 1gN \times 6.25	Kjeldahl method
Total crude lipids	Lipid-C = lipid \times 0.73gCg ⁻¹ lipid	Sukenik <i>et al.</i> , 1993 Geider and Roche, 2002
Total crude carbohydrates	Carbohydrate-C = carbohydrate \times 0.40gCg ⁻¹ carbohydrate	Geider and Roche, 2002
Total crude proteins	Protein-C = protein \times 0.53gCg ⁻¹ protein	Geider and Roche, 2002

3. Growth, elemental and biochemical composition of *Nannochloropsis oculata* (Droop) in a large-scale tubular photobioreactor

3.1 Introduction

Nannochloropsis oculata (Droop) is one of the microalgae most widely used as feedstock in aquaculture for its relatively high eicosapentaenoic acid (EPA) content, which is essential for fish larval and zooplankton nutrition (Brown *et al.*, 1997). Its growth stoichiometry and biochemical composition has been reported under various growth conditions in laboratory-scale experiments (Sukenik & Carmeli 1990; Flynn *et al.*, 1993; Sukenik *et al.* 1993; Fabregas *et al.* 2004). However, fewer studies combined measurements of elemental stoichiometry with biochemical analysis under dynamic growth conditions in mass culture systems. Reports from pilot-scale PBR was revealed that lipid productivity in *Nannochloropsis sp.* may attain over 60mg L⁻¹ d⁻¹, with lipid content varying between 21-31% of dry biomass in N-replete condition (Rodolfi *et al.*, 2009). Although the lipid content of *Nannochloropsis sp.* can attain up to 60% of dry biomass under N-deprivation, higher lipid productivity can only be achieved via the accumulation of biomass in nutrient replete batch culture (Rodolfi *et al.*, 2009; Huerlimann *et al.*, 2010). Therefore, a combination of N-replete batch culture (to obtain a substantial initial biomass) followed by an N-deprived batch culture (to promote lipid accumulation), of *Nannochloropsis sp.* was proposed (Rodolfi *et al.*, 2009). This approach has been shown to have nearly 3 times higher lipid yield than traditional batch culture (Su *et al.* 2011). Manipulation of the physiology of the microalgae via the operation of the bioreactor in this so call “two-stage cultivation” has been demonstrated to be an effective way to promote the lipid productivity. Actually, the method probably differs in its physiological implications to conditions generated in small scale laboratory systems; the problem

with large-scale PBRs is specifically ensuring the development of nutrient stress in a culture system that is so readily prone to light (and not nutrient) limitation due to the self-shading of culture.

The aims of the present study come from two angles. One is to exam the productivity of *Nannochloropsis oculata* (Droop) (CCAP 849/1) in a 600L tubular photobioreactor (PBR). The other is to seek a link between elemental ratios and biochemical composition for a typical dynamic growth in the PBR in order to provide data for model development.

3.2 Materials and Methods

Nannochloropsis oculata (Droop) (CCAP 849/1) (10% v/v inocula) was grown in a 600 L tubular photobioreactor (PBR) located in a greenhouse under continuously lighting (the physical description of PBR is given in Chapter 2.1.3). Natural seawater with $5\times f/2$ based nutrient medium was used (see Chapter 2.1.2 for preparation). Since a significant volume of inoculum was added into the system, the final concentration (after inoculation) of nutrients in the PBR equals $4.55\times f/2$ medium (as the residual nutrient levels in inoculums was rather low in comparison with the fresh nutrient). The PBR was operated initially in a batch culture mode until the external nutrients were depleted and then switched to semi-continuous mode for 3 days to obtain nutrient limitation growth. During semi-continuous growth, 150 L of seawater medium comprising 37.5 L of $5\times f/2$ nutrient medium was pumped into the system daily. Biomass was harvested daily to maintain 600 litre of culture remain inside the system. This equals a dilution rate of 0.2 d^{-1} ; when run for a long enough period, this dilution rate would thus enforce a growth rate of 0.2 d^{-1} .

The study was conducted during the winter time (December) when natural daylight and atmospheric temperature was low. Artificial lighting was provided continuously in addition to the daily sunlight. Heat produced by the light bulb also helped to maintain the room temperature inside the venue. Photon flux density was measured



using a QSL-100 probe (Biospherical Instruments Inc, San Diego, U.S.A) at least once a day, and always at 12:00 GMT, at six fixed positions across the surface of PBR. Daylight irradiance was estimated from the average of the six positions. Light irradiance during the night time was measured using the same methods as daylight period (PFD about $225 \mu\text{mol photons m}^{-2} \text{s}^{-1}$). This is considered to be the lowest light experience by the culture. Medium temperature and pH were recorded 5 times a day in the dark tank.

Sample collections and analysis see Chapter 2. Centrifugation was applied along with gravity filtration to collect the filtrate since the 13mm filters block at high cell densities.

Lipid extraction was performed using 2:1 (v/v) chloroform:methanol solution according to the method of Folch *et al.* (1957) as described in section 2.1.5.6 of Chapter 2. The C content of total lipid was then estimated using $0.73 \times$ total lipid content (see Chapter 2.3.1). Protein content was estimated using the conversion factor $6.25 \times$ N content measured from elemental analysis. The C of the protein was then calculated using $0.53 \times$ protein content according to the general chemical formula (Geider and La Roche, 2002). If we assume the C content consists of the C from lipid, protein and carbohydrate, then the carbohydrate-C can be calculated from the subtraction of lipid-C and protein-C from total cell-C.

3.3 Results

3.3.1 Growth conditions

The physical culture conditions are illustrated in Figure 3.1. The Medium temperature was maintained relatively constant at 26°C with transient decrease to 23°C . Irradiance at the surface of the PBR remained fairly constant, around $250 \mu\text{mol photons m}^{-2} \text{s}^{-1}$, although it was considerably higher at day 2. Irradiance also slightly decreased below the minimum light ($225 \mu\text{mol photons m}^{-2} \text{s}^{-1}$) measured at night

(see Chapter 2) at the end of the culture (around day 11). This was attributed to failing lamps (failed and obviously failing lamps were replaced as they were noted). Values of pH were maintained at around 8 after day 4. A fluctuation of pH value over 9 was observed around day 3. However, this was attributed to an inability of the CO₂ injection to keep pace with the CO₂ demands of the then rapidly growing algal population.

3.3.2 culture conditions

Changes in cell number are illustrated in Figure 3.2. Cell specific growth rate reached its maximum, 0.52 d⁻¹, at day 5; this rate was maintained for 3 days. A slight fluctuation on cell growth rate was observed within day samples. It may result from the higher irradiance in the afternoon in comparison with morning although the daylight irradiance was not significantly change except day 2 (Figure 3.1). When grown in a light/dark cycle, cell division is expected to occur in darkness; here there was continuous light, so the variation in growth rate may be attributed to a residual synchrony from the inoculum.

The relationship between C-biomass and biovolume is given in Figure 3.3. A strong linear relationship can be drawn out between cellular C and cell volume. Given an equation which can be used for estimation of the C-biomass from biovolume for *Nannochloropsis oculata* as following:

$$\text{Biovolume (L)} = 314 \times \text{C (g)}$$

At day 9 of the culture, C-biomass, N and chlorophyll_a (Chl) concentration attained around 600 mg L⁻¹, 70 mg L⁻¹ and 7 mg L⁻¹ respectively, as illustrated in Figure 3.4A. Recovery from lag phase extended until day 4. Exponential growth started at day 4 where C-specific growth rate peaked at 0.57 d⁻¹ and exceeded 0.5 d⁻¹ for about 3 days (day 4-6), declining after day 6 (Figure 3.4B). N and Chl specific growth rate both attained their maximum at day 5 around 0.54 and 0.6 d⁻¹ respectively. Similar to the

growth rate of C and N sustained around 0.5 d^{-1} for about 3 days (day 4-6).

Chl has a higher specific growth rate than either C or N. The initial Chl:C ratio is high and decrease 60% of original to attain minimum at day 4 when C growth attained the maximum. The Chl:C start to increase at day 7 when C and N growth decrease. This pattern likely reflects the initial acclimation to higher received irradiance at the cell surface when the inoculum was introduced to the PBR, and then a “re-greening” with acclimation to increasing light attenuation as biomass developed.

3.3.3 Nutrient assimilations

Nitrate and phosphate were depleted by day 9 and 7, respectively (Figure 3.5). Correspondently, the cellular N:C started to decrease at day 9 from around 0.14, at which level it had been maintained for the previous 4 days, when the nitrate was depleted (Figure 3.5A). The initial N:C is around 0.1 indicates a nutrient-stressed inoculum was employed to start the PBR culture. A high N:C ratio up to 0.17 was observed at day 3 when a relatively high medium pH (pH=9) was recorded (Figure 3.1). The cellular P:C started to decrease from 0.025 at day 6 when the phosphate was depleted (Figure 3.5B). The initial phosphate concentration was lower than expected (the phosphate initially added equated to $4.55 \times f/2$, which is $163 \mu\text{mol L}^{-1}$). Only about 70% of added phosphate was thus detected in the medium. This was probably due to the precipitation of phosphate with high concentration in seawater medium (ref). A high P:C ratio up to 0.06 is recorded with the high N:C (0.17) at day 3. The high pH at this time is likely to be coincidental with relative C-stress in the culture; C-stress equates to a N and P replete state, consistent with elevated N:C and P:C.

The nutrient status of the culture during growth is shown in Figure 3.6. Here, calculated from the temporal pattern of changes in N:C and P:C associated with changes in C-specific growth rate (Figure 3.6A, C), nutrient status can be

transformed into NCu and PCu (Figure 3.6D). These values, derived from the normalised quota equation ($^n\text{Quota}$, Flynn 2002; given in Figure 3.6B) indicate the level of nutrient stress; NCu and PCu vary between 0 and 1, where 1 indicates nutrient replete.

As illustrated in Figure 3.6C, N:C and P:C are closely correlated with C-specific growth rate. Maximum growth rate is achieved when N:C and P:C both attain their maximum (apart from the extreme quota, noted at day 3). The maximum N:C obtained from the regression fitting is 0.157 and KQN is typically >10. The maximum P:C obtain is 0.03 and KQP is 0.179. N:C has a linear relationship with growth rate while P:C are curvilinear, although some discrepancies are observed. The discrepancy in P:C may results from the phosphorus storage in inoculums before the exponential growth begins. The extreme quota ratio may be influenced by the elevated pH observed at day 3 (Figure 3.1).

From the nutrient status given in Figure 3.6D, a dynamic nutrient limitation can be interpreted. The lowest normalised quota ($^n\text{Quota}$; NCu or PCu) indicates the most limiting nutrient that limits the growth. Both nutrient $^n\text{Quota}$ are below 1 during much of the growth period. NCu is lower than the PCu before day 6. Then PCu decreased to the lowest between day 7-10 and then recovered during the semi-continuous culture phase. In contrast, NCu continued to decline, indicating a declining N-status in the semi-continuous culture phase, and also implying that the culture system had not entered steady-state by the end of the experiment..

3.3.4 Biochemical composition:

The lipid concentration in the culture attained approximately 250 mg L⁻¹ after 10 days in batch culture (Figure 3.7). Cellular lipid content decreased initially from a high value around 50% of cell-C to around 20% and then recovered to 30% of cell-C at the end of the batch culture. Lipid-C per cell-C slightly decreases during the semi-continuous phase. Lipid per cell has a similar trend as lipid-C but relatively stable at 1.5 pg cell⁻¹ during semi-continuous growth.

More changes in biochemical composition is illustrated in Figure 3.8A. Protein-C maintained nearly 50% of the cell-C for about 5 days (day 4-8) and decreased to around 30% of cell-C at the end of semi-continuous growth. Carbohydrate-C increases over 5 fold and attain nearly 50% of cell-C. Only very little carbohydrate is contained at the beginning of exponential growth (see Figure 3.4 for growth condition). The estimated amount of excess-C increased with the increase in C:N ratio, with most of that increase being associated with carbohydrate, and not with lipid (Figure 3.8.B).

3.4 Discussion

As microalgae have been suggested as a potential feedstock for third generation biofuels, much effort has been deployed to maximise lipid productivity (Rodolfi *et al.*, 2009; Huerlimann *et al.*, 2010). Physiological changes of microalgae with different bioreactor units have been considered less.

Lipid accumulation is in expense of the growth rate, or more precisely, depend on the nutrient status. Lipid content is closely linked to the physiological status of the cell. A common negative relationship between lipid content and growth rate has been suggested by Williams and Laurens (2010). When consider the concept within the word “productivity”, the best species for biodiesel is needed to accumulate relatively large amount of biomass with high lipid content in relatively short time. To achieve this, manipulation of nutrient status may provide a route.

3.4.1 Nutrient limitations

The degree and type of nutrient stress determents lipid or carbohydrate content of the cells. As the present study shows, C:N ratio and excess-C (sum of lipid-C and carbohydrate-C) are positively correlated (Figure 3.8B). It is worth to note that the increase of carbohydrate is also well correlated with C:N ratio. The C:N ratio of *Nannochloropsis oculata* has been reported to attain 28 in nutrient deplete batch culture (Flynn *et al.*, 1993), and the lipid content can be stimulated approximately 5 fold within 4 days in the starvation phase of *Nannochloropsis oculata* (Su *et al.* 2011). The highest C:N ratio and lipid content noted in this study were only half of these values, likely in consequence of light-limitation within a large scale PBR..

In general, N-starvation appears an effective way to increase C:N ratio and thus excess-C content. A N-starvation study of *Isochrysis galbana* shows that C:N ratios reach their maximum around 20 within 3 days in both ammonium and nitrate grown cells with their fatty acid content immediately increase (Flynn *et al.*, 1992).

N-starvation of *Phaeodactylum tricornutum* for 6 days yields a C:N ratio at 28 with approximately 76% of lipid content ($\text{gC}(\text{gC})^{-1}$), if assume C contained in lipid is about 73% of lipid weight (Larson and Rees, 1996).

The potential to enhance the excess-C accumulated by N-stress is great. However, it is of importance to know the nutrient status of the cells inside a particulate culture vessel and further to 1) meet their needs to support the maximum production of target chemicals by designing the photobioreactor (PBR) or 2) select the time to harvest.

Different nutrient source limitation has significant impact on the lipid and carbohydrate content (collectively call excess-C) for different species. In comparison with ammonium growth cell, nitrate grown cell has more lipid content and higher C:N ratio under the same growth condition (Flynn *et al.*, 1993; Fidalgo *et al.*, 1998). Often nitrate is the prefer N source used in algal mass culture due to the non-toxicity in high concentration level, although ammonium grown cells may have a higher growth rate in continues light culture (Levasseur *et al.*, 1993). Cells in relatively high light culture are more stressed than the cells in low light culture using nitrate as N source (Wood and Flynn, 1995). Higher irradiance will results in higher C:N ratio and thus potentially more excess-C (Thompson *et al.*, 1990; Fabregas *et al.*, 2004). For the present study, nitrate initially limited growth for 4 days and then the growth are co-limited by N and P (Figure 3.6D). According to the threshold theory, only one nutrient can be assumed to be limiting at a given instant (Droop, 1974). The most limiting nutrient results in the growth rate. Cellular lipid content dramatically decreased when the growth become N and P co-limited after day 4 (Figure 3.7). Then, P is the most limiting nutrient in the N and P co-limiting growth using *f/2* based medium.

Phosphorous is an important component in nucleic acids. Cells lacking P typically have a relatively low RNA content in comparison with N stressed cells, while N stressed cells have a significantly lower protein and chlorophyll content than

P-stressed cells (Berdalet *et al.*, 1994). P limitation may limit the transcription level from DNA to RNA while N limitation may affect the translation level from RNA to protein. P limitation may also result in elevation of C:N ratio potentially by control the N transport (Flynn, 2008b). Therefore, excess-C increases under P limitation. However, as the chemical analysis shows in the present study, the main excess-C increases as carbohydrate rather than as lipid. The types of excess-C may mainly subject to species-specific difference (Reitan *et al.*, 1994). It has been revealed under P starvation that neutral lipid significantly increase in select marine species while fresh water species are not (Rodolfi *et al.*, 2009). There is another possibility that N and P co-limitation may lead to an accumulation of carbohydrate and results in low lipid productivity as shown in cultures using *f/2* medium (Huerlimann *et al.*, 2010). A further research on the regulation of nutrient limitation type on the interrelationship between the excess-C groups (i.e. carbohydrate and lipid) is required.

Unfortunately, C-specific data are rarely reported in the literature. The true relationship between nutrient stress and cellular biochemical composition is thus unclear in respect to the various data types (see section 2.3). In most of the literature, chemical analyses are expressed as percentage of organic fraction or dry weight with or without ash content, or on mass per cell based. Transformations from bases such as cell or weight, to C are highly problematic (e.g. change of cell size during growth). The transformations are depending on species and nutrient status (Finkle *et al.*, 2010).

To determine the effects of nutrient status to the biochemical end products, elemental composition and biochemical composition data are both needed. Cellular N:C and P:C ratios are the more reliable parameters to determine the nutrient status of culture rather than the external nutrient concentration (Flynn, 2010a). Cell size and thus total biovolume is relatively easy to measure in non-colony forming algae, and are well correlated with total C biomass (for this study, see Figure 3.3). Nutrient concentrations are also relatively easy to measure. If one assumes that nutrient

“missing” equates to nutrient within the growing biomass, then estimates of cellular C:N and C:P should be possible without recourse to the expense of elemental analysis.

3.4.2 Chlorophyll synthesis and self shadings

High density biomass cultures often end up with light limitation by self-shading from the chlorophyll concentration of the culture. In batch culture, light availability inside the culture changes depending on the chlorophyll concentration during growth. N limitation leads to a significant decrease of chlorophyll content (Davidson *et al.*, 1991; Berdalet *et al.*, 1994). Therefore, light availability increases with N stress increase. However, P limitation may not directly affect the chlorophyll synthesis. Cells in P limitation have higher chlorophyll content than the N limited cells (Berdalet *et al.*, 1994).

As the present study shows, chlorophyll-specific growth maintained a high rate for one more day after C and N specific growth rates started to decrease (Figure 3.4B). The chlorophyll-specific growth rate started to decrease when the N-status decrease at day 8 (Figure 3.6B). The increase of Chl:C ratio may results from a differential decrease of chlorophyll and C synthesis since the growth rate is controlled by P limitation (the most limiting nutrient limits growth) while chlorophyll synthesis is controlled by N status. The increase of the Chl:C ratio indicates a decrease of light availability inside the culture. From the self-shading of the culture prospect, N limitation may be more efficient than P limitation in promotion of lipid accumulation in high density mass culture.

Two other interactions between chlorophyll synthesis and biomass production warrant mention at this stage. Firstly, the development of photo acclimation has a deleterious effect on total biomass growth (Flynn *et al.* 2010b). In consequence, it has been the subject of genetic modification studies, to limit the extent of self shading (Beckmann *et al.* 2009). Secondly, photodamage develops rapidly in

microalgae at the transition from nutrient-replete to nutrient depletion. Deployment of a two-stage culture approach may be expected to differ significantly from that of continuous culture in this regard, and warrants further study.

3.4.3 Culture productivity and operation

This study shows a supplementary culture scheme during winter time when the suitable growth temperature and illumination are scarce in high latitude area. However, the use of artificial lighting may not be viable in summer time due to the development of extreme high temperatures. The use of artificial lighting is also usually considered as uneconomical; a further comprehensive life cycle assessment (LCA) of this deployment would consider not only the productivity but also the social and ecological cost, such as carbon dioxide fixation and energy consumed etc associated with energy production (Williams, 2007).

Various papers report productivity of microalgal culture. Unfortunately they do so using a variety of methods that complicate comparison. For continuous production, the productivity is easily computed. For the system studied here, during the semi-continuous phase, lipid production was ca. 40mg lipid L⁻¹ d⁻¹; this is computed from a content of ca. 200mg lipid L⁻¹, with a dilution rate of 0.2 d⁻¹.

However, for batch cultures, calculations should be computed over a series of growth cycles, in order to take into account the contribution of the inoculum. More usually, production is considered just considering the period of growth and the increase in lipid content over that time. A comparison of the productivity of batch cultures is given in Table 3.1. The biomass and lipid productivity in the system studied here is relatively low (0.12g L⁻¹ d⁻¹ and 40mg L⁻¹ d⁻¹). Of the systems studied, this was by far the largest among the reports. There is potential for significant problems in up-scaling the production of microalgal biomass. However, productivity is highly subject to the culture condition and the scale applied, and as the nutrient statuses are rarely reported a full comparison of the biomass and lipid productivity must await further

study. Various factors, such as pH, may affect the nutrient acquisition of culture. In the present study, pH was elevated by 1 unit from the standard pH set for regulation (pH=8) at day 3. During photosynthesis, CO₂ is taken up from the culture medium. This action changes the equilibrium of DIC dynamic and results in an elevation of pH by increasing the CO₃²⁻ contribution to the medium (Falkowski and Raven, 2007). The insufficient CO₂ supplied in a large scale high density system slow the growth rate (Figure 3.4B) and result with a high N:C and P:C ratio (Figure 3.5). To prevent the increase of pH, continue CO₂ supplied regulated by medium pH is needed to be installed, especially in high density culture.

3.5. Conclusion

In conclusion, the physiology of nutrient uptake and biochemical composition of *Nannochloropsis oculata* has been studied in a large-scale tubular photobioreactor. The culture depleted the 5×f/2 nutrients within 10 days and then grew on into N and P co-limitation. The cellular lipid content did not significantly increase while carbohydrate appears as the main product accumulated. Biomass and lipid productivity equals 0.12 g L⁻¹ d⁻¹ and 24.5 mg L⁻¹ d⁻¹ respectively over the batch cycle; during the semi-continuous phase these rates were 600mg L⁻¹ d⁻¹ and 40mg L⁻¹ d⁻¹, respectively.

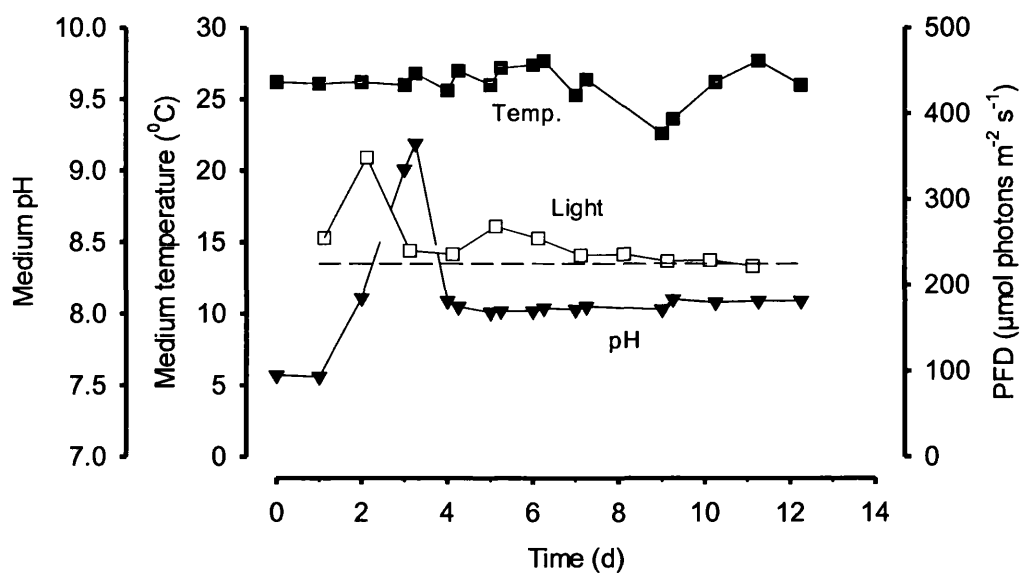


Figure 3.1: Change of daylight irradiance, medium temperature and pH during culture growth. (■) Temperature, (□) daylight irradiance at the surface of the PBR tubes, dashed line indicates the minimum irradiance at night time. (▼) pH.

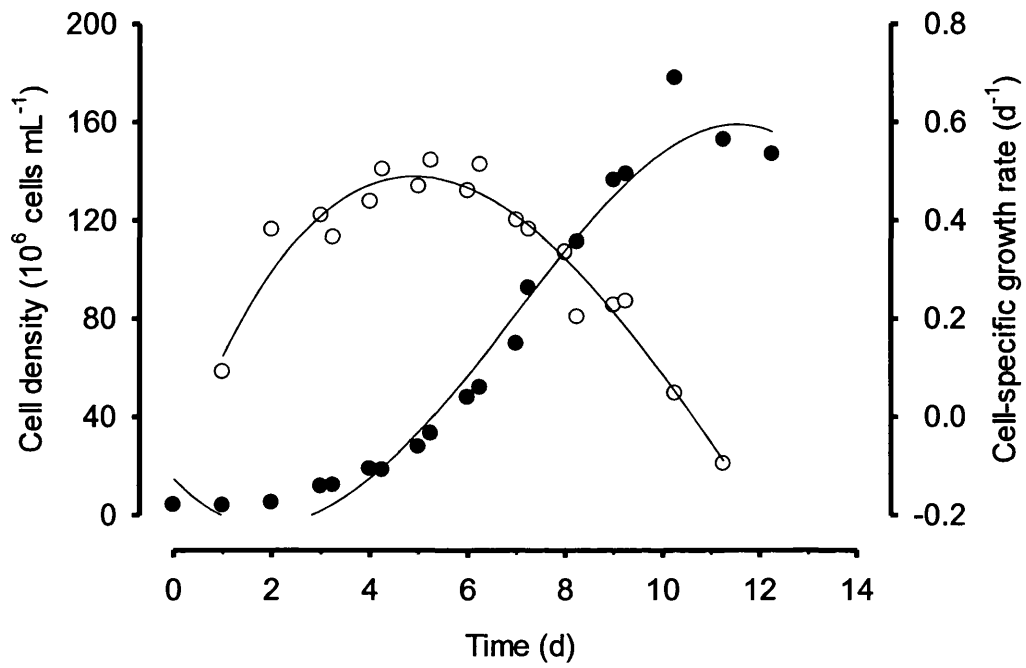


Figure 3.2 Change of cell density and cell specific growth rate. (●) cell density, (○) cell specific growth.

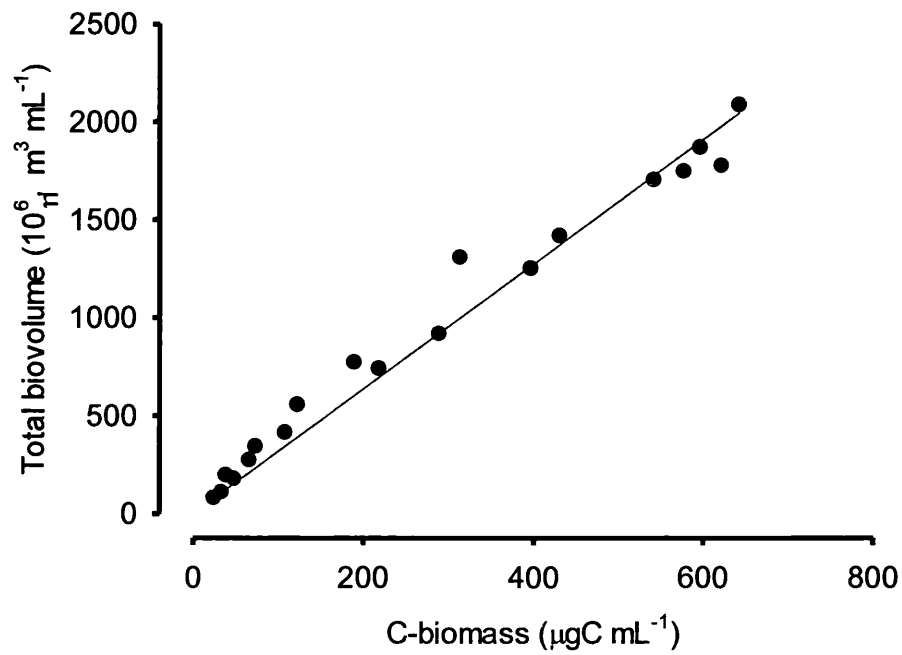


Figure 3.3 Relationship between C-biomass and total biovolume of the culture. Linear regression Biovolume (L) = $314 \times C$ (g) ($r^2=0.98$, $n=19$) was fitted through the data points.

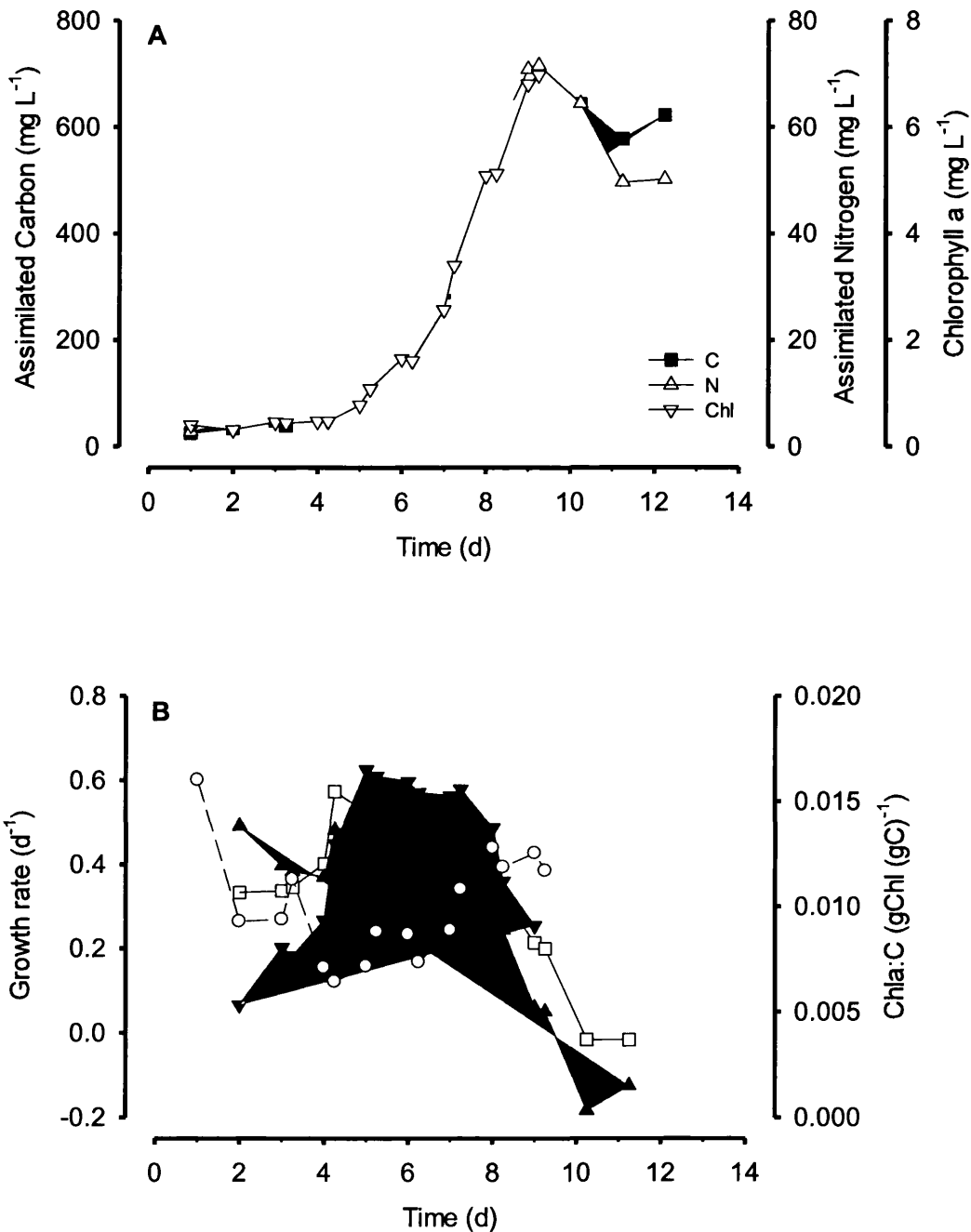


Figure 3.4: Panel A: Change of cellular C, N and Chlorophyll content during the culture (■) C-biomass concentration, (△) N concentration, (▽) Chlorophyll concentration. Panel B: Change of specific growth rate in terms of C, N and Chlorophyll and Chla:C ratios during the culture. (□) C-specific growth rate, (▲) N-specific growth rate, (▼) Chl-specific growth rate, (○) Chla:C ratio

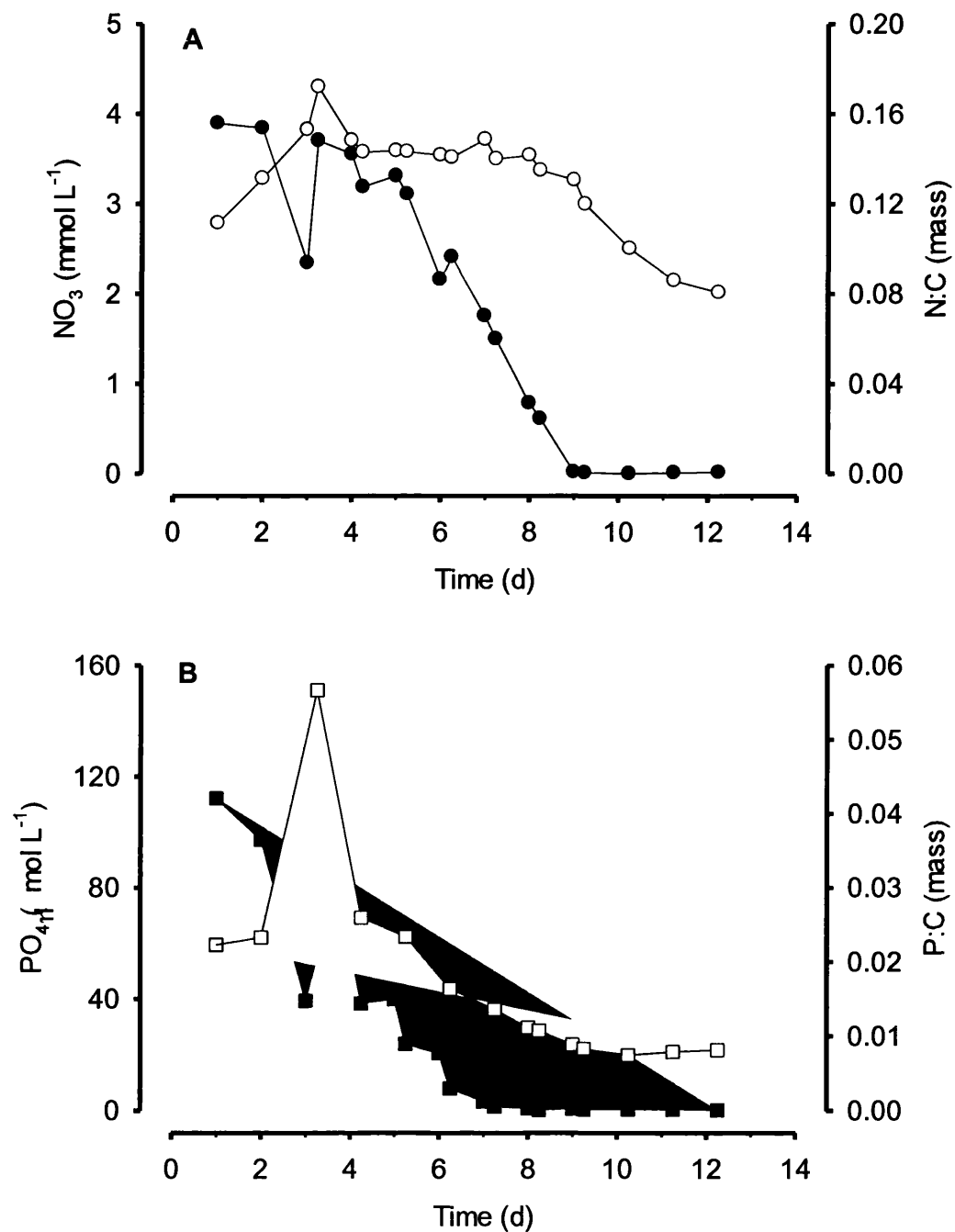


Figure 3.5 Change of medium nutrient concentration and cellular elemental ratios. A: (●) Nitrate concentration, (○) Cellular N:C ratios. B: (■) Phosphate concentration, (□) cellular P:C ratios. Data presented are the mean of duplicate measurements.

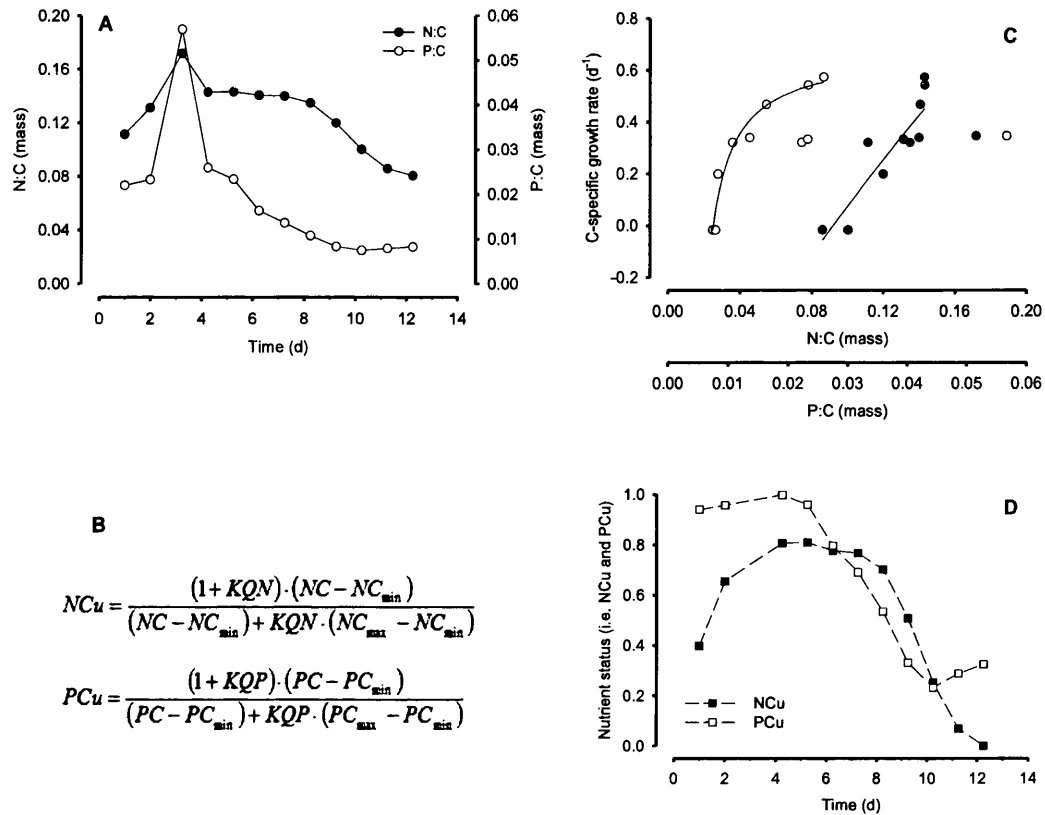


Figure 3.6 Conversion of cellular N:C, P:C ratios into nutrient status (NCu and PCu). A: Change of N:C and P:C ratios along the growth; (●) N:C ratio, (○) P:C ratio. B: Equations for nutrient status. C: Change of N:C and P:C with C-specific growth rate; symbols as in panel (A). Equations in B were fitted to the data in panel (C). D: Change of nutrient status during culture growth; (■) N-status (NCu), (□) P-status (PCu).

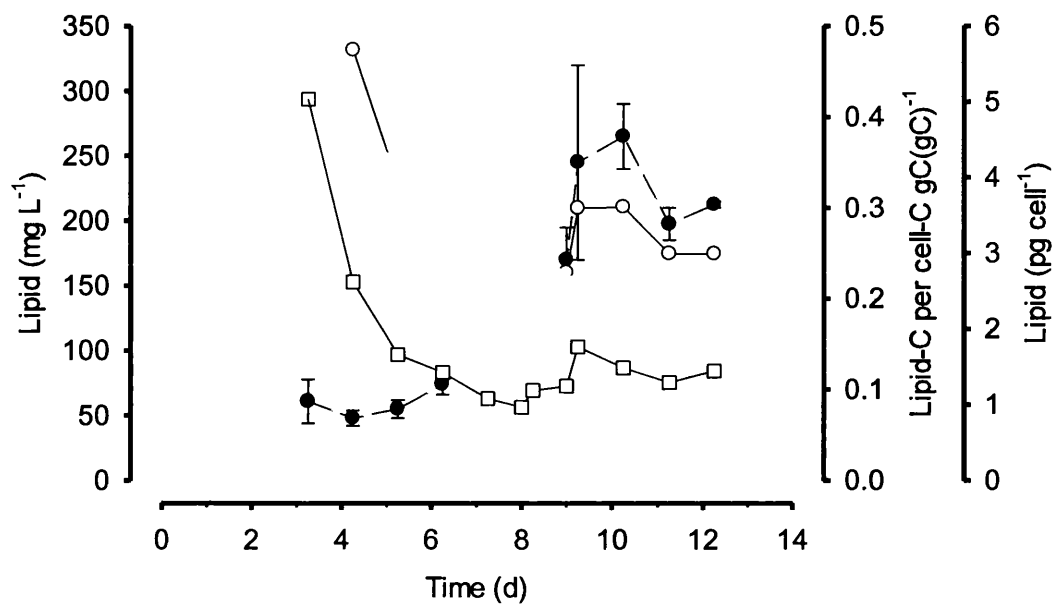


Figure 3.7 Change of total lipid content of culture and cellular lipid content in terms of C-based and per cell-based. (●) Total lipid concentration, Data presented as mean of duplicates with error bars. (○) lipid-C per cell-C. (□) lipid per cell.

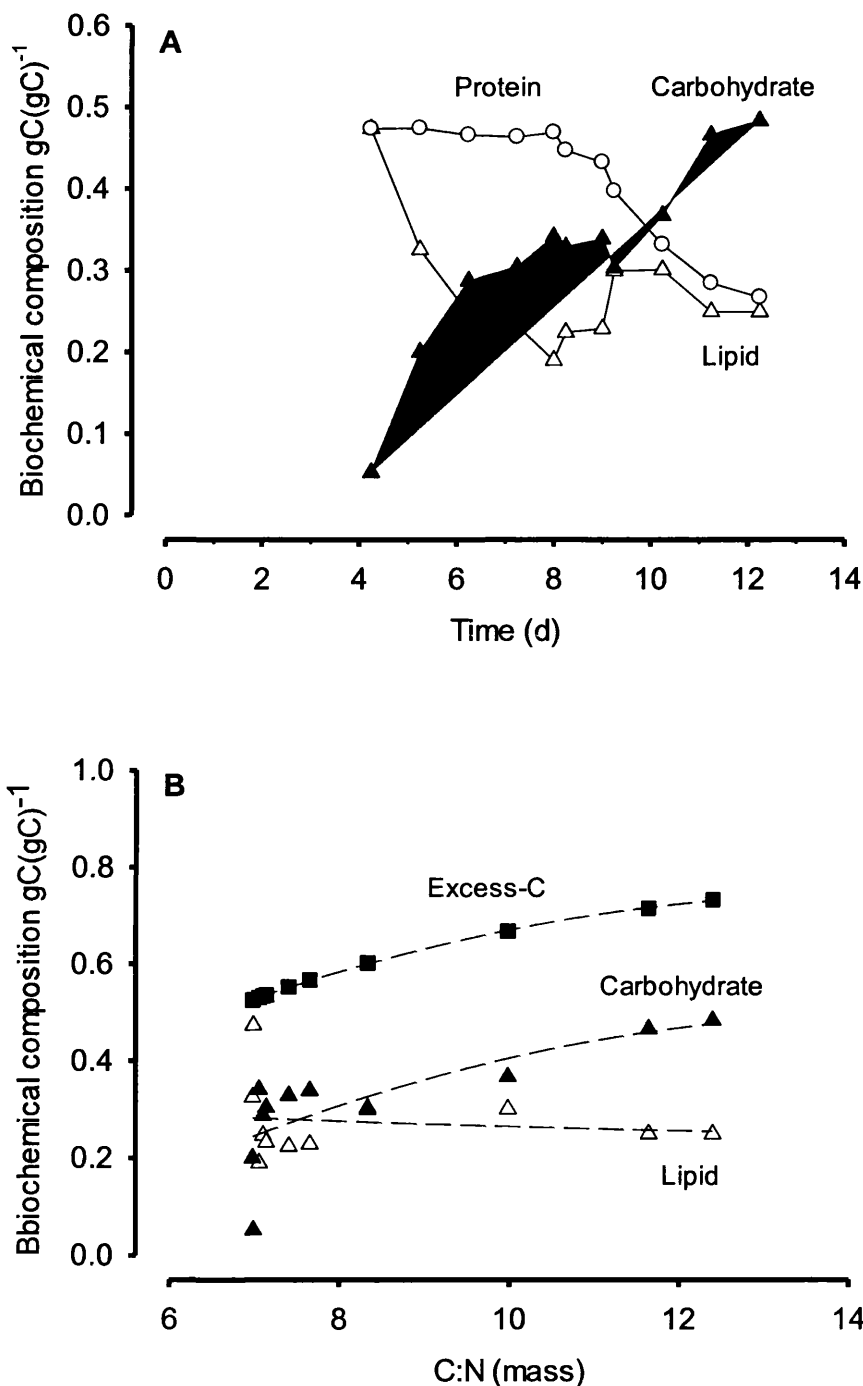


Figure 3.8 Change of biochemical compositions and their relationship with C:N ratios. Panel A: (○) Protein, (▲) Carbohydrate, (△) Lipid. Panel B: Change of excess-C (sum of the lipid-C and carbohydrate-C) with C:N ratio. (■) excess-C, (▲) Carbohydrate, (△) Lipid. Data presented are the mean of duplicate measurements. Carbohydrate content was calculated as the difference between total-C and protein-C plus lipid-C.

Table 3.1 Biomass and lipid productivity of genus *Nannochloropsis* under different batch culture conditions

Species and strain	PFD and light:dark cycle (μmol photons m ⁻² s ⁻¹)	Culture medium	Scale of culture (L)	Biomass productivity (g L ⁻¹ d ⁻¹)	Lipid content (% of dry weight)	Lipid productivity mg L ⁻¹ d ⁻¹)	Reference
<i>Nannochloropsis oculata</i> (NCTU-3)	300 (24)	f/2	0.8	0.37-0.48	22.7-29.7	82-142	Chiu <i>et al.</i> 2009
<i>Nannochloropsis</i> sp.	250 (12:12)	L1	15	0.061	32.7	20.0	Huerlimann <i>et al.</i> 2010
<i>Nannochloropsis</i> sp.	250 (12:12)	f/2	15	0.014	33.2	4.59	Huerlimann <i>et al.</i> 2010
<i>Nannochloropsis</i> sp CS 246	100 (24)	f	0.25	0.17	29.2	49.7	Rodolfi <i>et al.</i> 2009
<i>Nannochloropsis</i> sp F&M-M24	100 (24)	f	0.25	0.18	30.9	54.8	Rodolfi <i>et al.</i> 2009
<i>Nannochloropsis</i> sp F&M-M26	100 (24)	f	0.25	0.21	29.6	61.0	Rodolfi <i>et al.</i> 2009
<i>Nannochloropsis</i> sp F&M-M27	100 (24)	f	0.25	0.20	24.4	48.2	Rodolfi <i>et al.</i> 2009
<i>Nannochloropsis</i> sp F&M-M28	100 (24)	f	0.25	0.17	35.7	60.9	Rodolfi <i>et al.</i> 2009
<i>Nannochloropsis</i> sp F&M-M29	100 (24)	f	0.25	0.17	21.6	37.6	Rodolfi <i>et al.</i> 2009
<i>Nannochloropsis</i> sp F&M-M24	15.9 MJ/m ² /day (outdoor, August)	f	110	0.36	32.3	117	Rodolfi <i>et al.</i> 2009
<i>Nannochloropsis oculata</i> (CCAP 849/1)	250 (24)	5×f/2	600	0.12 ^(a)	20.9 ^(a)	40	Current study

Note: (a) calculated from cell-C by assuming C content is 50% of ashed free dry weight. C in lipid contain 73% of lipid weight.

4. Changes in fatty acid composition in relation to C:N:P:Chl stoichiometry within *Nannochloropsis oculata* during dynamic growth.

4.1 Introduction

The fatty acid profile of microalgae changes in response to changing environmental conditions. When growing in a batch culture, the fatty acid composition of microalgae is expected to be regulated by both changing nutrient status, any internal irradiance (via self-shading) over the growth cycle in a predictable manner assuming pH and temperature are maintained constant. Typically, the percentage contribution of total fatty acids (TFAs) attributed to saturated fatty acids (SFAs) plus monounsaturated fatty acids (MUFAs) increase while the polyunsaturated fatty acids (PUFAs) decrease with the development of various nutrient stresses through to starvation (Sukenik *et al.*, 1993; Reitan *et al.*, 1994; Xu *et al.*, 2001; James *et al.*, 2011). Similar patterns also can be found in gradually increase the light intensity of nitrate grown culture. High light acclimated cultures with nitrate as the N-source may accumulate more neutral lipid (i.e. TAG) in which SFAs and MUFAs are dominant, a situation contrasting with low light acclimated cultures (Sukenik *et al.*, 1989; Sukenik and Carmeli, 1990; Thompson *et al.*, 1990; Fabregas *et al.*, 2004). This may reflect the observation that nitrate-grown cells become more N-stressed during growth at high light than in low light culture, with the difference between growth rates of organisms grown on ammonium versus nitrate becoming greater at high irradiance (Wood and Flynn, 1995). On the contrary, high PUFA content has been suggested to be obtained under nutrient rich and low light condition (Sukenik *et al.*, 1989). The fatty acid profile of microalgae is thus a highly dynamic component

which can be physiologically manipulated.

With the growing interest of using microalgae for commercial exploration, the quality of fatty acid composition is a common target for research. Under “optimal” culture condition, microalgae, especially marine species, are naturally rich in long chain PUFAs which collectively comprise an essential nutritional property assessed as feed for aquaculture (Volkman *et al.*, 1989; Volkman *et al.*, 1993). Additionally, omega-3 fatty acid, such as eicosapentaenoic acid (EPA) and docosahexaenoic acid (DHA) from long chain PUFAs are valuable chemicals which have been used in feedstuffs for human consumption (Borowitzka 1995; Adarme-Vega *et al.*, 2012). However, for the bioenergy agenda, high PUFAs content in biodiesel products is undesirable as they tend to decrease the oxidative stability; a high content of short chain SFAs and MUFAs, which are normally obtained under conditions of nutrient stress, are more desirable (Hu *et al.*, 2008; Ramos *et al.*, 2009; Stansell *et al.*, 2012). It is thus of importance to know the fatty acid composition in a dynamic growth stage for distinctive purposes.

Nannochloropsis oculata, a marine eustigmatophyte, contains relatively large amount of valuable lipids. The predominant fatty acids are palmitic acid (C16:0), palmitoleic acid (C16:1(n-7)) and eicosapentaenoic acid (EPA; C20:5(n-3)) (Hodgson *et al.*, 1991; Volkman *et al.*, 1993) (see Chapter 2.3.2 for fatty acid nomenclature). It is one of the few species which is readily cultured in large scale outdoor ponds (Anderson, 2005). The EPA content of *Nannochloropsis oculata* has been reported to attain about 30% of TFAs under low light condition (Volkman *et al.*, 1993). Conversely, the sum of SFAs and MUFAs of *Nannochloropsis sp.* may attain >90% of TFAs under nitrogen deprivation (Rodolfi *et al.*, 2009). These characteristics make *Nannochloropsis oculata* an ideal candidate to exam the change of fatty acid composition in a batch culture for commercial exploration (e.g. biodiesel and Omega-3 fatty acids production).

Usually, only a few fatty acid profiles are presented in publications, selected as

representative of specific growth stages (i.e. logarithmic phase and stationary phase) (e.g. Fidalgo *et al.*, 1998). Inadequate fatty acid profile along the growth reflects the logistic (time, resource, expense) complexity of FA analysis. Only a few studies have followed changes of the fatty acid composition over the course of a growth cycle (Hodgson *et al.*, 1991; Liang *et al.*, 2006), and even fewer have related shifts of fatty acid composition during the growth with key physiological parameters (e.g. N:C, P:C & Chl:C). In consequence, while (as stated above) much is known about relative changes in FA composition, relating these objectively to the organism nutrient status is non-trivial.

With the development of nutrient limitation in the batch growth of culture, elemental ratios (e.g. N:C and/or P:C) decrease to a minimum (e.g., Flynn *et al.*, 1993), giving the so-called “subsistence quotas” (Droop 1968; Flynn 2008a). Elemental ratios, particularly N:C (or C:N) and P:C (or C:P), have been widely used as an indicator for food quality in trophic studies and ecological simulations (Hessen *et al.*, 2002; Jones and Flynn, 2005; Mitra and Flynn, 2006). It would be useful to establish a relationship between fatty acid content and physiological parameters, to develop a predictive tool in fatty acid synthesis and production.

The present chapter aims to explore the relationship between the fatty acid content and the existing physiological parameters used in the phytoplankton growth modelling. The daily fatty acid profile and organismal stoichiometric parameters (C:N:P:Chla) are reported along with the growth of *Nannochloropsis oculata* in a batch culture mode. The potential use of these parameters to monitor and predict the growth is discussed.

4.2 Methods and Materials

This is the same experiment as described in Chapter 3 but here the emphasis is placed upon the detailed fatty acid composition of *Nannochloropsis oculata*. Detail on the experimental settings is given in Chapter 3.2. Data for growth condition,

nutrient concentration, and gross biochemical composition are reported in Chapter 3.3 Nutrient limitation related to change of cellular C:N:P ratios are also given in Chapter 3.3.3.

In addition to the data noted above, duplicate samples for fatty acid analysis were taken daily from when culture entered exponential growth phase. After phosphate was depleted, samples were taken twice a day at 9am and 3pm (lighting was provide continuously for 24hr; see Chapter 3.3.1 for culture condition). The amount of algal biomass (in terms of mgC L⁻¹) was estimated from the biovolume concentration of the culture (see Chapter 3.3.2), and used to ensure that at least 0.5g of C-biomass was collected by gravity filtration per filter disc (ashed 13mm diameter AE) for subsequent fatty acid analysis. These filters were stored at -20 °C.

Lipid was extracted from the filters using 2:1 (v:v) chloroform: methanol solution according to the method of Folch *et al.* (1957). Fatty acid methyl ester (FAME) was prepared and analysed according to the methods described in Chapter 2.1.5.6. Quantitative fatty acid contents were transformed into C-based form (see Chapter 2.3.2). Units of fatty acid content are expressed in terms of C contained in specific fatty acid group per cellular C. The contribution of fatty acid-C (FAC) to total cellular C is then explicitly described using the C-based form.

Fatty acid data indicated in the figures have been grouped according to the nutrient status of the organisms according to the threshold theory for nutrients co-limitation analysis in Chapter 3.3.3. The culture was initially limited by N, then by P during the co-limitation phase of most of the batch culture period. When the culture was switched to semi-continuous mode, N was the most limiting nutrient (see Chapter 3.3.3 for Figure 3.6D).

Since the cost and time in conducting fatty acid analysis and large scale PBR experiment, the study reported here has not been reproduced in full under identical conditions. The general growth dynamics have, however, been repeated and the

experiment reported shows similar dynamics.

4.3 Results

4.3.1 Changes in fatty acid content during growth

Growth-related changes of total fatty acid content are illustrated in Figure 4.1. A maximum C-specific growth rate of 0.57 d^{-1} was recorded for *N. oculata* at day 4 when the culture entered exponential growth. Cellular total fatty acids (TFA) significantly increased by about two folds in stationary phase where the growth is halted and nutrient depletion is recorded (see Chapter 3.3.3). Total fatty acid-C (TFAC) contributed around 6% of cell-C during exponential growth and up to 12% of cell-C in the nutrient-stressed semi-continuous phase (after day 10). A small fluctuation of total fatty acid between day 8 and 9 was observed, which may have resulted from the influence of light between the morning and afternoon samples although the light irradiance was fairly constant between days (see Chapter 3.3.1). A slight evaluation of cellular fatty acid content was recorded at the beginning of exponential growth when an elevated medium pH (pH =9) occurred (Chapter 3.3.1).

As shown in Figure 4.2A, SFA decreased when the growth enters exponential phase and increased up to 54% of TFA during the semi-continuous growth (which commenced at day 9). On the contrary, PUFA increased up to 12% of TFA when the culture was in exponential growth and then decreased to 8% at the end of semi-continuous growth. MUFA content slightly decreased from 40% of TFA along with the growth. The sum of total SFAs and MUFA contributed $\approx 90\%$ of TFA under the conditions applied in this study. However, a higher PUFA and lower SFA content are observed at day 3 when a high medium pH was recorded (Figure 3.1).

As shown in Figure 4.2B, Palmitic acid (C16:0) and palmitoleic acid (C16:1(n-7)) have similar response as total SFA and MUFA respectively. EPA (C20:5(n-3)) content increases from 2% to 7.5% of TFA during the exponential growth and decrease back

to 5% at the semicontinues phase. Palmitic acid (C16:0) (31%-45% of TFA) and palmitoleic acid (C16:1(n-7)) (25%-32% of TFA) are the predominant fatty acids. Myristic acid (C14:0) and oleic acid (C18:1(n-9)) contributed 5.5%-7.3% and 5-10% of TFA respectively (Table 4.1). A full detailed breakdown of fatty acid composition is given in Table 4.1.

4.3.2 Changes of fatty acid composition with N:C

The expression of fatty acid data in the following sections are normalised to C based form (see Chapter 2.3.2).

The contribution of total fatty acid-C to cell-C (TFA) increased as the N:C ratio decreased from 0.14 to 0.08 (Figure 4.3A). A proximate linear relationship can be drawn out between N:C and total fatty acid content. The relationship between the N:C ratio and the saturated fatty acid-C to cell-C (SFA) has a similar response as the TFA; though with a lower gradient, the pro rata changes are similar (i.e. doubles over the range of the decrease in N:C) Considerable variation in fatty acid content was observed at high N:C ratio (0.17), possibly associated with changes in the C-status (due to insufficient CO₂ supply) induced by fluctuations in pH that are associated with an elevated N:C ratio (see Chapter 3.3.3) (Figure 4.3).

The contribution of PUFA -C and EPA-C to cell-C attained maximum values of 0.012 and 0.008 respectively at N:C ratio around 0.1 (Figure 4.3B) where, interestingly, P is the most limiting nutrient control the growth (Figure 3.6). The PUFA and EPA content also varied by a factor of ca. 2-fold with slight variation of N:C ratio around the maximum value. PUFAs synthesis may be regulated by factors other than N status when N is not the most limiting nutrient. Despite the different nutrient limiting types, N:C ratio are well correlated with total fatty acid content (Figure 4.3).

4.3.2 Changes of fatty acid composition with P:C

The relationship between fatty acid content and P:C ratio is given in Figure 4.4. Although no obvious trends are obtained for total fatty acid or saturated fatty acid content versus P:C ratio (Figure 4.4.A), P:C ratio did relate linearly with total PUFA as well as EPA content (Figure 4.4.B); the data point influenced by high growth pH (high P:C ratio, see Chapter 3.3.3) appears an outlier. Interestingly, PUFA and EPA content increased almost 3-fold with the P:C ratio decrease between 0.03 to 0.01. It demonstrated that the PUFA content does not necessarily decrease concurrently with a decrease in P:C during batch growth of *Nannochloropsis oculata*. When P is the most limiting nutrient (Chapter 3.3.3, Figure 3.6), PUFA content increased. It shows that P may not be the dominant factor in control of PUFA synthesis in this organism. The result indicated here challenges the common believe that PUFA content is positively correlated with P:C ratio, which is based upon the importance of P as an essential component in PUFA-rich phospholipids.

4.3.2 Changes of fatty acid composition with Chl:C

The relationship between N:C and Chl:C is given in Figure 4.5A, N:C from P limiting cells varies between 0.12-0.14. Cells from P limiting growth have more Chl than when nitrate is limiting growth. Relationships between PUFA and EPA content with Chl:C are illustrated in Figure 4.5B. A proximate linear regression is shown between Chl:C and total PUFA content. EPA content has a similar relationship against Chl:C. Together this could be taken to indicates a significant light regulation on PUFA synthesis when pigmentation developed in the culture. Most of the data from P limiting growth have higher Chl:C ratio than the N limiting data and therefore more PUFAs content. Unfortunately, Chl:C data are not available during the semi-continuous growth where N is limiting the growth.

4.4 Discussion

Fatty acid composition varies significantly with different culture conditions and culture age (Sukenik *et al.*, 1993). Cells in batch culture are likely to have a dynamic fluctuation of culture conditions (e.g. light and nutrients). Palmitic acid (C16:0), palmitoleic acid (C16:1(n-7)) and EPA (C20:5(n-3)) are the predominant fatty acids in *Nannochloropsis oculata* (Table 4.1). Changes of these three major fatty acids, C16:0, C16:1(n-7) and C20:5(n-3), are closely related to changes of total SFA, MUFA and PUFA content. Increase of irradiance and nutrient limitation have been reported as an effective way to increase the content of C16:0 and C16:1 while decreasing the content of C20:5(n-3) (Sukenik *et al.*, 1989; Sukenik *et al.*, 1993). The major fatty acid profiles reported here are similar to those reported previously under the high light condition (PFD over $220 \mu\text{mol m}^{-2} \text{s}^{-1}$) with 12h:12h light dark cycle (Fabregas *et al.*, 2004) and under continuous light (Sukenik *et al.*, 1989) in the exponential phase (nutrient in excess). However, the percentage of SFAs is higher while PUFA and EPA of total fatty acid are lower in comparison with the fatty acid composition under the same illumination during exponential growth. This probably resulted from the additional nutrient limitation found in the present study. PUFA and EPA content are even lower in semi-continuous phase, where nutrient limitation developed (Figure 4.2) in comparison with the nutrient replete culture (Sukenik *et al.*, 1989, Fabregas *et al.*, 2004).

Since the medium used in this study was based upon $f/2$, with an initial nutrient N:P (mole) >24 , P is expected to develop as the limiting nutrient in the culture if one expects the algal N:P ratio to accord with the value of 16:1 (Redfield, 1958). However, the previous growth study suggested that the culture is co-limited by both nitrate and phosphate (see Chapter 3.3.3). According to the threshold theory, only one nutrient can be assumed to be limiting at a given instant (Droop, 1974). The most limiting nutrient limits the growth rate. However, this does not mean that the response to the limiting nutrient is not affected by the sufficiency of other nutrients.

The batch growth is dynamically regulated by N and P limitation, where nitrate limits the growth initially (before day 6) and follow by P is the most limiting nutrient (day 7-10) during the batch culture (see Chapter 3.3.3 for Figure 3.6D). When the culture was switched to semi-continuous mode, N became the more limiting nutrient controlling growth. Cellular P:C and N:C ratios both decreased from nutrient saturating point observed earlier in the culture. The fatty acid profile presented here is more representative of a condition under N and P co-limitation. P limitation may also be associated with a decline in N:C ratios (Flynn, 2008), while P limitation also leads to accumulation of lipids and/or carbohydrates but less lipid is obtained in comparison with N limitation (Chen *et al* 2011).

4.4.1 N stress in relation to fatty acid accumulation

A decrease of N:C (i.e., a decline in the N-status) results in an increase of fatty acid content irrespective the N or P limitation (Figure 4.3A). Fatty acid composition changed with nutrient limitation types as well as degrees of stress during the batch culture period. Nitrate grown cells are relatively more N-stressed than ammonium grown cells (Wood & Flynn, 1995) which has implications not only in experiments but for ecophysiology under irradiance in light:dark cycles (Clark *et al.* 2002; Flynn *et al.* 2002). Accordingly, one may expect more fatty acids to be accumulated in cells grown on nitrate than on ammonium (Flynn *et al.*, 1992). Under high light conditions, ammonium grown cells grow faster than nitrate grown cells which have a relatively lower N:C ratio (Wood and Flynn, 1995). In other words, the increase of light irradiance may further increase the level of N-stress in nitrate grown cultures. There is thus a likely high accumulation of fatty acids under higher light irradiance when using nitrate as the N-source (Thompson *et al.*, 1990; Fabregas *et al.*, 2004). Nitrate limiting cells potentially have more total fatty acid content but less PUFA content than P limiting cells when similar N:C ratios are observed around maximum 0.14 (Figure 4.2). From all of this it can be seen that it is important to discriminate the limiting nutrient controlling the growth since the effects of nutrient and irradiance

upon fatty acid content may vary according to the prevailing conditions.

A similar C:N ratio (approximately 7 by mass) in exponential growth for *N. oculata* was obtained as the findings of Fabregas (Fabregas *et al.*, 1994) under high light culture (PFD=220 $\mu\text{mol m}^{-2} \text{s}^{-1}$). In the work described here, the N:C ratio varies from 0.14 to 0.08 by mass (i.e. C:N from 7 to 12) (Figure 4.2). The increased C:N ratio is mainly induced by the accumulation of excess-C, which could be in forms of lipid and/or carbohydrate. Lynn (Lynn *et al.*, 2000) found a close negative relationship between C:N and protein: carbohydrate ratios. Excess-C has partly been incorporated into fatty acids although most of the excess-C is partitioned into carbohydrates (see Chapter 3.3.4). The correlation between N:C ratio and total fatty acid-C per cell-C (TFA) can potentially be used for estimation of total fatty acid content (Figure 4.2). Similarly, the relationship between N:C and saturated fatty acid (SFA) may be useful. However, the correlation between N:C to SFA and N:C to TFA are expected to be species specific. SFA does not significantly vary for some species while MUFA is the main group that significantly changed when nutrient has been depleted (Lin and Lin, 2011). For some fresh water species, TFA remains constant while N:C ratio (molar) decreases from 5 to 20 (Park *et al.*, 2002). The accumulation of lipid also has not been found in N starvation of some fresh water species, which may only accumulated carbohydrates as storage (Rodolfi *et al.*, 2009).

4.4.2 PUFA accumulation under P limiting growth

It is important to determine the regulation of PUFA synthesis in relation to P limitation. The essential fatty acids, such as EPA and DHA, are proposed to be important factors affecting the growth of grazers in aquatic food web (Brett and Muller-Navarra, 1997; Muller-Navarra *et al.*, 2000). In fresh water species, the cellular P content (P:C ratio) is believed to be an indicator related to food quality to grazers (Hessen *et al.*, 2002). PUFA content and P content might be positively correlated to affect the quality of food to grazers, since P is the major composition of

phospholipids which is rich in PUFAs. Phospholipids, which are abundance in cell membranes, closely change with the nutrient status (Guschina and Harwood, 2006).

The results here show that a depressed P:C ratio does not necessarily result in a lower PUFA content in *Nannochloropsis oculata* (Figure 4.3B), although the P:C ratio shows here does decline as far as it may. For some fresh water microalgae, serious P limitation (P:C around 0.00325) has been shown to increase the saturated fatty acid and decrease the Omega-3 fatty acids in *Chlamydomonas reinhardtii* and result in a decreased growth rate of its predators (Weers and Gulati, 1997). However, For some fresh water species, PUFA and omega-3 fatty acid (expressed as $\text{gC}(\text{gC})^{-1}$) are not significantly affected by changes in P:C over 10-fold (Park *et al.*, 2002). P limitation decreases the PUFA content and increases the saturation level of fatty acids in many marine microalgae (Reitan *et al.*, 1994). However, a relatively higher PUFA content are reported in a P limitation culture than N limitation culture in the cryptophyte *Rhodomonas salina* in feeding experiment for zooplankton (Malzahn *et al.*, 2007). Distinctive effects of P limitation may subject to the different species or other factors such as light limitation at the end of batch growth.

Photoacclimation from self-shading affects PUFA content in mass culture under P limiting growth. The negative relationship between P:C ratio and PUFA as well as EPA content found in this study (Figure 4.4) would possibly result from the decrease of internal irradiance via self-shading from pigmentation. As shown in Figure 4.4, P limited cells have higher Chl:C ratio than the N limiting cells during the batch culture. When the culture is growing to certain density, high Chl concentration decreases the availability of light inside the culture. Cells acclimated to relatively low light promote the synthesis of Chl_a pigment (Richardson *et al.*, 1983; Geider, 1998). The optimal condition for high EPA culture of *Nannochloropsis sp.* has been suggested as low light with excess nutrients (Sukenic *et al.*, 1989).

The synthesis of photosynthetic reaction centres may result in an increase of the cellular EPA content under low light conditions. EPA contributes around 50% of fatty

acid content in monogalactosyldiacylglycerol (MGDG) which is the most abundant polar lipid group in *Nannochloropsis oculata* (Schneider and Roessler, 1994; Thompson, 1996). This P-free galactolipid lipid (MGDG) is associated with the D1 protein in the photosynthesis reaction centre (Mizusawa and Wada, 2012). Lacking the ability to readily synthesis EPA may thus result in a difficulty to assembly photosynthetic components (Schneider *et al.*, 1995). It is likely that the increase of EPA observed comes from the synthesis of photosynthesis reaction centres by photoacclimate to relatively low light condition if N is not limiting the synthesis of light harvesting component. P limitation may not have direct effects on depression of Chl component synthesis since Chl growth can be maintain when P is limiting the growth (Chapter 3.4.2). N limitation is expected to decrease the PUFA content in *Nannochloropsis oculata* by degrading the Chl content and D1 protein associated with MGDG in the photosynthesis reaction centre (Falkowski *et al.*, 1989). The relationship between Chl:C and PUFA has not been shown under serious N limitation (extreme low N:C ratio), although the EPA and PUFA content start to decrease when N:C below 0.1 (Figure 4.2B).

4.5 Conclusion

The present study shows a day to day change of fatty acid profile of *Nannochloropsis oculata* when grown in a large-scale tubular photobioreactor under batch growth conditions. The fatty acid composition changed significantly in relation to changes in light and nutrients (N &/or P limiting). It is important to discriminate the effects between N and P limitation (and likely also light limitation) during growth. The decrease of N:C and P:C to some extent (nutrient stress) may not necessarily indicate a low PUFA content and further be implicated in a deterioration in food quality. Photoacclimation processes also play an important role in regulation of PUFA as well as EPA synthesis in *Nannochloropsis oculata*. However, N:C ratios may be better and more reliable indicators for total fatty acid content, and potentially PUFA content under N-stress condition (Figure 4.2). A fine tuning of N:C ratios is expected to

optimize the total fatty acid content. Chl:C could potentially be used as an indicator for EPA and PUFA content in *Nannochloropsis oculata*. However, as the correlation between elemental stoichiometry and fatty acid composition indicates, single elemental ratios alone may not be an effective indicator of cellular fatty acid contents and hence food quality. C partitioning into different biochemical groups (Anderson *et al.*, 2004) may well be desirable (if not essential) in culture systems where natural illumination likely results in unpredictable changes in overall physiological responses.

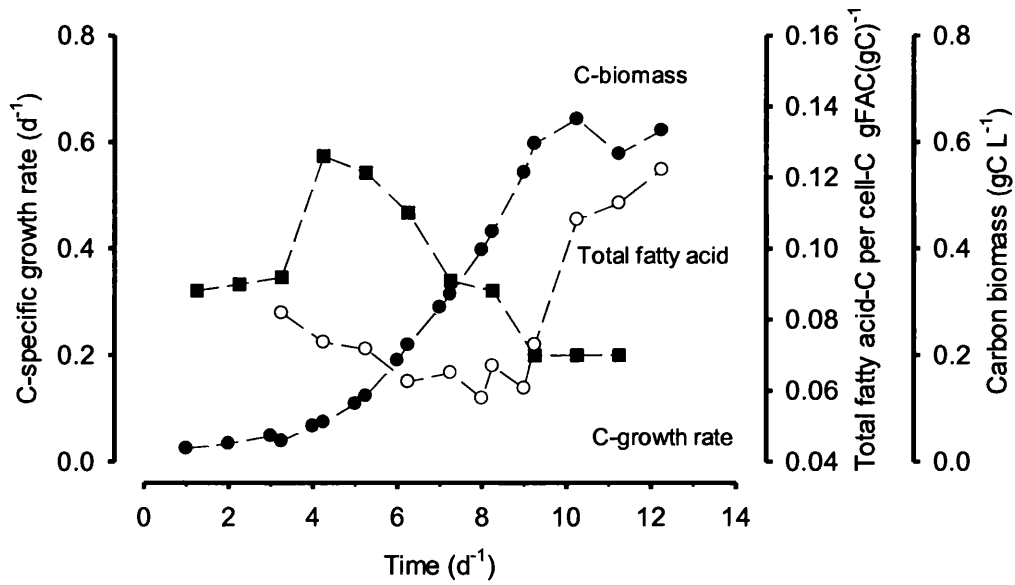


Figure 4.1 Changes of C growth and total fatty acid content. (■) C-specific growth rate; (●) carbon biomass; (○) total cellular fatty acid content.

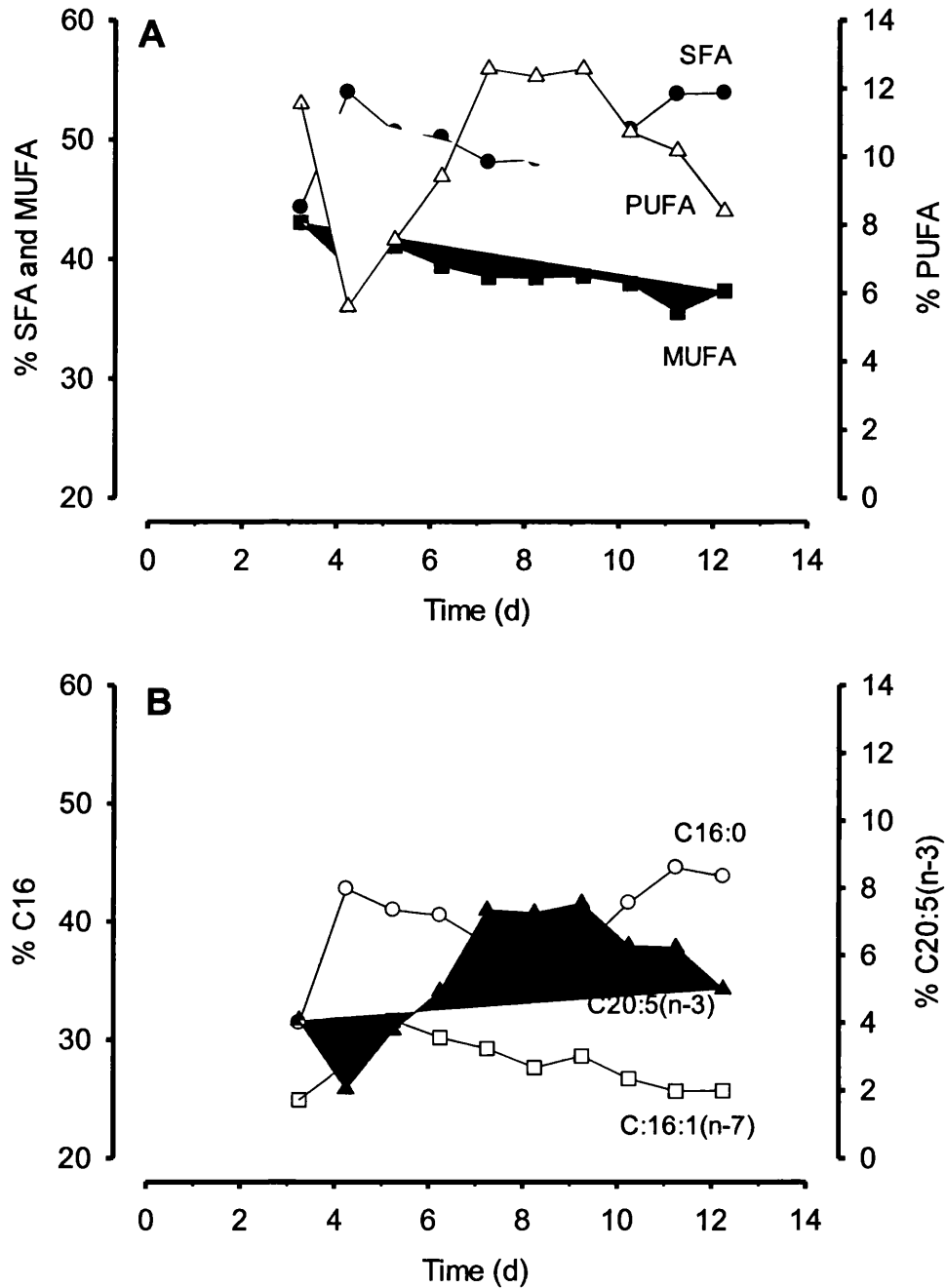


Figure 4.2 Change of the fatty acids composition along the growth. This is shown as % of fatty acid C relative to total fatty acid C by weight. Semi-continuous growth commenced at day 9. A: (●) SFA, (■) MUFA, (△) PUFA; B:(○) palmitic acid C16:0, (□) palmitoleic acid C16:1(n-7), (▲) EPA C20:5(n-3).

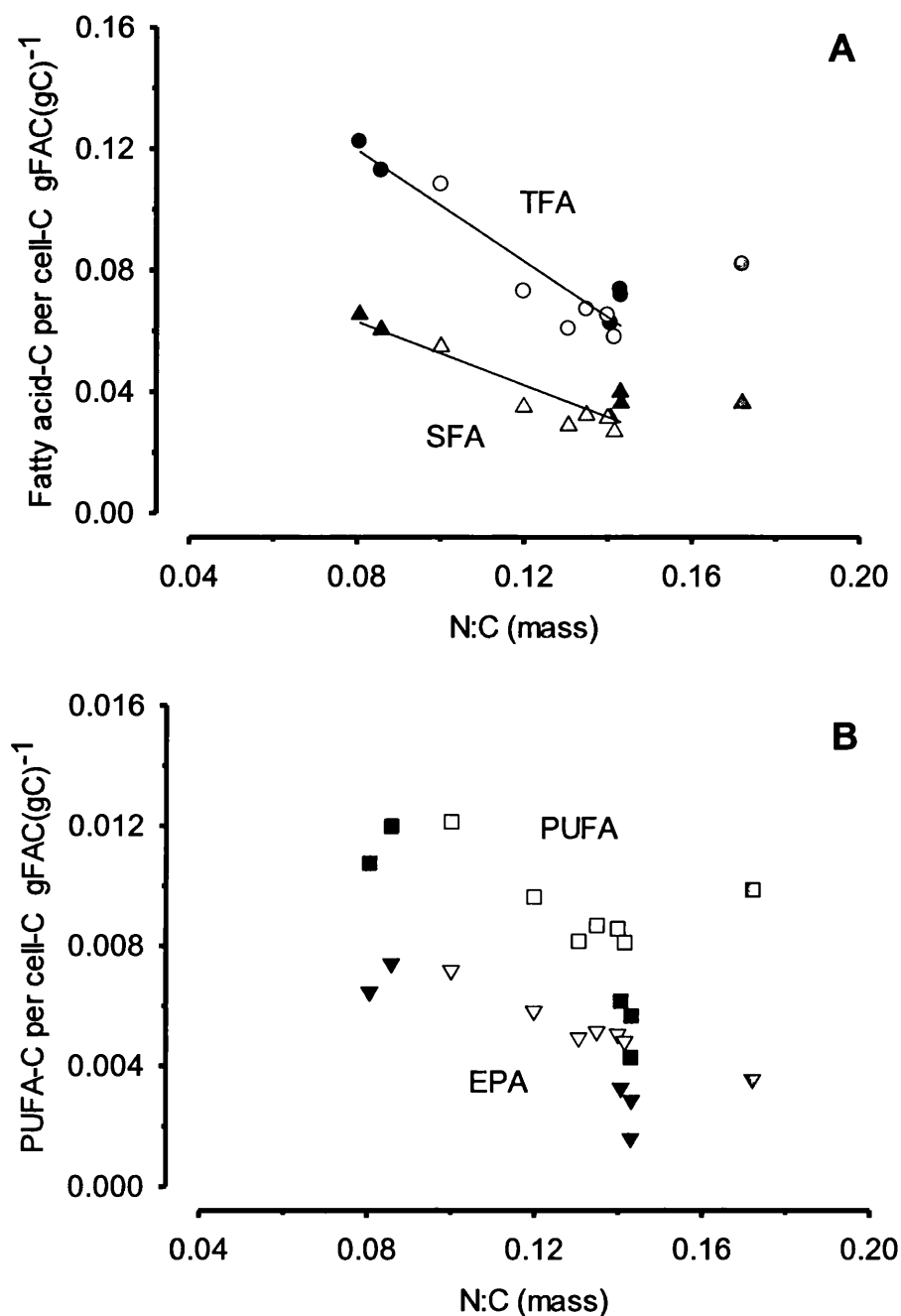


Figure 4.3 Variations of specific fatty acid content with N:C ratios; A: Total fatty acid (TFA) (circle), Saturated fatty acid (SFA) (up triangle). Linear regression fitting $r^2=0.889$; $n=11$ and $r^2=0.847$; $n=11$ for TFA and SFA respectively. B: Polyunsaturated fatty acid (PUFA) (square), eicosapentaenoic acid (EPA) (down triangle). Closed symbols: N-limiting growth; Open symbols: P-limiting growth; Gray symbol: C-limiting growth.

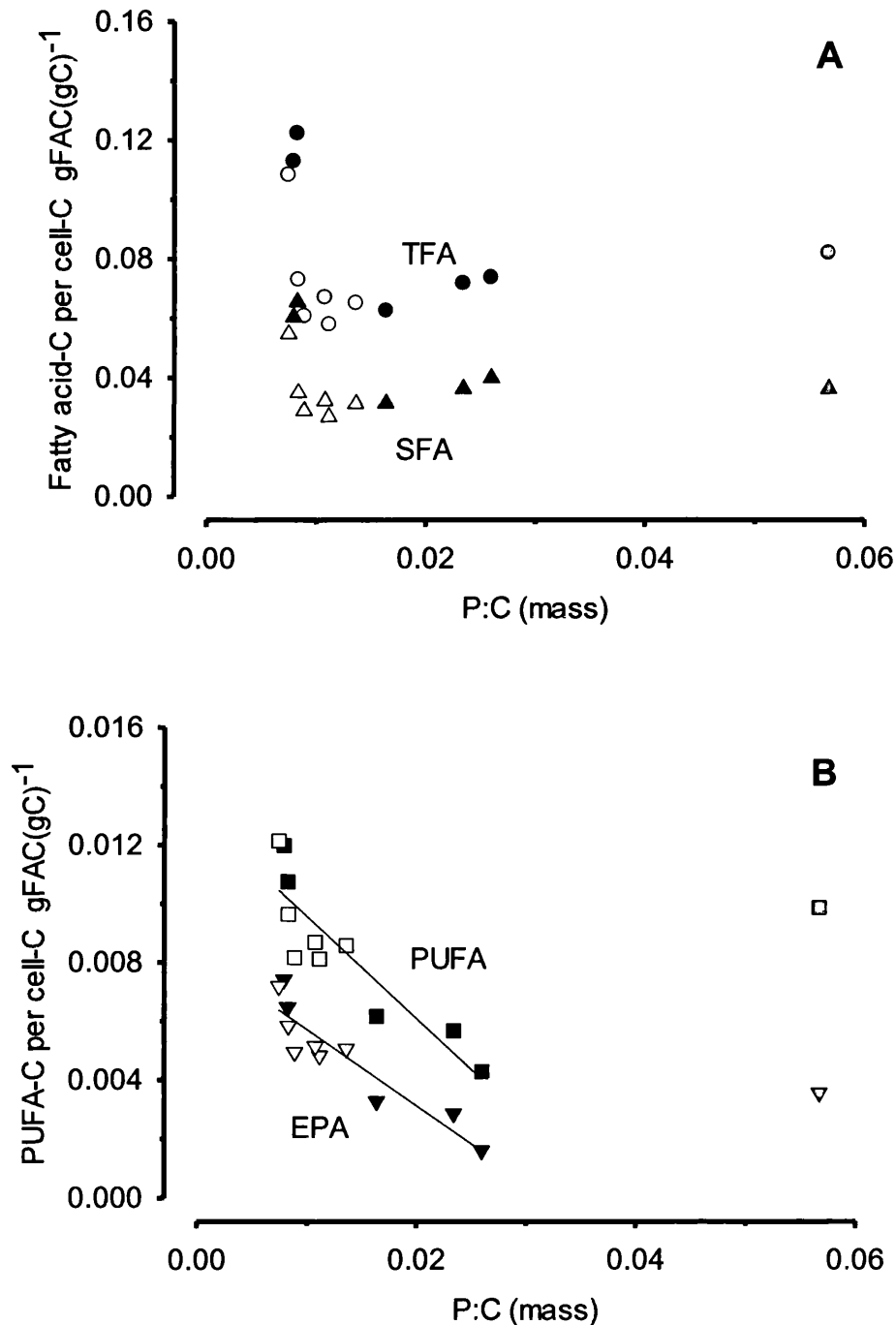


Figure 4.4 Variations of specific fatty acid content with P:C ratios; A: Total fatty acid (TFA) (circle), Saturated fatty acid (SFA) (up triangle); B: Polyunsaturated fatty acid (PUFA) (square), eicosapentaenoic acid (EPA) (down triangle). Linear regression fitting $r^2=0.792$; $n=11$ and $r^2=0.851$; $n=11$ for PUFA and EPA respectively. Close symbols: N-limiting growth; Open symbols: P-limiting growth; Gray symbol: C-limiting growth.

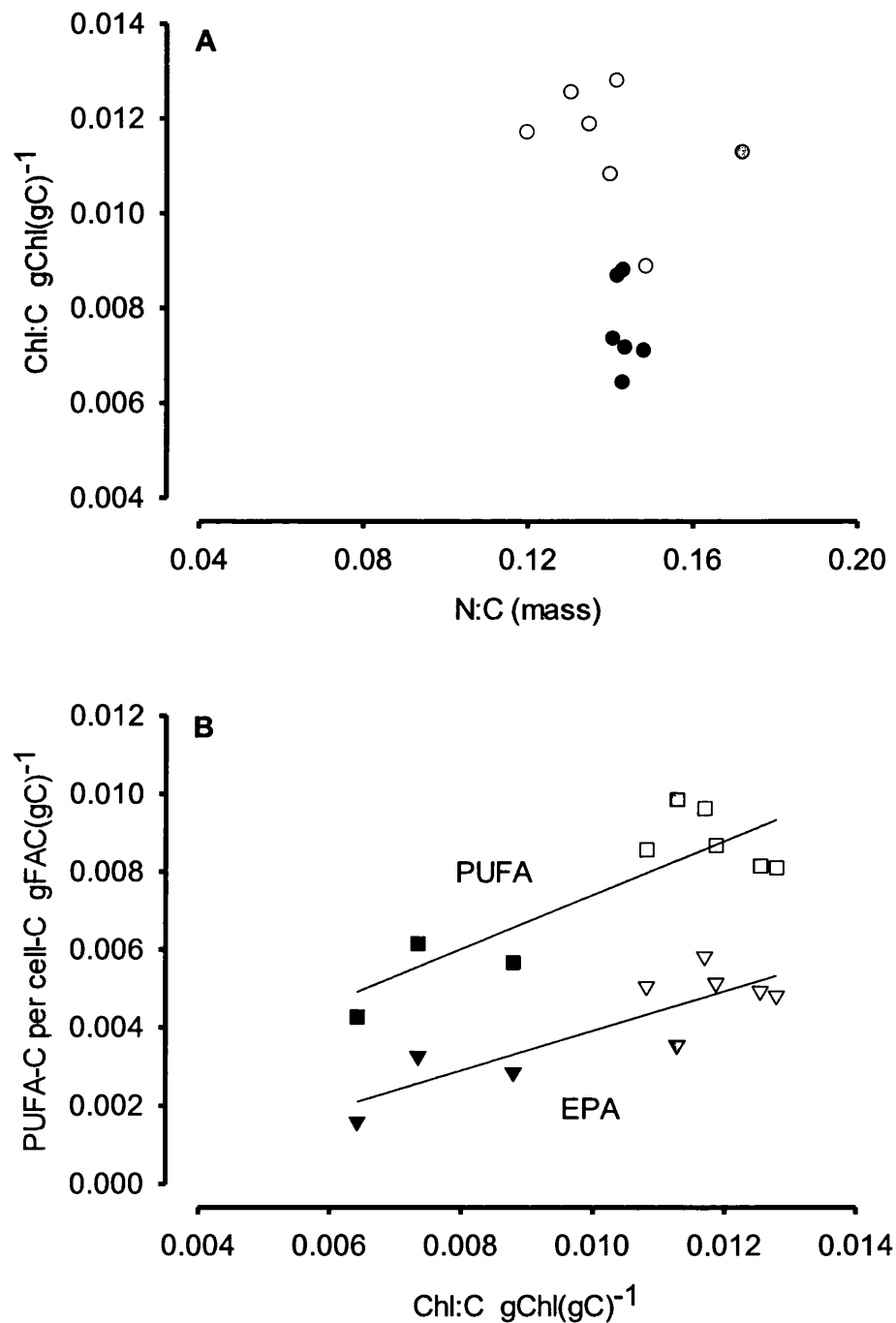


Figure 4.5 Variations of N:C and specific fatty acid content with Chl:C ratios during the batch growth; A. Relationship between N:C and Chl:C; B: Relationship between Chl:C and PUFA, Polyunsaturated fatty acid (PUFA) (square), eicosapentaenoic acid (EPA) (down triangle). Linear regression fitting $r^2=0.72$; $n=9$ and $r^2=0.733$; $n=9$ for PUFA and EPA respectively. Close symbols: N-limiting growth; Open symbols: P-limiting growth; Gray symbol: C-limiting growth.

Fatty acid composition 4.19

Table 7.1: Fatty acid composition of *Nannochloropsis oculata* (w/w % of total fatty acid) during the batch culture (<=day 9) and semi-continues culture (>day 9). Fatty acid value represents the mean of duplicates with SD in bracket. Note: tr represents the fatty acid content <1%.

Fatty acids	Day of culture									
	3	4	5	6	7	8	9	10	11	12
14:0	6.63 (0.03)	5.53 (0.21)	5.75 (0.22)	6.47 (0.18)	6.87 (0.07)	7.30 (0.15)	7.26 (0.35)	6.18 (0.27)	6.63(0.04)	6.96 (0.19)
16:0	31.42 (0.02)	42.78 (0.98)	40.99 (0.27)	40.54 (0.06)	38.10 (0.23)	37.49 (0.06)	37.80 (0.20)	41.60 (0.13)	44.58 (0.59)	43.84 (0.32)
18:0	3.61 (0.00)	3.07 (0.34)	1.94 (0.08)	1.29 (0.10)	1.46 (0.06)	1.63 (0.18)	1.49 (0.11)	1.65 (0.04)	1.06 (0.03)	1.18 (0.06)
16:1n-9	1.34 (0.16)	2.32 (0.08)	2.59 (0.06)	3.15 (0.10)	2.70 (0.06)	2.78 (0.03)	2.64 (0.00)	1.94 (0.00)	1.53 (0.01)	1.40 (0.08)
16:1n-7	24.92 (0.31)	27.92 (2.68)	31.64 (0.17)	30.18 (0.31)	29.26 (0.34)	27.64 (1.84)	28.62 (0.75)	26.70 (0.04)	25.66 (0.13)	25.69 (0.24)
18:1n-9	10.28 (0.23)	5.79 (1.12)	5.08 (0.11)	4.92 (0.22)	5.40 (0.14)	6.00 (0.53)	6.09 (0.19)	8.12 (0.04)	7.40 (0.01)	9.11 (0.09)
18:1n-7	1.80 (0.10)	1.14 (0.12)	tr	tr	tr	tr	tr	tr	tr	tr
20:1n-9	1.29 (0.16)	tr	tr	tr	tr	tr	tr	tr	tr	tr
22:1n-11	1.59(0.27)	tr	tr	tr	tr	tr	tr	tr	tr	tr
24:1n-9	1.61 (0.55)	1.11 (0.02)	tr	tr	tr	tr	tr	tr	tr	tr
18:2n-6	4.10 (0.87)	1.82 (0.26)	2.02 (0.05)	2.46 (0.02)	2.78 (0.03)	2.41 (0.04)	2.23 (0.04)	1.99 (0.01)	1.72 (0.03)	1.69 (0.06)
20:4n-6	tr	tr	tr	1.23 (0.05)	1.74 (0.01)	1.77 (0.09)	1.96 (0.08)	1.62 (0.04)	1.51 (0.11)	1.17 (0.10)
20:5n-3	4.07 (0.17)	2.04 (0.07)	3.77 (0.04)	4.93 (0.15)	7.35 (0.03)	7.26 (0.41)	7.54 (0.43)	6.29 (0.08)	6.24 (0.48)	5.00 (0.52)
22:6n-3	1.28(0.06)	tr	tr	tr	tr	tr	tr	tr	tr	tr
ΣSFA	44.31 (0.11)	53.96 (0.10)	50.64 (0.05)	50.18 (0.17)	48.11 (0.20)	48.33 (0.21)	48.03 (0.73)	50.85 (0.23)	53.82 (0.69)	53.90 (0.39)
ΣMUFA	43.06 (0.42)	39.39 (0.91)	41.07 (0.10)	39.44 (0.02)	38.48 (0.03)	38.46 (0.73)	38.57 (0.30)	37.93 (0.10)	35.56 (0.09)	37.34 (0.20)
ΣPUFA	11.55 (0.48)	5.60 (0.38)	7.56 (0.05)	9.42 (0.19)	12.57 (0.15)	12.35 (0.51)	12.57 (0.43)	10.72 (0.13)	10.17 (0.59)	8.40 (0.59)

5. Development and exploration of a mechanistic model of microalgal growth in bioreactors for biofuel production

5.1 Introduction

Microalgae are unicellular organisms using light energy to convert CO₂ into biomass and various valuable chemicals, although some species can be grown heterotrophically using organic carbon or mixotrophically using both inorganic and organic carbon (Chen *et al.*, 2011). Many microalgal species have been used as the feedstock for aquaculture feedings for many decades (Brown *et al.*, 1997). Growing microalgae for their valuable compounds (e.g. polyunsaturated fatty acids; DHA and EPA) for human consumption were also proposed for commercial exploitation (Borowitzka, 1995). More recently, the great potential of using microalgae as feedstocks for biodiesel and bioethanol production have attracted global attentions (Chisti, 2007; Markou *et al.*, 2012). The advantages of using microalgae for biofuel production are not only sustained in the potentially high proportion of biochemical compounds for fuel production but also minimized the ecological cost by not competing with agriculture land, potentially combining CO₂ mitigation and waste water treatment (Williams, 2007; McGinn *et al.*, 2011). Mass cultivation of microalgae became a fundamental issue which may limit the potential of the exploitation of microalgae.

Model simulations have been developed from various aspects in evaluation and prediction of commercial culture of microalgae for different types of reactor units. The potential of computer based mathematical models to explore the options for optimization of biomass production in PBR has been shown to be of values (Yu *et al.*, 2009). Existing mathematical models often focus on the impact of light utilization on biomass production with no consideration of nutrient availability or assuming

nutrients are not a limiting factor (Murphy and Berberoglu, 2011; Slegers *et al.*, 2011). In reality, nutrient inputs as dilution rate (controlling growth rate) is a key factor affecting both quantity and quality of the biomass as feedstock for chemical production. Employing mechanistic model of algal physiology may provide a better understanding of the physiological changes of cell growth in PBRs of various designs (Greenwell *et al.*, 2010; Flynn *et al.*, 2010).

The development of phytoplankton growth model has a long history since the Monod model firstly was employed for describing the growth of microorganisms (see Chapter 1). The quota type model (Droop, 1968) was developed when the Monod model was found to be inadequate in describing the relationship of growth rate and nutrient concentration. Thereafter, several models based on Droop's quota model were developed to describe the relationship between growth rate and cell quota under steady-state growth condition (Caperon and Meyer's, 1972; Burmaster, 1979). Unlike these classic quota models, Flynn (2001) presented a mechanistic model of algal physiology (MAP) with a normalized quota type function to describe the multiple nutrient uptakes in a dynamic growth condition. Coupled with a chlorophyll (Chl) synthesis term, the MAP is able to describe the change of photosynthesis rate calculated from the Poisson equation of the P-I curve (Jassby and Platt, 1976) in response to different light regime via photoacclimated regulation of Chl synthesis (Flynn, 2001; Flynn *et al.*, 2001). The MAP is structured with a set of differential equations describing the change of cellular organic materials (such as C:N:P:Si:Fe:Chl) with variant external nutrient and light availability (Flynn 2003). This model has been incorporated into an oceanographic model to explore the implications of nutrient limitation in oceanographic scenarios (Fasham *et al.*, 2006).

Here, the MAP is simplified to describe cellular C:N:P:Chl dynamics according to the suggestions by Flynn (2003) and extended to PBR descriptions, defined as total volumes and optical depth, with depth integrated photosynthesis calculation and biofuel descriptions defined as biochemical ends (excess-C) calculated from cellular

C:N ratio. The PBR model constructed from the MAP was simulated into series of scenarios that mimic the condition from species selection to microalgal cultivation. The implication from the interactions of physiological characteristic of selected species, nutrient inputs and PBR design and operation are discussed. Modeling technique as a potential aid in optimization of biofuel production for commercial gains is also discussed.

5.2 Model and scenarios description

Model structure and modelling platform is given in Chapter 2. List of state variables, auxiliary and constants used in the model are given in Appendix A. Detail equations are provided in ASCII form in Appendix B. Model structure descriptions are explained in the followings.

5.2.1 Model descriptions

5.2.1.1 Nutrients assimilation

External nutrient X_a (X refers to nitrogen (N) or phosphorus (P) source, a refer to the amount of nutrient source, with unit gram X) are consumed by algal cells (Eq. 1&2). The nutrient uptake function is a mass balance function that N uptake from medium is assimilated into cellular material. The external nutrient concentration (X) can be calculated from nutrient amount (X_a) and bioreactor volume ($React_V$) is driven the transport of external nutrients (Eq. 3 & Eq. 5). Cellular X:C (i.e. nutrient X to C quota) is determined by algal nutrient ($algX$) and $algC$ amounts (Eq. 4). Cellular X:C vary typically between X_{Co} (minimum nutrient quota) and X_{Cm} (maximum nutrient quota). The uptake of X:C (X_{Cup} , with unit $gX(gC)^{-1}$) is determined by two steps of nutrient uptake which are controlled by external nutrient transport and internal nutrient status defined by X:C (Eq. 5).

Nutrient transport is described as a hyperbolic function of external nutrient

concentration and half saturation constant XK_u (Eq. 5) and controlled by the internal nutrient status (XC_u), which is developed from the quota type growth equation (Eq. 6) (Flynn, 2001). The normalized the XC_u changing between 0 and 1 is used to describe the nutrient condition for the current XC ratio. If XC reaches XC_m , XC_u is given a value of 1; otherwise XC_u is computed using Eq. 6. The NPC_u is an interaction term describing N and P limiting growth (Eq. 7). According to Droop's threshold theory, only one nutrient can be limiting at a given of time and therefore the most limiting nutrient results in controlling the growth rate (Droop, 1974). The logical statement of NPC_u varied between 0 and 1 indicates when two nutrients are limiting and the most limiting nutrient quota takes effect. If the nutrient (either N or P) is not the most limiting nutrient, maximum uptake rate is $U_m \cdot XC_m$, otherwise NPC_u will restrict the maximum uptake rate. The NPC_u controls the nutrient uptake by activating the threshold cell quota control function (Eq. 5). Feedback control (Eq. 5) written as a sigmoid function is applied to restrict the X:C quota since there seems to be a absolute maximum physiological value for X:C quota (Flynn, 2003). With the sigmoid function, XC will not exceed the absolute maximum (XC_{abs}) even the external nutrient concentration is replete.

$$\frac{d}{dt}Xa = -algC \cdot XCup \quad (1)$$

$$\frac{d}{dt}algX = algC \cdot XCup \quad (2)$$

$$X = \frac{Xa}{React_V} \quad (3)$$

$$XC = \frac{algX}{algC} \quad (4)$$

$$\begin{aligned}
 XCu_p = & \underbrace{Um \cdot Xcm \cdot \left\{ \underbrace{(XCu > NPCu) \cdot NPCu + (NPCu = XCu)}_{\text{cell quota control}} \right\}}_{\text{maximum transport rate}} \cdot \underbrace{\frac{X}{X + XKu}}_{\text{nutrient uptake}} \\
 & \cdot \frac{\left(1 - \frac{XC}{XCabs}\right)^{Qh}}{\underbrace{\left(1 - \frac{XC}{XCabs}\right)^{Qh} + Kxi}_{\text{feedback control}}}
 \end{aligned}
 \tag{5}$$

$$XCu = (XC < Xcm) \cdot \frac{(1 + KQX) \cdot (XC - XC_0)}{[(XC - XC_0) + KQX \cdot (Xcm - XC_0)]} + (XC \geq Xcm)
 \tag{6}$$

$$NPCu = MIN(NCu, PCu)
 \tag{7}$$

5.2.1.2 Chlorophyll a synthesis

Regulation of the Chl:C ratio can be written as a function of nutrients and relative photosynthesis (PS) rate (Eq. 8). The maximum Chl:C synthesis rate is indexed to Um and $ChlCm$. Constant M acts as a function of acceleration to control the rate of chlorophyll (Chl) synthesis during photoacclimation (Anning *et al.*, 1998). The function of the PS ratio controls the requirement of ChlC to reach the maximum PS rate with a feedback control to restrict the ChlC within the maximum ChlC ratio ($ChlCm$). ChlC is diluted by algal growth. The breakdown term is a function of N availability and degrades the ChlC synthesis when N status is poor since there is no N for protein synthesis for photosynthetic units. Therefore, Chl will be broken down to maintain the basic growth. Chlorophyll concentration is calculated as Chl:C ratio times carbon concentration (C).

$$\frac{d}{dt} ChlC = Um \cdot ChlCm \cdot M \cdot NPCu \cdot \left(1 - \frac{PS}{Pqm}\right) \cdot \frac{\left(1 - \frac{ChlC}{ChlCm}\right)}{\left(1 - \frac{ChlC}{ChlCm}\right) + 0.005} - \underbrace{ChlC \cdot Cu}_{Chlremove} - \underbrace{ChlC \cdot (1 - NCu) \cdot Um}_{breakdown} \quad (8)$$

$$Chl = ChlC \cdot C \quad (9)$$

5.2.1.3 Determined carbon specific growth

Carbon assimilation rate (Cu) is calculated as the difference between photosynthesis rate (PS) and respiration rate (res) (Eq. 10). As the only N source is assumed to be nitrate, the respiration rate (res) is included the cost of nitrate reduction (redco) and metabolic cost to assimilate nitrogen. The value of C-specific cost of nitrate reduction (redco) is measured as 1.71 gC(gN)⁻¹ (Flynn *et al.*, 1997). The metabolic cost to assimilate nitrogen is estimated as 1.5 gC(gN)⁻¹ (Flynn and Hipkin, 1999). The nitrate specific respiration rate can be calculated as Eq. 11 where basal respiration (basres) is assumed to be a rate of 5% of Um subjected to the NC status (Eq. 12). A normalized function of NC status has been employed to make the cell cease respiration when there is no C to consume. When NC approaches NCabs, the value of basres is down-regulated to zero. A mathematical trap is placed to prevent respiration below a value of zero. The growth of cell carbon therefore can be computed as Eq. 13

$$Cu = PS - res \quad (10)$$

$$res = \underbrace{\text{redco} \cdot Nup}_{\text{nitrate reduction cost}} + \underbrace{Nup \cdot 1.5}_{\text{nitrogen respiratory cost}} + basres \quad (11)$$

$$basres = Um \cdot 0.05 \cdot 1.01 \cdot \frac{\frac{NCabs - NC}{NCabs - NCo}}{[(NCabs - NCo) + 0.01]} \cdot \underbrace{(NC < NCabs)}_{\text{trap}} \quad (12)$$

$$\frac{d}{dt} \lg C = \lg C \cdot Cu \quad (13)$$

5.2.1.4 Determined depth integrated photosynthesis rate

Photosynthesis (PS) is a process using light energy to convert CO₂ into organic carbon. Light distribution in a deep water column is decreased with increase in depth. Therefore, the PS is decreases as the light path increase. Calculation of PS for cell growth in a water column with certain depth is needed to consider the light penetration. According to the Beer's Law, light penetration inside a liquid medium can be stated as:

$$I_z = I_0 \cdot e^{-Kz} \quad (14)$$

Where, z is the depth penetrating by light. I_z is the irradiance at the depth of z . I_0 is the surface irradiance. K is the attenuation coefficient of the medium. For microalgal cultivation, the attenuation effects of light can be counted mainly from the attenuation of water used for cultivation and the pigments of microalgae within the culture. Here we assume most of the light is absorbed by the chlorophyll a which is the most abundance pigment in microalgae. Hence, attenuation coefficient can be described as:

$$K = K_w + K_p \cdot C_{chl} \quad (15)$$

Where, K_w is the attenuation coefficient of certain water type. K_w increase with the increase of the turbidity of water (Sverdrup, 1945). Here, we take $K_w=0.0323 \text{ m}^{-1}$ as the value for pure seawater used for cultivation. K_p is the attenuation coefficient due to the chlorophyll in microalgae. C_{chl} is the concentration of Chlorophyll in culture. Therefore, substituting Eq 15 into Eq 14, the average light attenuated over mixing

depth z can be given as:

$$I_z = \frac{I_0}{z} \int_z^0 e^{-z(K_w + K_p \cdot C_{chl})} \quad (16)$$

To calculate the depth integrated rate of photosynthesis, the Smith equation (Smith, 1936) empirically describing the P-I curve is the only suitable form that can be integrated analytically (Jassby and Platt, 1976). Therefore, the photosynthetic rate at the given mixing depth (z) and time (t) can be calculated as Eq.17 and depth integrated average photosynthesis rate (PS_a) can be calculated as Eq. 18. Here, the calculation assumes the algal biomass in the system is homogenous (i.e. fully mixed) across the mixing depth. The carbon fixation assumes CO_2 in the system is not a limiting factor.

$$PS(z, t) = \frac{P_{qm} \cdot \alpha \cdot ChlC \cdot I_z(z, t)}{\sqrt{P_{qm}^2 + (\alpha \cdot ChlC \cdot I_z(z, t))^2}} \quad (17)$$

$$PS_a(t) = \frac{1}{Z} \int_z^0 PS(z, t) dz \quad (18)$$

$$P_{qm} = [U_m + basres + NC_m \cdot U_m \cdot (redco + 1.5)] \cdot NPCu \quad (19)$$

Where, α , with the unit ($gCgChl^{-1} d^{-1} (\mu mol \text{ photons } m^{-2})^{-1}$), is the initial slope of the P-I curve. $I_z(z, t)$ having a unit ($\mu mol \text{ photons } m^{-2}$) is the irradiance at depth z at time t . P_{qm} is the maximum photosynthetic rate. Here we define the P_{qm} as Eq. 19, where the maximum growth rate U_m can be achieved under the growth on nitrate (Flynn and Flynn, 1998). With the function of $NPCu$ in Eq.19, P_{qm} is a function of nutrient status. P_{qm} decrease proportionally with nutrient status decrease. Detailed

mathematical deduction of Eq. 18 is given in Appendix C.

To substitute the PS in Eq. 10 with the depth integrated average PS_a in Eq. 18, the averaged C-specific growth rate over the mixing depth z at the time t is given in Eq.20, where the respiration function is given in Eq. 11.

$$Cu(t) = PS_a(t) - res(t) \quad (20)$$

5.2.1.5. Determined the “biochemical composition”

Cell-C can be divided into two major groups subject to the association with nitrogen, nitrogenous-C and non-nitrogenous-C. Nitrogenous-C is mainly associated with protein and nucleic acids. Non-nitrogenous-C is the sum of total lipid and carbohydrates. Since the C and N content in protein and nucleic acids are similar, a N dependent core material comprised protein and nucleic acids having a constant C:N ratio can be assumed here. This ratio can be termed as CN_{core} . Calculation of C and N content in this core under nutrient replete and nutrient deplete respectively reveals that the CN ratio of CN_{core} is relatively constant with a value of 3.20 gC(gN)^{-1} (calculated from Geider and La Roche, 2002). Therefore, non-nitrogenous-C (C_{nonN}) is given as Eq.21:

$$C_{nonN} = \frac{CN_{cell} - CN_{core}}{CN_{cell}} \quad (21)$$

Where, CN_{cell} is the cellular C:N ratio. CN_{core} is the constant value ($CN_{core}=3.20 \text{ gC(gN)}^{-1}$) for the nitrogenous core material.

Non-nitrogenous-C contains structural components (e.g. membrane-C and cell wall-C) and excess-C as energy reserved. Although the non-nitrogenous-C (total lipid and carbohydrate) can be used as feedstock for biofuel production, the quality of fuel is influenced by the structure material which varies with nutrient status. Membrane-C

is associated with long chain unsaturated fatty acid which is expected to decrease the fuel stability (Hu et al., 2008).

To deprive the excess-C, we assume there is a minimum CN ratio (CN_{min} , i.e. NCabs) where no excess-C is accumulated. This CN_{min} can be obtained under light limited ammonium grown culture. Moreover, this CN_{min} is expected to be taxon-dependant. For example, diatoms have Si-based cell walls, coccolithophores have $CaCO_3$ -based cell wall, while *Dunaliella* sp. is lack of cell wall. Therefore, excess-C (C_{ex}) can be calculated as Eq. 22 and the structure components (C_{struc}) can be deprived as the difference between C_{nonN} and C_{ex} (Eq.23).

$$C_{ex} = \frac{CN_{cell} - CN_{min}}{CN_{cell}} \quad (22)$$

$$C_{struc} = C_{nonN} - C_{ex} \quad (23)$$

5.2.1.6 Determined steady-state condition

Steady-state is a special growth condition where the rates of change are constant (Chapter 2.2.2). Operating the PBR steady-state growth can be realized by continuous inflow of fresh medium with outflow of cultures (where the volume of inflow=outflow). In the PBR model set here, dilution rate (D) is determined by the inflow volume of medium (Inflow) and the total volume of PBR (React_V) (Eq.24).

$$D = \frac{Inflow}{React_V} \quad (24)$$

During steady-state growth, dilution rate controls the growth rate and eventually the cellular biochemical composition. However, if light is the most limiting source in the PBR, steady-state growth is difficult to achieve due to the changing internal light

availability with the inflow of medium. The outflow of nutrient and biomass are determined by the dilution rate of the system. Therefore, the change of nutrient (X_a) and algal biomass ($algX$ and $algC$) during the steady-state growth can be given as Eq. 25-27:

$$\frac{d}{dt} X_a = D \cdot extX \cdot React_V - algC \cdot XCup - D \cdot X_a \quad (25)$$

$$\frac{d}{dt} algX = algC \cdot XCup - D \cdot algX \quad (26)$$

$$\frac{d}{dt} algC = algC \cdot Cu - algC \cdot D \quad (27)$$

Where, X_a (unit, gX) is the amount of nutrient. $extX$ (unit, gXm^{-3}) is the concentration of external nutrient. $React_V$ (unit, m^3) is the total volume of bioreactor. $algX$ (unit, gX) represents the N or P specific algal biomass, $algC$ (unit, gC) is the algal C-biomass. $XCup$ (unit $gX(gC)^{-1}$) is the change of X:C ratio defined in Eq. 5. Cu (unit, $gC(gC)^{-1}d^{-1} = d^{-1}$) is the C-specific growth rate defined in Eq. 20.

5.2.1.6 Determined volumetric and areal productivity

Volumetric productivity (VP , $gC m^{-3} d^{-1}$) and areal productivity (AP , $gC m^{-2} d^{-1}$) are the key parameters to judge the feasibility of production system. High VP may indicate a high biomass concentration system decreasing the cost of dewatering. High AP may indicate an efficient land use. Using AP as the production index is able to directly compare with the traditional crops. Here, the VP and AP of algal biomass (VP_{BM} and AP_{BM}) can be calculated as followings:

$$VP_{BM}(t) = \frac{\frac{algC \cdot Cu}{React_V}(t_2) - \frac{algC \cdot Cu}{React_V}(t_1)}{t_2 - t_1} \quad (28)$$

$$AP_{BM}(t) = VP_{BM}(t) \cdot z \quad (29)$$

The productivity is calculated in terms of algal carbon productivity on a daily basis. AP is calculated from the VP and z (the mixing depth of the system, see section 5.1.2.4).

If we assume all the excess-C (C_{ex}) can be converted into biofuel products, the VP and AP of biofuel products (VP_{fuel} and AP_{fuel}) can be calculated as:

$$VP_{fuel}(t) = VP_{BM}(t) \cdot C_{ex} \quad (30)$$

$$AP_{fuel}(t) = AP_{BM}(t) \cdot C_{ex} \quad (31)$$

5.2.2 Scenarios description

As the microalgal growth model in a PBR system (i.e. PBR model) is described above, this numerical model is simulating into 3 designed scenarios which may encounter in microalgal cultivation process. Model parameters are using the default values listed in the Table 5.1 as the model configuration. During the scenario, the test values of designed parameters are altered to conduct the simulation in hypothetical conditions. The aims of these 3 scenarios is to explore the options of species selection, PBR system and operation design by using numerical model simulations. Scenario details are giving as below:

5.2.2.1 Species selection for a given PBR

During this section, the PBR model is used to explore the potential way of optimizing algal productivity by selecting the species with various target parameters. Three species specific parameters (U_m , $N:C$ and $Chl:C$, see Table 5.1) are test in a given 1 m^3 PBR system with $500 \text{ } \mu\text{mol photons m}^{-2} \text{ s}^{-1}$ continuous lighting (24hr) and 0.03m mixing depth (z) (i.e. tube diameter). Model is simulated into continuous culture of designed algal species with $5 \times f/2$ nutrient medium (i.e. $4410 \text{ } \mu\text{M NO}_3^-$ and $181 \text{ } \mu\text{M PO}_4^-$, or) under various operational dilution rates (D , see Table 5.1). For the maximum growth rate (U_m) simulation, dilution rates are chosen from $0.1\text{-}0.9 \text{ d}^{-1}$. For the minimum $N:C$ and maximum $Chl:C$ ratio simulation, maximum growth rate is set at 0.693 d^{-1} (i.e. one division per day) and dilution rates are selected from $0.07\text{-}0.624 \text{ d}^{-1}$ which is equal to 10%-90% of its maximum growth rate.

5.2.2.2 Bioreactor design for a giving species

In this scenario, the PBR model is used to explore the considerations of PBR system design and operations in order to reveal the relationship among the productivity, mixing depth (z) and operational dilution rate (D) under different light regime. A fast growing hypothetical species with maximum growth rate (U_m) as 1.386 d^{-1} is selected (parameters configuration listed in Table 5.1) to grow in a 1 m^3 PBR system with $5 \times f/2$ nutrient medium. The Model is operated in either continuous culture mode under $500 \text{ } \mu\text{mol photons m}^{-2} \text{ s}^{-1}$ continuous artificial lighting (24hr) or simulated natural light-dark cycle during summer time near the equator (with peak irradiance near $2000 \text{ } \mu\text{mol photons m}^{-2} \text{ s}^{-1}$ during noon time, more detail see Appendix. D). Biomass is harvested at the mid-day in the daylight cycle to maximise productivity.

5.2.2.3 Two-stage cultivation process

As the idea of two-stage cultivation process (a combination of N-replete culture

followed by an N-deprived culture to promote the lipid productivity) has been proposed (Rodolfi *et al.*, 2009), there is no experimental work concerning the two-stage cultivation in large scale continuous culture system although the lab scale batch experiment has shown the advantage in employing the two-stage cultivation (Su *et al.* 2011). In this scenario, the mechanistic model (i.e. PBR model) as previously described is modified into a two-stage cultivation model (see Figure 5.1) to evaluate the production and design consideration of the continuous culture system.

Within the two-stage model, two individual PBR models sharing the same numerical structure are connected together. Algal cells with nutrients grow inside the systems of two stages. To mimic the commercial scale cultivation, we operate the two-stage cultivation in continuous culture in both stages. During the stage 1, cells are growing in a closed PBR with nutrients support 90% of maximum growth rate (U_m) as operational dilution rate (D) under continuous lighting as the inocula supply for stage 2. Continuous cultures run from stage 1 into stage 2 at a given flow rate (equals operational dilution rate (D) at stage 1) Flow from the PBR in stage 1 into the reactor (containing only water initially) in stage 2 is algal broth containing residue nutrients and algal biomass. During stage 2, there is no external nutrient into the system in order to create a nutrient starvation stage, and then the algal broth is harvested at the stage 2 as the overflow from the system.

The reactor in stage 2 could be either a closed PBR or an open raceway system. Raceway systems are commonly chosen in commercial scale production. To design the dimensions of raceway in stage 2, we assume the volume of reactor in stage 2 (RV) is depended on the operational dilution rate (D_2) in the stage 2 (Eq.32). Surface area (Surface) is calculated from the determined optical depth (OD) and volume (RV) of the raceway system (Eq. 33).

$$RV = \frac{Flow}{D_2}$$

(32)

$$Surface = \frac{RV}{OD} \quad (33)$$

In Eq.32, dilution rate (D_2) will result in a smaller reactor volume (RV). The assumption here is that the algal broth will be overflow at the designed volume with certain optical depth (OD) and eventually to harvest. The Flow rate in Eq. 32 equals the dilution rate (D) in the stage 1. In Eq. 33, smaller optical depth will result in a larger surface area.

A hypothetical species with maximum growth rate (U_m) as 0.693 d^{-1} is chosen to grow in the two-stage system (more parameter configuration see Table 5.1). The PBR design in the stage 1 is used the same configuration in scenario 1 (1 m^3 reactor volume with 0.03m tube diameter). $5 \times f/2$ nutrient medium is applied in stage 1. Light regime in stage 1 is used artificial continuous lighting ($500 \mu\text{mol photons m}^{-2} \text{ s}^{-1}$). Light regime in stage 2 could be either simulated into artificial continuous lighting ($500 \mu\text{mol photons m}^{-2} \text{ s}^{-1}$) or natural light-dark cycle during summer time near the equator as previously experiment (see Scenario 5.2.2.2).

5.3 Results and Discussion

5.3.1 Model simulation as a tool in strain selection and modification

Selection of strains with high productivity of biofuel material is the first step to realize the biofuel production from microalgae. Physiological features (e.g. growth rate, storage carbon and pigment content etc.) of microalgae species are naturally selected during evolution. These physiological features are generally obtained during experimental work on microalgal cultivation. With the dataset in microalgal cultivation, the mechanistic model of microalgal growth described by these physiological parameters can be used to explore the bulk productivity of microalgae

under various physical-chemical conditions.

The optimal species under optimal condition (light and nutrients are sufficient) for biofuel production can be summarized into the following three characteristics: 1) high growth rate which is able to accumulate biomass within relatively short time; 2) high cellular biofuel material content; 3) less pigment content which is able to reduce the self-shading effects and eventually accumulate relatively large amount of biomass.

In Figure 5.2, panel A the simulation shows the best areal productivity of biomass and biofuel occurs at high maximum growth rate in combination with high dilution rate for the given photobioreactor design. Obtaining a fast growing species is always beneficial for both biomass and biofuel production. At low maximum growth rate with high dilution rate, biomass growth is not able to compensate the dilution rate and thereby is washed out of the system resulting in a low productivity of both biomass and biofuel. Cellular biofuel material content is low under nutrient sufficient condition (i.e. low maximum growth rate with high dilution rate) but reach its maximum around 60% of cell carbon at nutrient limited condition (i.e. high maximum growth rate with low dilution rate). The relative growth rate indexed to maximum growth rate is the ultimate factor to determine the cellular biofuel content.

In Figure 5.2, panel B the simulation illustrates the best combination for areal productivity of biomass and biofuel occurs at middle dilution rate (around 0.35 d^{-1} , i.e. 50% of maximum growth rate) with low minimum N:C ratio. Minimum N:C ratio (i.e. maximum C:N ratio) is a physiological parameter indicating the maximum cellular carbon content refer to cell-N. Lowering 5 folds of the minimum N:C ratio (from 0.1 to 0.02, with unit $\text{gN}(\text{gC})^{-1}$) can increase areal productivity of biofuel material by 2 fold but the biomass productivity increases less. At high dilution rate, biofuel productivity and cellular biofuel material content is sharply decreased. Although the cellular biofuel material content obtains maximum around 60% of cell-C at lowest dilution rate, the biofuel productivity is low due to the low biomass

productivity. There is a trade-off between biomass and cellular biofuel material content.

In Figure 5.2, panel C the simulation shows that the maximum Chl:C content does not affect the productivity of biomass and biofuel for the designed shallow light path (mixing depth =0.03m) PBR with $5 \times f/2$ nutrient medium. The productivity is driven by the dilution rate only. Higher dilution rate results in higher biomass productivity but lower biofuel material content. The optimal biofuel productivity occurs in the middle of the test dilution rate. The simulation here indicates that maximum Chl:C ratio is not a critical feature to consider in the present production system. However, Maximum Chl:C ratio is an important parameter in high density culture where light availability is limited due to self-shading via the pigment synthesis (mainly chlorophyll synthesis). Decrease the maximum Chl:C ratio 10 fold can potentially increase the areal productivity of biomass 10 fold under the system with 1 m light path and $10 \times f/2$ nutrient medium (Flynn *et al.*, 2010).

Model simulations can aid in two ways of strain selection for optimisation of biofuel production: 1) select the strain that naturally exist; 2) select the strain that been genetically modified. The parameter value for microalgae indicated in the simulation can potentially be achieved via genetic modification. The simulation suggest that increase the maximum growth rate and decrease the minimum N:C ratio are both useful features in potentially increase the biofuel productivity in current production system. It is of difficulty to increase the maximum growth rate by genetic engineering. Engineering the maximum growth rate may involve alteration of cell cycle and limitation of respiration cost (Flynn, 2009). To decrease the cellular minimum N:C ratio may potentially achieve via increase the lipid droplet size to increase the ability of carbon storage (Radakovits *et al.*, 2010). Moreover, decreasing the Chl antenna size of photosynthesis system of cell via genetic engineering has been demonstrated to be of value of increasing growth in high density or high light path culture due to increase the light penetration (Beckman *et al.*, 2009). However,

physiological changes via genetic or biochemical modification are unlikely happen alone. Cells of *Chlamydomonas reinhardtii* are susceptible to high light damage of photosystem when starch synthesis is inhibited, although the cellular lipid content is significantly increased (Li *et al.*, 2010). Less carbohydrate is accumulated when fatty acid synthesis are depressed has been also reported in *Haematococcus pluvialis* (Recht *et al.*, 2012). Despite of the uncertainty of physiological changes via genetic or biochemical engineering, the model can work as a guideline to target the key parameters.

5.3.2 Model simulation as a tool in culture system and operational design.

5.3.2.1 Photobioreactor system

Light availability is the primary consideration in photobioreactor design (Richmond, 1992, 2004). Microalgal cultures are eventually grown to light limitation, if nutrients can be added as excess, due to the self-shading from dense cell pigments decrease the light availability within the population. To optimise the productivity of biomass, the light path (i.e. z , mixing depth) of the photobioreactor are needed to be as small as possible and nutrients must be supplied sufficiently. However, cellular biofuel feedstock (i.e. neutral lipid and carbohydrates) are accumulated under nutrient limitation condition. Excess nutrient may result in low biofuel productivity. Modelling the combination of nutrient and light availability is of benefit to optimise the productivity of biofuel in the culture system.

In the continuous light simulation (Figure 5.3), highest cellular biofuel material content is achieved around 60% of cell-C at lowest dilution rate 0.1d^{-1} with mixing depth below 0.1m while biomass concentration is highest around 1kgC m^{-3} . Volumetric productivity of biomass results in $400\text{ gC m}^{-3}\text{ d}^{-1}$ at dilution rate 0.8 d^{-1} (this equals 58% of maximum growth rate applied here) while the maximum

volumetric productivity of biofuel at dilution rate 0.6 d^{-1} (equals 43% of maximum growth rate) with the mixing depth value below 0.1m. The areal productivity of biomass reach c.a. $40 \text{ gC m}^{-2} \text{ d}^{-1}$ at highest dilution rate 0.8 d^{-1} , while the maximum biofuel productivity (c.a. $20 \text{ gC m}^{-2} \text{ d}^{-1}$) is achieved at dilution rate 0.6 d^{-1} with mixing depth at 0.1m. The areal productivity is low at shallow mixing depth system. The areal and volumetric productivities are both low with mixing depth of bioreactor above 0.1m due to the decrease of light penetration in the deep culture system. High volumetric productivity is a benefit to harvest with decreasing dewatering cost while high areal productivity can minimise the land use. To obtain the best combination of areal and volumetric productivity, a mixing depth at 0.1m appears to be the best option for PBR manufacturing at current nutrient and light settings.

In comparison with a continuous lighting system, simulation using natural light-dark cycle was evaluated under the same culture conditions. In Figure 5.4, the maximum volumetric productivities of biomass and biofuel are 4 fold lower than the continuous light culture at tropical summer day, although the peak values of biomass concentration and cellular biofuel material content are similar. The maximum areal productivities of biomass and biofuel are almost 10 fold lower than the continuous light culture. The maximum volumetric productivity of biomass is appeared at dilution rate 0.5 d^{-1} with shallow mixing depth at 0.03m while the optimal volumetric productivity of biofuel can be obtained under even lower dilution rate. Under the high dilution rate, the growth of cells are not able to compensate the lost from dilution (i.e. dilution rate is higher than growth rate) under light-dark cycle. The duration of the light period is critically important for the increase of productivity of biomass and biofuel. Simulation for a flat panel photobioreactor has also revealed the day length effects on the productivity over the year (Slegers *et al.*, 2011).

Increasing the duration of light period may be benefit to increase the growth of algal cultures, although the cost from artificial lighting may not benefit commercial production. However, the use of microalgae is not only focus on the economic

benefit but also the ecological benefit (Williams, 2007). The production of biofuels from microalgae may combine the process of waste water treatment and CO₂ fixation (McGinn *et al.*, 2011). Moreover, high value products (such as pigments and unsaturated fatty acids, see Spolaore *et al.*, 2006) as addition to biofuel products should be considered systematically. With these benefits from microalgae, continuous lighting with continuous culture may be cost-effective but the assumption here needs a detailed life cycle assessment which should include a comprehensive microalgal cultivation model.

5.3.2.1 Two-stage cultivation system

Microalgal cultivation processes are critically important for manipulation of algal physiology. It is difficult to actually built a large scale system and test it in commercial production. Mass cultivation process can be designed via model simulation. To mimic the commercial production, cultivation is designed into continuous system. However, the two-stage cultivation system can be operated into batch culture but the maintenance efforts (e.g. clean the system) after each batch is making the batch system commercially unreliable.

From the simulation under continuous lighting (Figure 5.5A), total production rate of biofuel at stage 2 can be increased by 5 fold than the production rate in stage 1 (arrows indicate) with optical depth below 0.1m under low dilution rate in stage 2. Within high optical depth (>0.1m) raceway, cells barely grow due to the self-shading within populations. Cellular biofuel material content is increased by over 2 fold at stage 2 cultivation. Since the light is not available at optical depth over 0.1m, cells are not getting nutrient limitation and thereby cellular biofuel content (c.a. 20%) is lower than the cells in stage 1. From the simulation under natural light-dark cycle at stage 2 (Figure 5.5B), total production rate and cellular biofuel content only reach similar values as the simulation with continuous light at shallow optical depth (0.03m) and low dilution rate (0.2d⁻¹). The implication is that the optical depth of nutrient

starvation growth stage is needed to be smaller than the nutrient sufficient growth stage to maximise the light use and thereby promote the accumulation of biofuel material. In reality, it is difficult to achieve this. Raceways with shallow optical depth will need larger land area (surface area) to maintain the relatively large scale of production system (Figure 5.6). Additionally, water evaporation in shallow optical depth system may become significant although increase of salinity to certain level may increase the cellular lipid content (Larson and Rees, 1996). Moreover, shallow optical depth system with nutrient starvation may raise a severe issue of photodamage of cells and eventually photoinhibition (decrease the rate of carbon fixation).

5.4 Conclusion

Prediction of microalgal growth in PBR is the fundamental work to evaluate the productivity of the system, while numerical models may work as a tool in optimisation the productivity of target chemicals. A mechanistic model based PBR model is presented in this chapter to explore the options in optimisation of biofuel productivity in different culture scenarios. Model simulation suggest species with high maximum growth rate and low minimum cellular N:C ratio are able to obtain high biofuel productivity in shallow mixing depth system. Employing GM species may be able to increase the biofuel productivity. In comparison with culture under natural light-dark cycle, the biofuel productivity of culture with continuous light can achieve nearly 10 folds higher under different combination of mixing depth and dilution rate. A two-stage cultivation process is designed. The simulation from two-stage cultivation process suggests the optical depth in nutrient starvation stage is needed to be shallower than the nutrient sufficient stage. Modelling technique is a powerful tool in prediction and optimisation of system productivity.

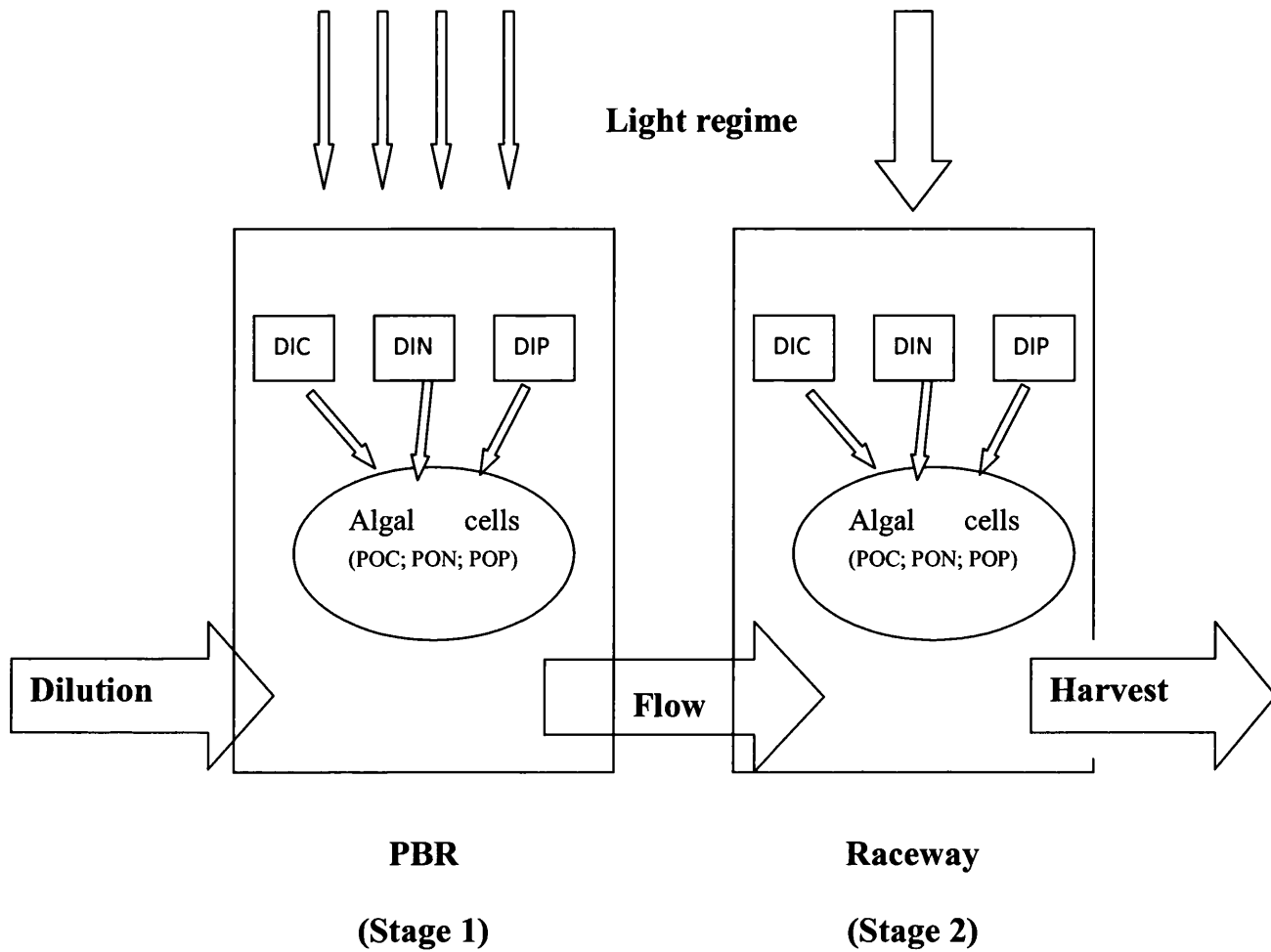


Figure 5.1: A schematic figure shows the PBR-Raceway linked model. Two models are coupled using a flow control function. Culture in PBR (stage 1) flows into a designed raceway (stage 2) with different regime applied. Detailed explanation see text in section 5.2.2.3

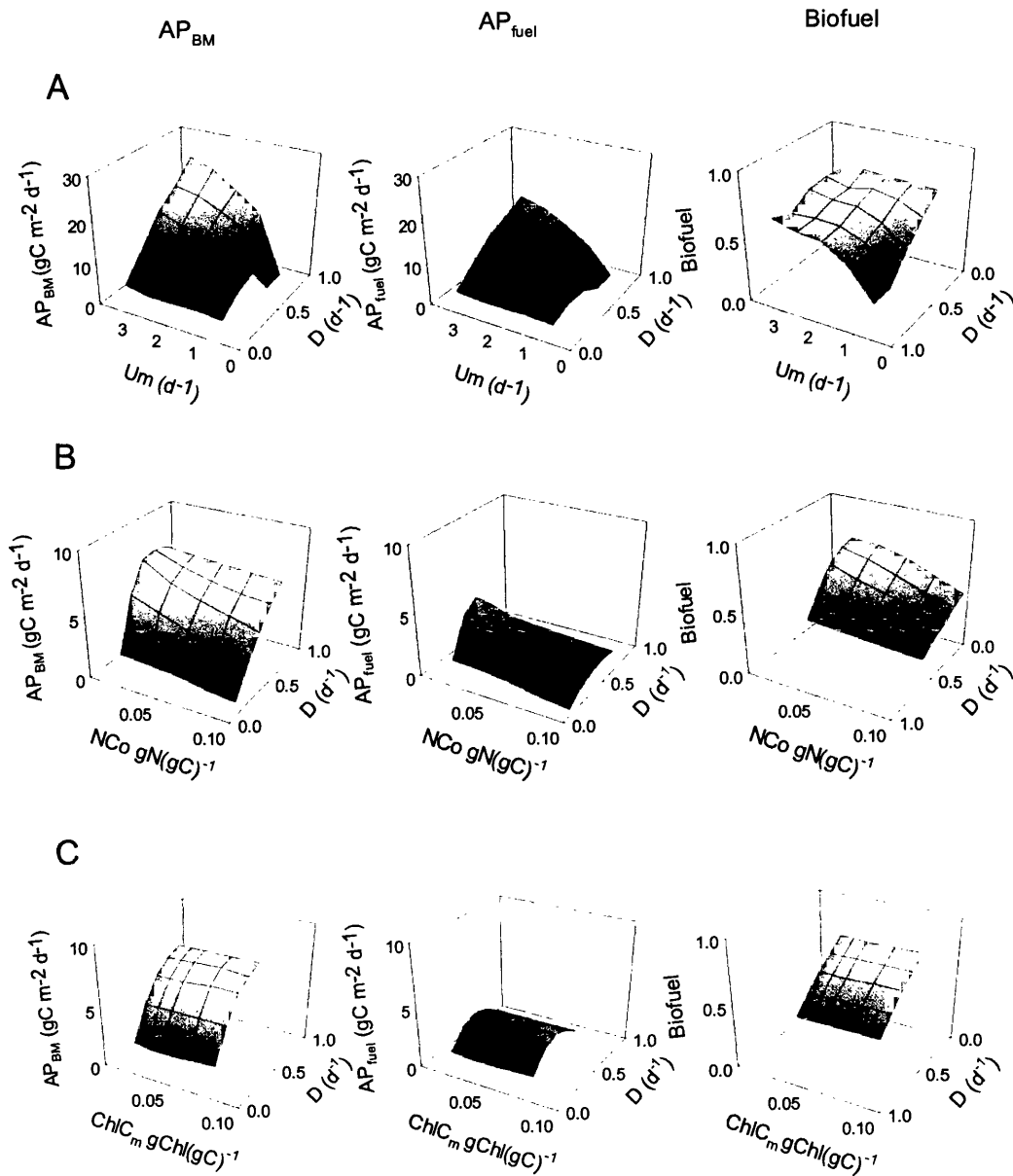


Figure 5.2: Simulation of continuous growth of algal species with selected figures under $500 \mu\text{mol photons m}^{-2} \text{s}^{-1}$ continuous lighting. Notice the different orientation of scale of dilution rate in biofuel column. AP_{BM} : areal productivity of algal biomass; AP_{fuel} : areal productivity of biofuel materials; Biofuel: proportion of biofuel materials in cell. D : Dilution rate. Panel A: Maximum growth rate (U_m), B: minimum N:C ratio (N_{Co} , gN(gC) $^{-1}$), C: Maximum Chl:C ratio ($ChlC_m$, gChl(gC) $^{-1}$).

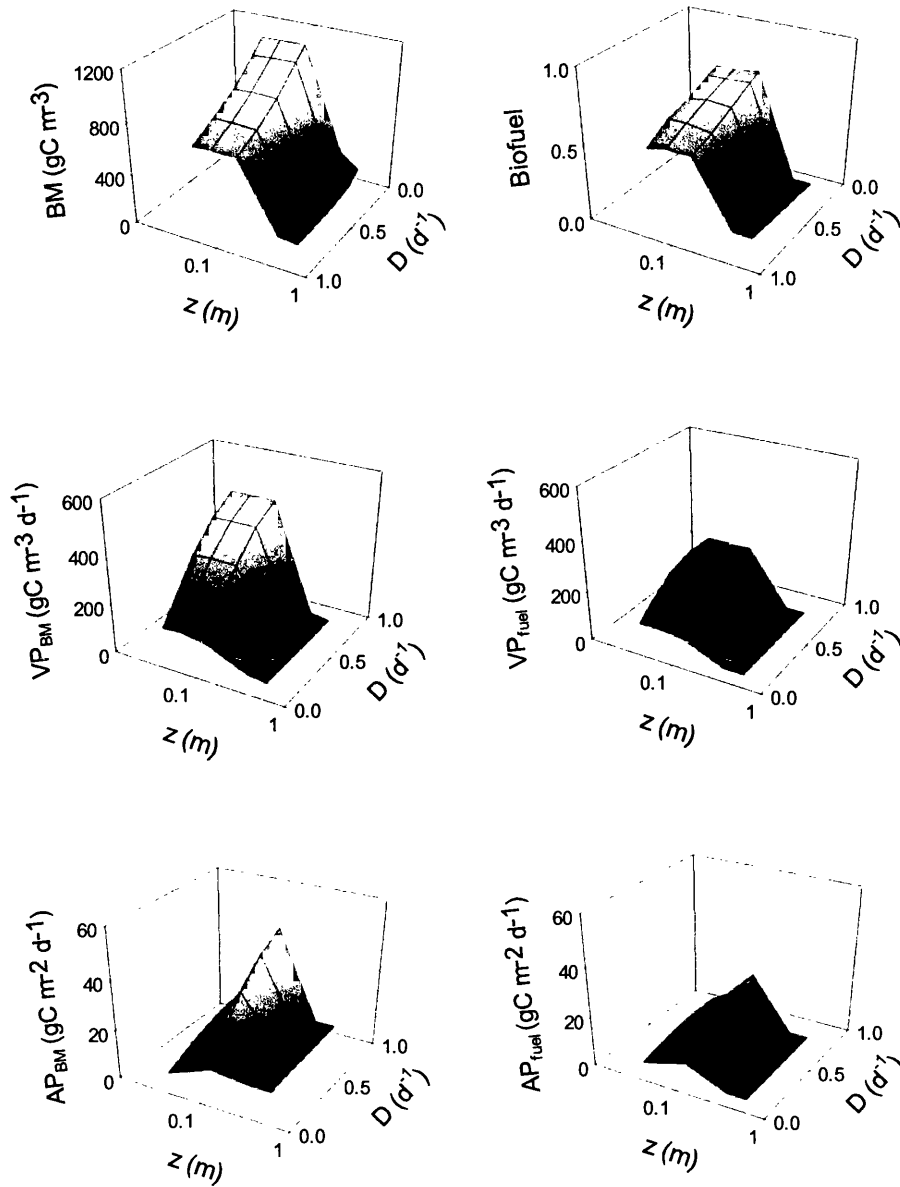


Figure 5.3: Continuous lighting ($500 \mu\text{mol photons m}^{-2} \text{s}^{-1}$) simulations of continuous growth of virtual species in a designed PBR. Notice the different orientation in scale of dilution rate. D : dilution rate. z : mixing depth. BM : algal biomass concentration; AP_{BM} : areal productivity of algal biomass; AP_{fuel} : areal productivity of biofuel materials; Biofuel : proportion of biofuel materials in cell. VP_{BM} : volumetric productivity of algal biomass; VP_{fuel} : volumetric productivity of biofuel materials.

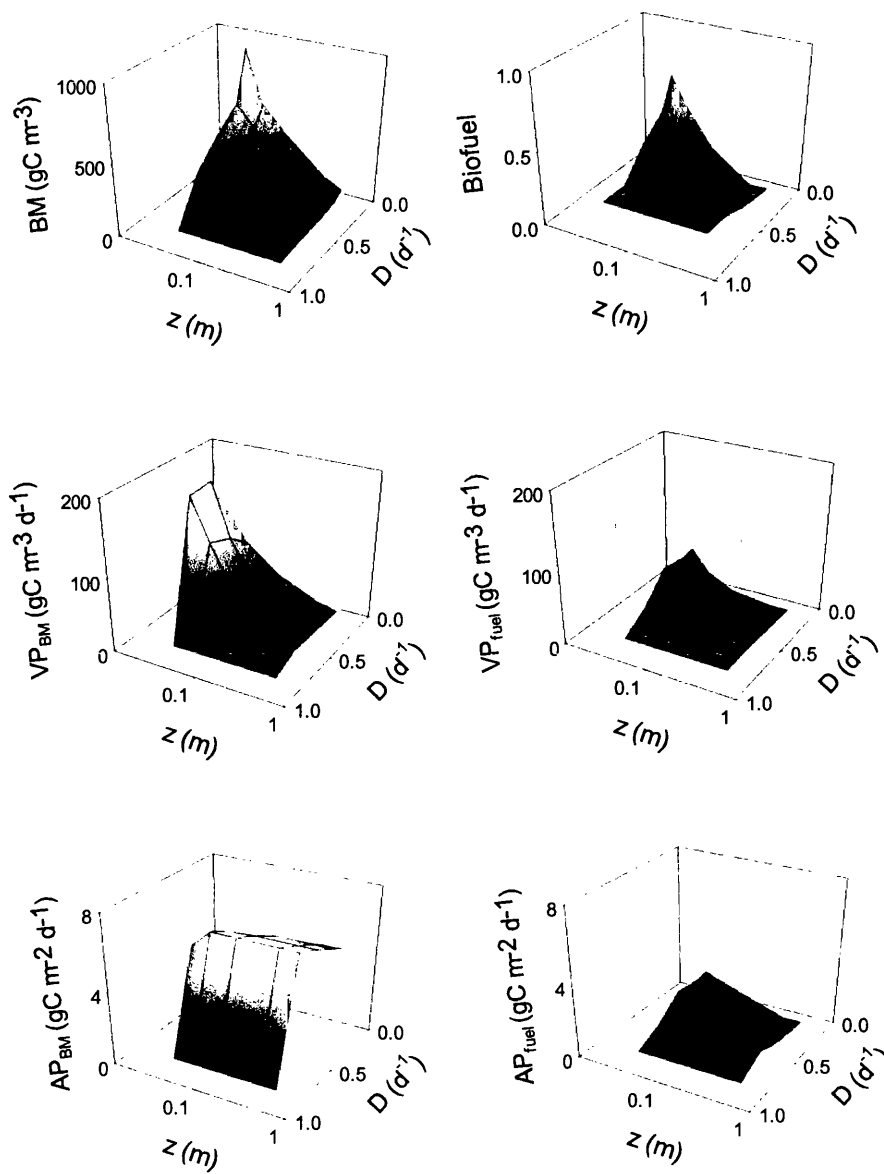


Figure 5.4: Natural light-dark cycle simulations of continuous growth of virtual species in a designed PBR. Notice the different orientation in scale of dilution rate. Nominations of parameters in axes see text in Figure 5.3.

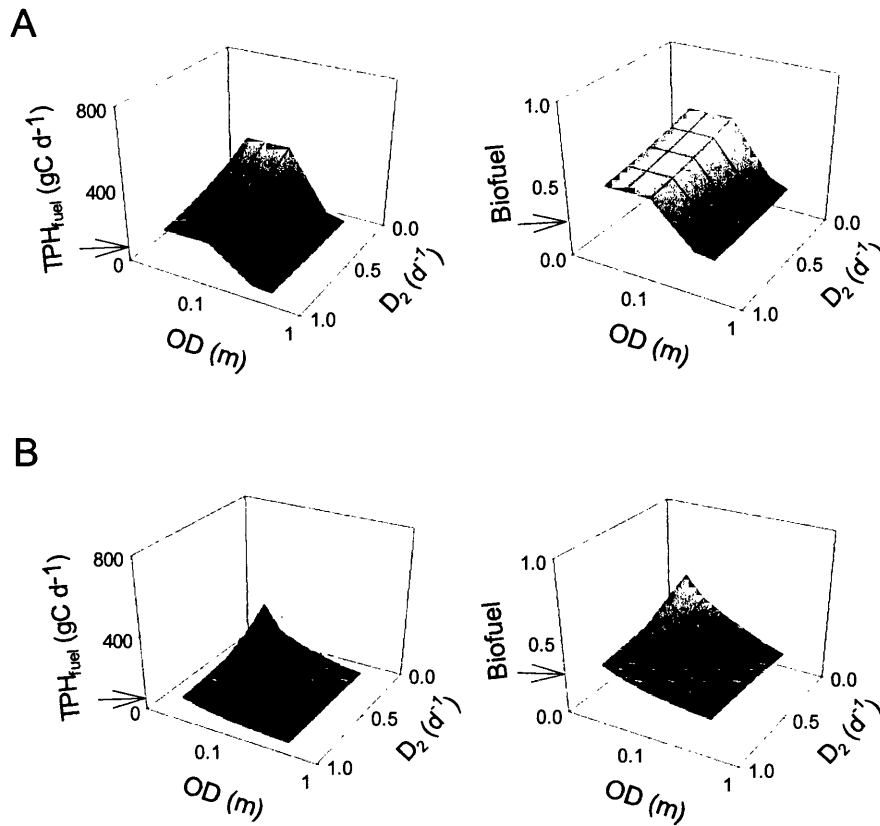


Figure 5.5: Two-stage (PBR-raceway) cultivation simulations of continuous growth of virtual species under various light regimes. Panel A: Continuous lighting ($500 \mu\text{mol photons m}^{-2} \text{s}^{-1}$) in both stages. Panel B: Continuous lighting in stage 1 ($500 \mu\text{mol photons m}^{-2} \text{s}^{-1}$) and natural light-dark cycle in stage 2. Arrows indicates the parameter in PBR (stage 1) only. TPH_{fuel} : Total production rate of biofuel material of the two-stage system in harvest stage (stage 2); Biofuel: proportion of biofuel materials in cell in stage 2.

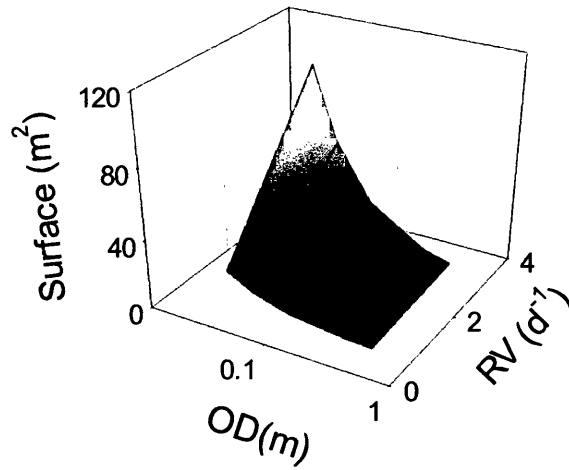


Figure 5.6: Relationship simulation of raceway reactor volume (RV), optical depth (OD) and surface area (Surface) in the stage 2.

Table 5.1: Parameters used in designed scenarios simulations. “NA” means not applicable; “-” means default setting is applied in the scenario simulation.

Parameters	Descriptions with units	Default settings	Scenario 5.2.2.1	Scenario 5.2.2.2	Scenario 5.2.2.3
Lighting	Continuous light (c-light) or daylight cycle (d-light); $\mu\text{mol photons m}^{-2} \text{ s}^{-1}$	NA	c-light	c-light and d-light	c-light and d-light
z	Mixing depth of PBR; m	0.03	-	0.03-0.5	-
OD	Optical depth in stage 2 in two-stage model; m	NA	-	-	0.03-0.5
React_V	Volume of PBR; m^3	1	-	-	-
N	N content in $5 \times f/2$ medium; gN m^{-3}	61.74	-	-	-
P	P content in $5 \times f/2$ medium; gP m^{-3}	5.61	-	-	-
D	Dilution rate in PBR model; d^{-1}	NA	0.1-0.9 and 0.07-0.624	0.1-0.8	0.624
D₂	Dilution rate in stage 2 in two-stage model; d^{-1}	NA	-	-	0.2-1.0
Um	Maximum growth rate under continuous light; d^{-1}	0.693	0.693-3.465	1.386	-
ChlCm	maximum pigment content; $\text{gChl}(\text{gC})^{-1}$	0.06	0.02-0.08	-	-
α^{Chl}	initial slope of photosynthesis irradiance curve; $(\text{gC mol}^{-1} \text{ photon}) \times (\text{m}^2 \text{ g}^{-1} \text{ Chl})$	7	-	-	-
M	photoacclimation rate controls; dl	2	-	-	-
NCo	Minimum N quota; $\text{gN}(\text{gC})^{-1}$	0.05	0.02-0.1	-	-
NCm	Maximum N quota; $\text{gN}(\text{gC})^{-1}$	0.16	-	-	-
NCabs	Absolute value of N quota; $\text{gN}(\text{gC})^{-1}$	0.2	-	-	-
NKu	Half saturation constant of N transport; gN m^{-3}	0.028	-	-	-
KQN	Curve control constant for N uptake; dl	10	-	-	-
PCo	Minimum P quota; $\text{gP}(\text{gC})^{-1}$	0.005	-	-	-
PCm	Maximum P quota; $\text{gP}(\text{gC})^{-1}$	0.02	-	-	-
PCabs	Absolute value of P quota; $\text{gP}(\text{gC})^{-1}$	0.04	-	-	-
PKu	Half saturation constant of P transport; gP m^{-3}	0.062	-	-	-
KQP	Curve control constant for P uptake; dl	0.1	-	-	-
Kxi	Feedback control constant; dl	0.001	-	-	-
Qh	Hill number of feedback control; dl	2	-	-	-
CN_{core}	C : N for the nitrogenous core of the cell; $\text{gC}(\text{gN})^{-1}$	3.20	-	-	-

6. Modelling the growth of *Nannochloropsis oculata* (Droop) in a 600L tubular photobioreactor

6.1 Introduction

Commercial scale cultures of photoautotrophic microalgae provide relatively low biomass productivity in current culturing techniques (Ugwu *et al.*, 2008). This has become a fundamental issue limiting the exploitation of microalgae for commercial applications (e.g., production of pigments and polyunsaturated fatty acids). Microalgae have also been demonstrated to have various advantages for biofuels production in comparison with traditional crops (Chisti, 2007), and increasing interests from various angles have further explored the use of microalgae for alternative fuels production (Greenwell *et al.*, 2010; Williams and Laurens, 2010; Mata *et al.*, 2010; Huang *et al.*, 2010). The challenge of increasing the productivity of biomass or of targeted products (e.g. biofuels) again has been placed on the priority list.

There are plenty of experiments conducted to assess the biomass and potential biofuel productivity of selected strains. The “productivity” (calculated using a variety of methods) varies depends on the culture conditions (Chen *et al.*, 2011). Nutrient stress appears to be an effective way to enhance the lipid and/or carbohydrate (collectively called excess-C) accumulation (Shifrin and Chisholm 1981; Lynn *et al.* 2000; Rodolfi *et al.*, 2009; Chen *et al.* 2011). However, high excess-C content and high growth rate seem to be mutually exclusive. Nutrient stress decreases the growth rate and eventually decreases the biomass productivity. There is a clear trade-off between the biomass and biofuel production (Williams and Laurens 2010).

Modelling the growth and excess-C accumulation of microalgae with detailed descriptions of nutrient acquisition and photoacclimation appears to have numerous

advantages in optimization of microalgal growth and target chemical products. Manipulation of nutrient inputs and hence growth conditions in photobioreactor (PBR) can potentially be exploited via computer based mathematical modelling. This is needed as a first step prior to actually building and testing a real system (Greenwell *et al.*, 2010). Simulations of algal growth in PBRs have typically focussed upon impacts of irradiance and lack of descriptions of nutrient status (e.g. Sukenik *et al.*, 1991, Fernandez *et al.*, 1998). Although detailed phytoplankton growth models have been constructed (Geider, 1998; Flynn, 2001), they have not been parameterized for the purposes of optimizing biomass and biofuels production in a PBR. Once such a mechanistic model has been parameterized, it can serve as a useful tool to estimate the production of the biomass and target chemicals. More importantly, it can provide information of physiological status of organisms during the growth enabling a better understanding of an otherwise poorly defined system. This not only can be employed to promote the growth via altering the design and operation of the bioreactor but may also benefit the understanding of the ecology of phytoplankton blooms (i.e. high density cultures).

Both ecological and commercial interests in modelling the dynamics of excess-C synthesis are best served with C-specific data, for which there are surprisingly few published data sets. The vast bulk of data report either whole cell elemental composition (typically C:N, fewer as C:N:P; Geider and La Roche, 2002) or they report carbohydrate or lipid (either as bulk determinants or as specific compounds) on a cell basis (Sukenik and Wahnou, 1991; Demadariaga and Joint, 1992; Lourenco *et al.*, 1997). Reporting biochemical composition on a cell basis, with no rigorous concurrent measurement of cell biomass (ideally as C) is of little utility for modelling because of the variation in cell size that occurs over the light-dark cycle and with nutrient stress (Finkel *et al.*, 2010). Unsurprisingly then, while models of microalgae simulating changes in C:N:P are not uncommon, there are none simulating changes in excess-C in a manner appropriate for placement in biomass-based simulators such as that used by Flynn *et al.* (Flynn *et al.*, 2010).

In this study, a PBR model previously developed from MAP2 (Flynn 2003), coupled with a bulk estimation of biochemical composition model (see Chapter 5.2.1.5) is modified to meet the configuration of a 600L tubular PBR (Chapter 2.1.3). Validation of the PBR model is conducted using the experimental culture of *Nannochloropsis oculata* (Chapter 3). Key physiological parameters (e.g. N:C, P:C and Chla:C) described in the model have been examined both by modelling and in reality and discussed with respect to their usefulness of monitoring the culture and estimate the production of biomass and target chemicals.

6.2 Materials and Methods

The photobioreactor model as described in Chapter 5 was configured using the physical-chemical condition listed in Table 6.1 as employed in the actual 600L photobioreactor. Detailed explanation of the model structure and algorithms are given in Chapter 5. The simulation was run for 10 days in batch mode and 2 days in semi-continuous mode (fresh medium was injected continuously at a fixed rate into the system, and biomass was harvested daily at fixed time), mimicking the configuration of the PBR system. Experimental data from Chapter 3 are used to tune the PBR model. Simulation starts from day 1 using measured data as initial parameters to model operation. Model parameters were tuned to obtain the best fit of the data using Powersim Solver (see Chapter 2.2.5). Constants obtained from the tuning process are given in Table 6.2.

6.3 Results

6.3.1 C-biomass accumulation

Cellular C-biomass accumulated up to 622 mgC L⁻¹; simulation results from the model agree well with the data in general (Figure 6.1). A steeper slope (higher growth rate) was observed in the data during exponential growth in comparison with the model simulation. However, the final C-biomass agreed with the simulation in

both batch and semi-continuous phase.

6.3.2 Nutrient uptake from the medium

Nitrate (NO_3) and phosphate (PO_4) are the macro-nutrients in the *f/2* based nutrient medium which has been widely used in marine microalgal cultivation.

Dissolved Inorganic Nitrogen (DIN) measured as nitrate and nitrite are well described by the model (Figure 6.2). Particulate organic nitrogen (PON) accumulation can be also described by the model, although the PON content was underestimated by around 10 mg L^{-1} at the end of batch culture from the simulation. The input of DIN is far less than the PON accumulated in the system. It indicates another nitrogen source may be consumed by the cells when nitrate was depleted.

Phosphorus removal and accumulation were less well described by the model in comparison with nitrogen. The initial phosphate concentration added into the system equals 4.5 times *f/2* medium (i.e. around $163\ \mu\text{mol L}^{-1} = 5\ \text{mg L}^{-1}$). Only 70% of added phosphate (i.e. $3.5\ \text{mg L}^{-1} = 112\ \mu\text{mol L}^{-1}$) was detected chemically as soluble reactive phosphate (SRP) in the medium at the beginning of growth. This was probably due to the precipitation of phosphate with high concentration in seawater medium. Despite of the discrepancy at day 3, SRP removal is well described by the model simulation (Figure 6.3). Simulation of particulate organic phosphorus (POP) accumulation was under estimated in the system by using SRP data. The increase of POP after SRP was depleted is likely to be explained by the resolubilisation of previously precipitated phosphate in the seawater medium. The POP attained around 5 mg L^{-1} which is equal to the amount added initially. In comparison with the simulation using initial Dissolved Inorganic Phosphate (DIP) (i.e. $5\ \text{mg L}^{-1}$) with the same constants using in the SRP simulation, the POP uptake was slower using SRP (Figure 6.3).

6.3.3 Cellular N and P Quota

The model simulations are able to describe most of the data points with the change of N:C and P:C ratios. Simulation results are slightly discrepant with N:C ratio at the first few days (Figure 6.4). It indicates the culture was relatively more nutrient replete than the model indicates. The P:C ratio is well described by the model, although the simulation slightly underestimates the results in semi-continuous phase. The simulation does not catch the data points for either N:C or P:C at day 3. It probably results from the insufficient CO₂ supply induced C-limitation (Chapter 3.3.1), which is not included in the model structure.

6.3.4 Pigmentation

Chlorophyll_a (Chl) synthesis is regulated by the availability of light and nutrients (mainly N) in the system (Geider *et al.* 1998; Kruskopf and Flynn 2006). The concentration of Chlorophyll was significantly influenced by biomass production via self-shading. An initial decrease of Chl:C indicates a photoacclimation process of the cells to relative high light condition at the beginning of growth and increase back at the end of batch culture (Figure 6.5). The changes in ChlC are well described by the model simulation, although data around day 3 are underestimated in the simulation. The bias between simulation and data are probably the same reason as found in N:C and P:C data (C-limitation).

6.3.5 Biochemical composition

Usually protein, lipid and carbohydrate are the three main biochemical groups measured in aquaculture nutrition. In the PBR model presented here, biochemical groups were simulated using the term defined as non-nitrogenous C (nonN-C), membrane-C (mem-C) and excess-C (XS-C) in order to investigate the relationship between growth and C-specific storage groups (See Chapter 5 for more details). nonN-C is the sum of lipid-C and carbohydrate-C, which is well described with

model simulation (Figure 6.6). Excess-C (XS-C) is a potential biofuel component consisting of neutral lipid-C and/or carbohydrate-C. This component can be assigned to either when the species only accumulate single storage product. For the species using in this study, lipid content and carbohydrate content of *Nannochloropsis oculata* is not fit well for the group that defined in the model (Figure 6.6).

6.4 Discussion

6.4.1 The role of N dynamics

Determining the utilization and release of different forms of soluble N is of importance when considering biomass production, especially for utilization of waste water treatment. The mechanism of organic N metabolism still remains unclear, although the interactions of inorganic N source (NH_4 and NO_3) were well understood (e.g., Dortch 1990; Flynn *et al.*, 1997). More measurements were needed to clarify the N footprint in high density seawater culture.

In natural seawater, N sources present as dissolve inorganic N (DIN) and dissolve organic N (DON) (Flynn and Butler, 1986). Despite the common emphasis on DIN (e.g. NH_4^+ and NO_3^-) used for algal culture, microalgae cells are able to use organic N sources in the aquatic environment (Flynn and Butler, 1986; Berman and Chava, 1999). Urea is the most common one with the reputation of relatively low cost and even “better” growth in comparison with NO_3^- and NH_4^+ for some cyanobacteria and diatom species used in aquaculture (Lourenco *et al.*, 2002; Meiser *et al.*, 2004). Meanwhile, N also can be released in terms of dissolved free amino acid (DFAA) from living cells but the net amount released by healthy cells is likely to be trivial (Flynn and Berry, 1999). At the laboratory scale, system N can be balanced by adding up DIN and PON (e.g. Harrison *et al.*, 1989; Flynn *et al.*, 1993), assuming the amount lost by adherence of cells to the culture vessel is minor. When considering nitrate as the only N-source added for cultivation, the increase of PON is expected to equal the decrease of DIN (nitrate and nitrite) as the model result suggested.

However, a higher PON content is observed at the end of batch culture (Figure 6.2). This indicates an alternative N source has been used in addition to nitrate. Considering the use of natural seawater and relatively large volume of inocula, an alternative N source cannot be ruled out DON might be used as an additional parameter to system N in mass culture with nutrient limiting condition.

6.4.2 The role of P dynamics

Phosphate precipitation is a common phenomena found in high concentration phosphate seawater-based media, and is exacerbated by changes in temperature and pH; precipitation decreases with high temperature and increases with elevated pH (Ferguson *et al.* 1973; Olsen *et al.* 2006). Simulations of phosphate uptake are thus challenged by coupling the prediction of bioavailable phosphorus, the so called soluble reactive phosphate (SRP) which is measured by chemical analysis, and any forms that not biologically usable or detected. In a closed or semi-closed PBR system without aeration, the pH of cultures may reach >10 induced by photosynthetic activity; phosphate precipitation occurs in alkaline pH range even in relatively low input concentration (Olsen *et al.* 2006). The pH stress can be easily avoided by applying a pH regulator program with suitable input of CO₂ concentration in closed PBR system. In the present study, pH value exceeded 9 at day 3 probably due to the insufficient DIC remain in the system (Fig. 3.1). A significant drop of SRP measured at day 3 could thus possibly reflect the precipitation of phosphate in high pH seawater. Interestingly, a significant increase of POP and PC values were observed at day 3 when lower SRP concentration was detected (Figure. 6.2B and Figure 6.3). The re-solubilisation of phosphate was barely observed but indicated from the increase of POP after SRP was depleted (Figure 6.3). There is a concern that the re-solubilisation rate of precipitated phosphate might limit the rate of P uptake. Additionally, according to the Redfield ratio (N:P=16:1), media based upon f/2 macro-nutrients (N:P=24:1) tend towards being P-limiting at the end of culture. Although P limitation is able to decrease N:C ratio (Flynn 2008) and thereby increase lipid content in some

oily species (Reitan *et al.*, 1994; Lynn *et al.*, 2000; Chen *et al.*, 2011), the complexity of phosphate dynamics needs to be clarified before P can be used as a reliable parameters to interpret the biomass productivity.

6.4.3 Simulating biochemicals using C:N ratios

Elemental stoichiometry is often used in models to explain the growth status of organism and their interactions in the ecosystem (e.g. Flynn, 2001; Mitra and Flynn, 2006). The simulation results agree well with the data for both N:C and P:C in general (Figure 6.5). With the concept of CN_{core} described in Chapter 5, algal C can be separated into two major groups, nitrogenous-C and non-nitrogenous-C. It is upon this core component that growth depends as it defines the proteinaceous biochemical machinery that drives growth. As it is “diluted” by excess C accumulating during N-starvation the growth rate declines, halting when cellular CN attains a maximum value (i.e., when the model state variable describing cellular N:C attains the minimum quota). Concurrent with the rise in CN_{cell} , there is a redirection of newly fixed C to synthesize the non-nitrogenous C “storage” lipid and carbohydrate (Flynn *et al.*, 1992; Livne and Sukenik, 1992; Larson and Rees, 1996). The non-nitrogenous C group (lipid+carbohydrate) derived from CN ratio is well described by the model (Figure 6.6).

While the accumulation of excess-C (XS-C) described in the model has not been partitioned into specific chemical groups (e.g., neutral lipid or carbohydrate). If one assumed that carbohydrate is the main chemical accumulated in the modelled XSC group, then the model cannot well describe such a fraction (Figure 6.6). It is probably that carbohydrate is not the only excess-C that accumulated during the group. As demonstrated for other microalgae such as *Isochrysis galbana*, neutral lipid and carbohydrate are both accumulated under N limitation (Lacour *et al.*, 2012; Recht *et al.*, 2012). Interrelationships between these two chemical groups remain unclear. Excess-C can be transformed into neutral lipid when starch synthesis is inhibited (Li *et al.*, 2010). Alternatively, inhibition of the synthesis of fatty acid may result in less

carbohydrate being accumulated (Recht *et al.*, 2012). It is of little use to describe the accumulation of certain chemicals with unknown interchangeable mechanism using Michaelis–Menten equations, although it is an enzymatic related function. The CN ratio has been applied for several models of neutral lipid synthesis under steady-state and dynamic conditions in laboratory scale experiments (Mairet *et al.*, 2011; Packer *et al.*, 2011). The model has the potential to partition the forms of excess-C into neutral lipid and carbohydrates. However, modelling the accumulation of excess-C offers a convenient generic approach to optimize the potential production of C-rich products for different purposes.

Partitioning between different forms of excess-C is a taxon-specific activity. For aquaculture and biofuel purposes, selected algal strains are grown to provide particular chemical compositions. At the extreme, one could consider a genetically modified microalga producing all excess-C as lipid or carbohydrate as one chemical class (Li *et al.*, 2010).

6.4.4 Model applications and limitations

The model used here had successfully described most of the data point in this dynamic batch culture. The same type of model has been used successfully for various other simulations (e.g. Flynn 2008a,b; Flynn *et al.*, 2013 in express). Unlike a steady-state model which can only described a fix growth stage, the dynamic model is designed for a changing condition. Algal cultures rarely achieve steady-state growth under natural environment. Operations of steady-state cultures with continuous dilutions are often costly in large scale cultivation. A comprehensive model with the capability of modelling the batch culture in changing environment is urgently needed to evaluate the reliability of the production in large scale system. In addition to the estimation of the productivity of the system, the growth stage can be monitoring by interpretation of the physiological parameters. Powerful physiological parameters (e.g. CN ratio) can be coupled with models describing the physical-chemical conditions for *in situ* simulation of the organisms in response to

changing culture condition. Prediction of cellular chemical products from cell physiological status is given more information to explore the use of algal biomass, which may make the biofuel from microalgae more reliable in large scale system.

The model presented here is intended to predict the internal changes of physiological status as response from the elemental stoichiometry via external dynamic conditions. However, building a complete model with capability of describing light, nutrient, temperature and pH effects are still in their infancy. The present model study shows the complexity of interactions between limiting factors during a dynamic growth of *Nannochloropsis oculata*, although the effects of limiting factors (e.g. DIC, nutrients) can be minimised via operations, the lack of knowledge of the interactions between these environmental factors and of comprehensive datasets is limiting the development and testing of mechanistic models. Noticeably, the photoacclimation part in our model does not incorporate the ability to describe photoinhibition which is potentially found in shallow optical depth bioreactors or raceway ponds during initial batch growth. The next generation of model should be able to explicit the interaction of light and nutrient availability in terms of their effects on growth rate. Another predominate factor that should be incorporated is temperature, which is closely linked to the irradiances. In reality, the dynamic of these limiting factors interact to shape the growth of organisms and their communities.

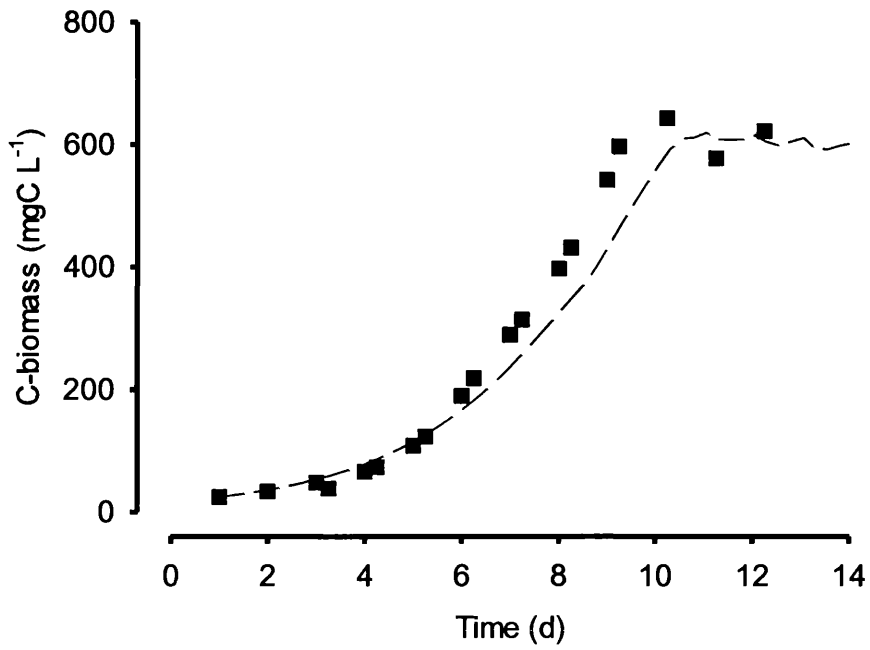


Figure 6.1 Simulation results and data (■) of C-biomass.

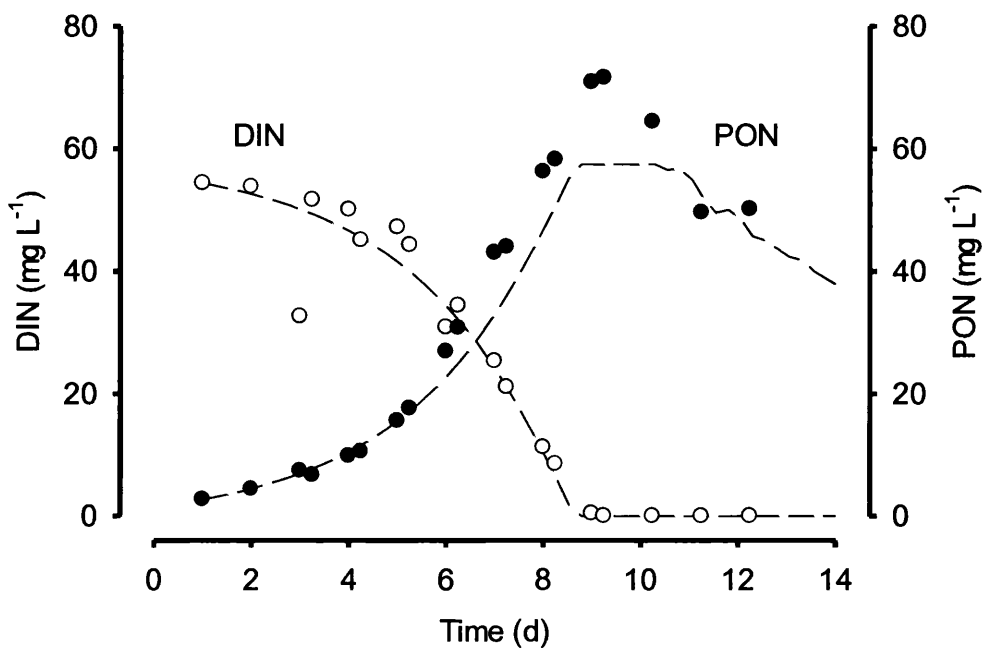


Figure 6.2: Simulation results of N-uptake from DIN (nitrate+nitrite) to particulate organic nitrogen (PON). (○) DIN (nitrate+nitrite); (●) PON; Dash line presented as model fit.

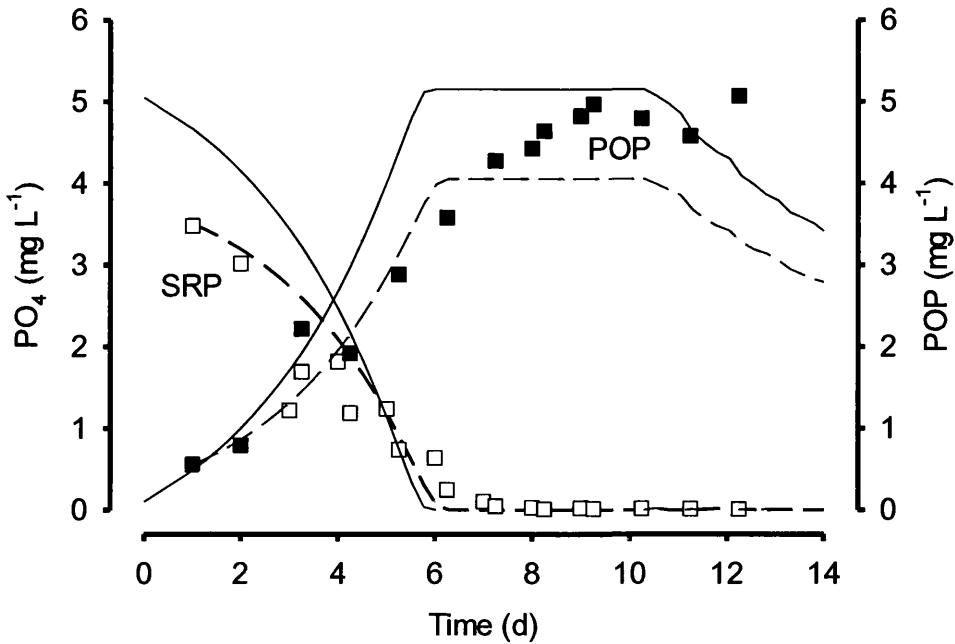


Figure 6.3: Simulation results versus data of P- uptake. (□) Soluble reactive phosphate (SRP); (■) Particular organic phosphorus (POP); Dash line presented as the simulation result using SRP in the medium; Solid line presented as the simulation result using initial phosphate concentration that added in.

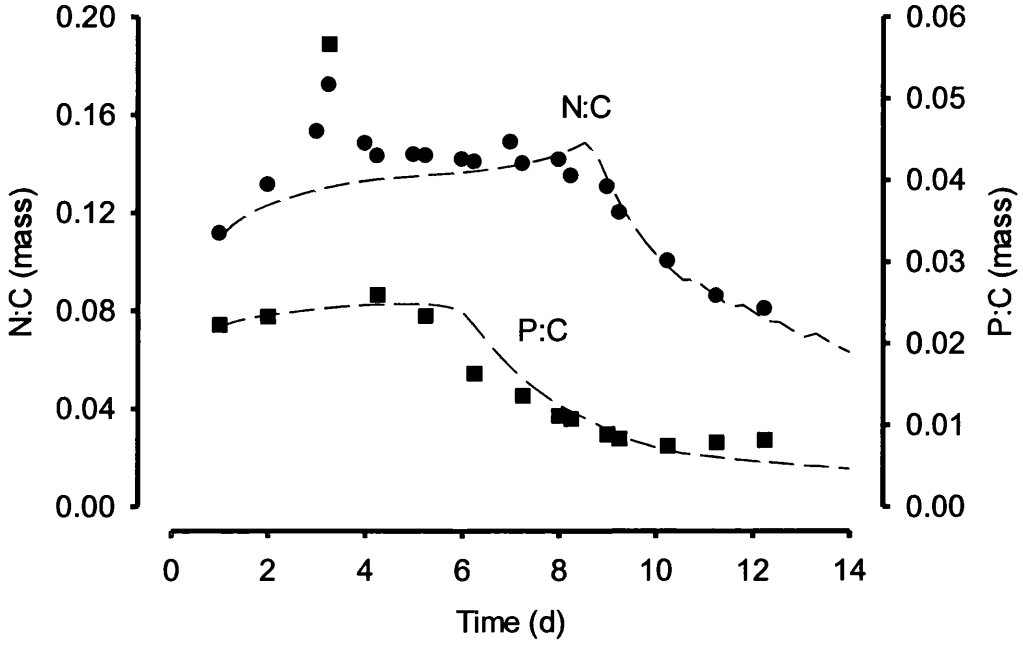


Figure 6.4: Simulation results versus data of N:C and P:C. (●)N:C; (■)P:C; Dash line presented as model fit.

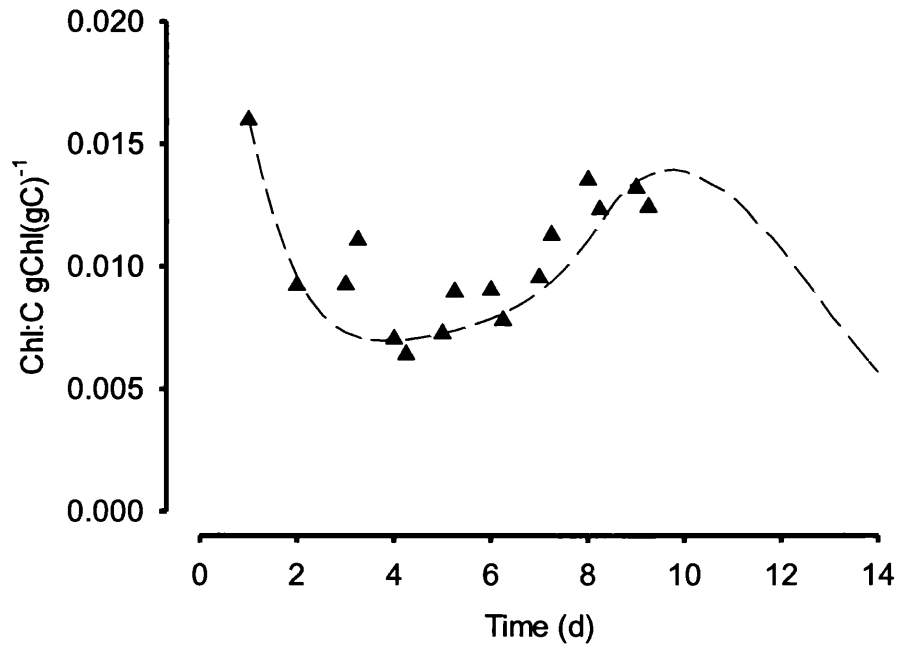


Figure 6.5: Simulation results versus data of Chl:C ratio. Dash line presented as the model fit.

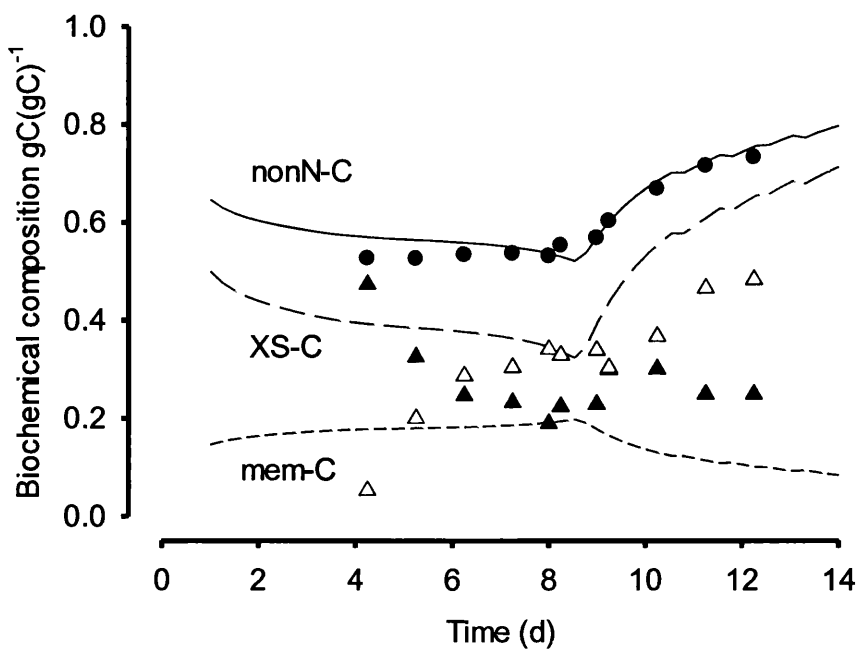


Figure 6.6: Simulation results versus data of cellular biochemical composition. (●) non-nitrogenous C (lipid-C+carbohydrate-C, nonN-C); Solid line as model fit to the nonN-C. (△) carbohydrate; long dash line as modelled XS-C content. (▲) lipid; short dash line as modelled membrane-C (mem-C).

Table 6.1: Physical-chemical parameters set in the model simulation.

Parameters	Descriptions	Values	Unit
PFD	Surface photon flux density	250	$\mu\text{mol photons m}^{-2} \text{s}^{-1}$
Mix_depth	Diameter of the culture vessel	0.03	m
Ini_BV	Initial bioreactor volume (including volume of inoculums)	660	l
Tank	Standard volume of the bioreactor	600	l
Flow	Fresh medium flow in semi-continuous mode	6.25	l/hr
f2NO₃	Concentration of NO ₃ in f/2 medium	882	$\mu\text{mol/l}$
f2P	Concentration of P in f/2 medium	36.2	$\mu\text{mol/l}$
AMP	Nutrient concentration amplifier (multiplier of the f/2 composition)	5	Dimensionless

Table 6.2: List of constants used in the model simulation

Parameters	Descriptions	Values	Unites
ChlCm	Maximum chlorophyll carbon ratio	0.06	$\text{gChl}(\text{gC})^{-1}$
M	Photoacclination rate coefficient	0.55	Dimensionless
NCabs	Absolute maximum NC ratio	0.22	$\text{gN}(\text{gC})^{-1}$
NCm	Maximum NC ratio	0.16	$\text{gN}(\text{gC})^{-1}$
NCo	Minimum NC ratio	0.033	$\text{gN}(\text{gC})^{-1}$
NKu	Half saturation constant of N transportation	2.59	$\mu\text{mol/L}$
KQN	quota control constant for N	12	Dimensionless
PCabs	Abslue PC ratio	0.045	$\text{gP}(\text{gC})^{-1}$
PCm	Maximum PC ratio	0.028	$\text{gP}(\text{gC})^{-1}$
PCo	Minimum PC ratio	0.0027	$\text{gP}(\text{gC})^{-1}$
PKu	Half saturation constant of P transportation	4.76	$\mu\text{mol/l}$
Qh	Uptake feedback control Hill number	1.5	Dimensionless
Um	Maximum growth rate	0.617	d^{-1}

7. Conclusion

A comprehensive study was presented with coupling experimental and modelling study in microalgal cultivation of *Nannochloropsis oculata*. Experimental study again reveals the difficulty in mass cultivation primarily due to the low productivity. However, the datasets were used to inform the development of algal growth models. The microalgal growth model mimicking the PBR system fits the dataset generally well. Model simulation suggest species with high maximum growth rate and low minimum cellular N:C ratio are able to obtain high biofuel productivity in shallow mixing depth system. In comparison with culture under natural light-dark cycle, the biofuel productivity of culture with continuous light can achieve nearly 10 fold higher under different combination of mixing depth and dilution rate. The implication from the modelling study suggests the potential of scale-up the mass culture by selecting the genetically modified species as well as changing the operational scheme.

Fatty acid composition of *Nannochloropsis oculata* in relation to elemental stoichiometry are further studied. The fatty acid composition is closely linked to the nutrient status (i.e. C:N). It is important to discriminate the effects between N and P limitation (and likely also light limitation) during growth. The decrease of N:C and P:C to some extent (nutrient stress) may not necessarily indicate a low PUFA content and further be implicated in a deterioration in food quality. Photoacclimation processes also play an important role in regulation of PUFA as well as EPA synthesis in *Nannochloropsis oculata*. However, N:C ratios may be better and more reliable indicators for total fatty acid content, and potentially PUFA content under N-stress condition (Figure 4.2). A fine tuning of N:C ratios is expected to optimize the total fatty acid content. Chl:C could potentially be used as an indicator for EPA and PUFA content in *Nannochloropsis oculata*. However, as the correlation between elemental stoichiometry and fatty acid composition indicates, single elemental ratios alone may

not be an effective indicator of cellular fatty acid contents and hence food quality. C partitioning into different biochemical groups (Anderson *et al.*, 2004) may well be desirable (if not essential) in culture systems where natural illumination likely results in unpredictable changes in overall physiological responses.

Using a bulk description of energy reserve (excess-C), the model can be used to evaluate the potential biomass and biofuels production while the development of a fully functional model of microalgae growth capable of describing biochemical stoichiometry is still in its infancy. Prediction of microalgal growth in PBR is the fundamental work to evaluate the productivity of the system, while numerical models may work as a tool in optimisation the productivity of target chemicals. The work described here indicates the potential value and scope of developing the functional model of microalgae growth for biofuels and valuable chemicals production. Modelling technique is a powerful tool in prediction and optimisation of system productivity.

References:

- Adarme-vega, T. C., Lim, D. K. Y., Timmins, Matthew, F., et al. (2012) Microalgal biofactories: a promising approach towards sustainable omega-3 fatty acid production. *Microb. Cell. Fact.* **11**, 96
- Amin S (2009). Review on biofuel oil and gas production processes from microalgae. *Energ. Convers. Manag.* **50**, 1834-1840
- Anderson, T. R., Boersma, M. and Raubenheimer, D. (2004) Stoichiometry: Linking elements to biochemicals. *Ecology*, **85**, 1193-1202.
- Anderson, R. A. (2005) Algal culturing technique. Elsevier Academic Press, Burlington, U.S.A
- Anning, T., Macintyre, H. L., Pratt, S. M., Sammes, P. J., Gibb, S. & Geider, R. J. 2000 Photoacclimation in the marine diatom *Skeletonema costatum*. *Limnol. Oceanogr.* **45**, 1807–1817.
- Beckmann, J., Lehrb, F., Finazzic, G., Hankamerd, B., Postenb, C., Wobbee, L. & Krusea, O. 2009 Improvement of light to biomass conversion by de-regulation of light-harvesting protein translation in *Chlamydomonas reinhardtii*. *J. Biotech.* **142**, 70–77.
- Beer, L. L., Boyd, E. S., Peters, J. W. & Posewitz, M. C. 2009 Engineering algae for biohydrogen and biofuel production. *Curr. Opin. Biotech.* **20**, 264-271.
- Berdalet, E., Latasa, M. and Estrada, M. (1994) Effects of nitrogen and phosphorus starvation on nucleic-acid and protein-content of *Heterocapsa sp.* *J. Plankton Res.*, **16**, 303-316.

-
- Berman, T and Chava, S (1999) Algal growth on organic compounds as nitrogen sources. *J. Plankton. Res.* **21**, 1423-1437
- Borowitzka, M. A. (1995) Microalgae as sources of pharmaceuticals and other biologically-active compounds. *J. App. Phycol.* **7**, 3-15
- Brett, M. T. and Muller-Navarra, D. C. (1997) The role of highly unsaturated fatty acids in aquatic food web processes. *Freshwater biol.* **38**, 483-499
- Brown, M.R., Jeffrey, S.W., Volkman, J.K., Dunstan, G.A. (1997) Nutritional properties of microalgae for mariculture. *Aquaculture.* **151**, 315-331
- Burmester, D. E. (1979). The unsteady continuous culture of phosphate-limited *Monochrysis lutheri* Droop: experimental and theoretical analysis. *J. Exp. Mar. Biol. Ecol.* **39**, 167–186
- Caperon, J. and Meyer, J. (1972) Nitrogen-limited growth of marine phytoplankton .2. Uptake kinetics and their role in nutrient limited growth of phytoplankton. *Deep-Sea Res.*, **19**, 619-632.
- Chen C.Y., Yeh K.L., Aisyah R., Lee D.J. & Chang J.S. 2011 Cultivation, photobioreactor design and harvesting of microalgae for biodiesel production: A critical review. *Bioresour. Technol.* **102**, 71-81
- Chen, M., Tang, H. Y., Ma, H. Z., et al. (2011) Effect of nutrients on growth and lipid accumulation in the green algae *Dunaliella tertiolecta*. *Bioresour. Technol.* **102**, 1649-1655
- Chisti, Y. (2007) Biodiesel from microalgae. *Biotechnol. Adv.*, **25**, 294-306.
- Christie, W.W., 2003. Lipid Analysis, 3rd Edition; The Oily Press, Bridgewater, UK. pp. 205-224.

-
- Clark, D. R., Flynn, K. J. and Owens, N. J. P. (2002) The large capacity for dark nitrate-assimilation in diatoms may overcome nitrate limitation of growth. *New Phytol.*, **155**, 101-108.
- Clarens, A. F., Resurreccion, E. P., White, M. A., & Colosi, L. M. 2010 Environmental life cycle comparison of algae to other bioenergy feedstock, *Environ. Sci. Technol.*, **44**, 1813–1819.
- Courchesne, N. M. D., Parisien, A., Wang, B. & Lan, C. Q. 2009 Enhancement of lipid production using biochemical, genetic and transcription factor engineering approaches *J. Biotech.* **141**, 31–41.
- Davidson, K., Flynn, K. J. and Cunningham, A (1991) Relationships between photopigments, cell carbon, cell nitrogen and growth-rate for a marine nanoflagellate. *J. Exp. Mar. Bio. Eco.* **153**, 87-96
- Davidson, K., Flynn, K. J. and Cunningham, A. (1992) Non-steady state ammonium-limited growth of the marine phytoflagellate *Isochrysis galbana* Parke. *New Phytol.*, **122**, 433-438.
- Demadariaga, I. and Joint, I. (1992) A comparative-study of phytoplankton physiological indicators. *J. Exp. Mar. Biol. Ecol.*, **158**, 149-165.
- Droop, M. R. 1968 Vitamin B12 and marine ecology. IV. The kinetics of uptake, growth, and inhibition in *Monochrysis lutheri*. *J. Mar. Biol. Assoc. U.K.* **48**, 689–733.
- Droop, M. R. (1974) Nutrient status of algal cells in continuous culture. *J. Mar. Biol. Assoc. U.K.* **54**, 825-855
- Dortch, Q. (1990) The interaction between ammonium and nitrate uptake in phytoplankton. *Mar Ecol Prog Ser.* **61**, 183-201

-
- Eriksen, N. T. (2008) The technology of microalgal culturing. *Biotechnol. Lett.* **30**, 1525-1536
- Fabregas, J., Maseda, A., Dominguez, A., *et al.* (2004) The cell composition of *Nannochloropsis* sp changes under different irradiances in semicontinuous culture. *World. J. Microb. Biot.* **20**, 31-35
- Falkowski, P. G., Sukenik, A., Herzig, R. (1989) Nitrogen limitation in *Isochrysis-galbana* (Haptophyceae) 2. relative abundance of chloroplast proteins. *J Phycol.* **25**, 471-478
- Falkowski, P. G. and Raven, J. A. (1997). Aquatic photosynthesis. Blackwell Science, London.
- Fasham, M. J. R., Flynn, K. J., Pondaven, P., Anderson, T. R. & Boyd, P. W. 2006 Development of a robust ecosystem model to predict the role of iron on biogeochemical cycles: a comparison of results for iron-replete and iron-limited areas, and the SOIREE iron-enrichment experiment. *Deep-Sea Res. I* **53**, 333-366.
- Fernandez, F.G.A., Camacho, F. G., Perez, J.A.S. *et al.*, (1998) Modelling of biomass productivity in tubular photobioreactors for microalgal cultures: effects of dilution rate, tube diameter, and solar irradiance. *Biotechnol. Bioeng.* **58**, 605-616
- Ferguson, J. F., Jenkins, D and Eastman, J (1973) Calcium phosphate precipitation at slightly alkaline pH values. *Journal (Water Pollution Control Federation)*. **45**, 620-631
- Fidalgo, J. P., Cid, A., Torres, E., *et al.* (1998) Effects of nitrogen source and growth phase on proximate biochemical composition, lipid classes and fatty acid profile of the marine microalga *Isochrysis galbana*. *Aquaculture*. **166**, 105-116

-
- Finkel, Z. V., Beardall, J., Flynn, K. J., Quigg, A., Rees, T. a. V. and Raven, J. A. (2010) Phytoplankton in a changing world: Cell size and elemental stoichiometry. *J. Plankton Res.*, **32**, 119-137.
- Flynn, K. J. and Butler, I (1986) Nitrogen source for the growth of marine microalgae: role of dissolved free amino acids. *Mar Ecol Prog Ser.* **34**, 281-304
- Flynn, K. J., Garrido, J. L., Zapata, M., Opik, H. and Hipkin, C. R. (1992) Changes in fatty acids, amino-acids and carbon nitrogen biomass during nitrogen starvation of ammonium-grown and nitrate grown *Isochrysis galbana*. *J. Appl. Phycol.*, **4**, 95-104.
- Flynn, K. J., Davidson, K., Cunningham, A. (1993) Relations between carbon and nitrogen during growth of *Nannochloropsis oculata* (droop) hibberd under continuous illumination. *New Phytol.* **125**, 717-722
- Flynn, K. J. Fasham, M. J. and Hipkin, C.R. (1997) Modelling the interactions between ammonium and nitrate uptake in marine phytoplankton. *Phil. Trans. R. Soc. Lond. B* **352**, 1625-1645
- Flynn, K.. J.and Flynn,,K. (1998) The release of nitrite by marine dinoflagellates development of a mathematical simulation. *Mar. Biol.* **130**, 455–470.
- Flynn, K. J. & Hipkin, C. R. (1999) Interactions between iron, light, ammonium and nitrate; insights from the construction of a dynamic model of algal physiology. *J. Phycol.* **35**, 1171-1190.
- Flynn, K. J. and Berry, L. S (1999) The loss of organic nitrogen during marine primary production may be significantly over estimated when using ¹⁵N substrates. *Proc. R. Soc. Lond. B* **266**, 641-647

-
- Flynn, K. (2001) A mechanistic model for describing dynamic multi-nutrient, light, temperature interactions in phytoplankton. *J. Plankton Res.*, **23**, 977-997.
- Flynn, K. J., Marshall, H. & Geider, R. J. 2001 A comparison of two N-irradiance models of phytoplankton growth. *Limnol. Oceanogr.* **46**, 1794-1802.
- Flynn, K. J. (2002) How critical is the critical N:P ratio? *J. Phycol.* **38**, 961-970.
- Flynn KJ, Clark DR, Owens NJP (2002) Modelling suggests that optimization of dark nitrogen-assimilation need not be a critical selective feature in phytoplankton. *New Phytologist* **155**; 109-119.
- Flynn, K. J. (2003) Modelling multi-nutrient interactions in phytoplankton; balancing simplicity and realism. *Prog. Oceanogr.*, **56**, 249-279.
- Flynn, K. J. (2008a) Use, abuse, misconceptions and insights from quota models - the droop cell quota model 40 years on. *Oceanogr. Mar. Biol.*, **46**, 1-23.
- Flynn, K. J. (2008b) The importance of the form of the quota curve and control of non-limiting nutrient transport in phytoplankton models. *J. Plankton Res.*, **30**, 423-438.
- Flynn, K. J., Clark, D. R. & Xue, Y. (2008) Modelling the release of dissolved organic matter by phytoplankton. *J. Phycol.* **44**, 1171-1187
- Flynn, K. J. (2009) Going for the slow burn: why should possession of a low maximum growth rate be advantageous for microalgae? *Plant Ecol. Diversity* **2**, 179-189.
- Flynn, K. J. (2010) Do external resource ratios matter? Implications for modelling eutrophication events and controlling harmful algal blooms. *J. Mar. Sys.* **83**, 170-180

-
- Flynn, K. J., Greenwell, H. C., Lovitt, R. W. and Shields, R. J. (2010) Selection for fitness at the individual or population levels: Modelling effects of genetic modifications in microalgae on productivity and environmental safety. *J. Theor. Biol.*, **263**, 269-280.
- Flynn, K. J., Mitra, A., Greenwell, H. C. and Sui, J. (2013) Monster potential meets potential monster: pros and cons deploying genetically modified microalgae for biofuels production. *Interface Focus* 3 in express
- Folch J, Lees M and Sloane-Stanley GH 1957. A simple method for the isolation and purification of total lipids from animal tissues. *J. Biol. Chem.*, **226**, 497-509.
- Greenwell, H. C., Laurens, L. M. L., Shields, R. J., Lovitt, R. W. and Flynn, K. J. (2010) Placing microalgae on the biofuels priority list: A review of the technological challenges. *J. R. Soc. Interface*, **7**, 703-726.
- Geider, R. J.; Macintyre, H. L., Kana, T. M. (1998) A dynamic regulatory model of phytoplanktonic acclimation to light, nutrients, and temperature. *Limnol. Oceanogr.* **43**, 679-694
- Geider, R. J. and La Roche, J. (2002) Redfield revisited: Variability of C : N : P in marine microalgae and its biochemical basis. *Eur. J. Phycol.*, **37**, 1-17.
- Ghioni, C., Bell, J.G., Sargent, J.R., 1996. Polyunsaturated fatty acids in neutral lipids and phospholipids of some freshwater insects. *Comp. Biochem. Physiol.* **114B**, 161-170.
- Guillard, R. L. L. & Ryther, J. H. 1962. Studies on marine planktonic diatoms I. *Cyclotella nana* Hustedt and *Detonula confervacea* (Cleve). *Trans Can J Microbiol* **8**, 229-239.

-
- Guschina, I. A. and Harwood, J. L. (2006) Lipids and lipid metabolism in eukaryotic algae. *Prog. Lipid Res.*, **45**, 160-186.
- Haefner, J. W. (1996) Modelling biological systems: Principles and applications. Chapman&Hall, New York.
- Harrison, P. J. Parslow, J. S. and Conway, H. L. (1989) Determination of nutrient uptake kinetic parameters- A comparison of methods. *Mar Ecol Prog Ser.* **52**, 301-312
- Hessen, D (1992) Nutrient element limitation of zooplankton production. *Amer. Nat.* **140**, 799-814
- Hessen, D., Faerovig, P. J., Andersen, T. (2002) Light, nutrients, and P: C ratios in algae: grazer performance related to food quality and quantity. *Ecology.* **83**, 1886-1898
- Hodgson, P. A., Henderson, R. J., Sargent, J. R., et al. (1991) Patterns of variation in the lipid class and fatty-acid composition of *Nannochloropsis-oculata* (eustigmatophyceae) during batch culture. 1. The growth-cycle. *J. App. Phycol.* **3**, 169-181
- Hu, Q., Sommerfeld, M., Jarvis, E. et al. (2008) Microalgal triacylglycerols as feedstocks for biofuel production: perspectives and advances. *Plant J.* **54**, 621-639
- Huang, G. H., Chen, F., Wei, D. et al. (2010) Biodiesel production by microalgal biotechnology. *App Engerg*, **87**, 38-46
- Huerlimann, R., de Nys Rocky and Heimann K. (2010) Growth, lipid content, productivity, and fatty acid composition of tropical microalgae for scale-up production . *Biotechnol. Bioemg.* **107**, 245-257

-
- Inskip and Bloom (1985) Extinction Coefficients of Chlorophyll a and b in N,N-Dimethylformamide and 80% Acetone. *Plant Physiol.* **77**, 483-485
- James, G.O., Hocart, C.H., Hillier, W., et al. (2011) Fatty acid profiling of *Chlamydomonas reinhardtii* under nitrogen deprivation *Bioresource Technol.* **102**, 3343-3351
- Jassby, A. D. and Platt, T. (1976) Mathematical formulations of the relationship between photosynthesis and light for phytoplankton. *Limnol. Oceanogr.*, **21**, 540–547.
- Jeffrey, S. W. and Humphrey, G. F. (1975) New spectrophotometric equations for determining chlorophylls a, b, c1 and c2 in higher plants, algae and natural phytoplankton. *Biochem. Physiol. Pflanzen.* **167**, 191 – 194.
- Jimenez, C. Cossio, B. R. Niell, F. X., (2003) Relationship between physicochemical variables and productivity in open ponds for the production of *Spirulina*: a predictive model of algal yield, *Aquaculture*, **221**, 331–345.
- John, E. H. and Flynn, K. J. (2000) Modelling phosphate transport and assimilation in microalgae; how much complexity is warranted? *Ecol. Model.*, **125**, 145-157.
- Jones, R. H and Flynn, K. J. (2005) Nutritional status and diet composition affect the value of diatoms as copepod prey. *Science.* **307**, 1457-1459
- Kruskopf, M. and Flynn, K. J. (2006) Chlorophyll content and fluorescence responses cannot be used to gauge reliably phytoplankton biomass, nutrient status or growth rate. *New Phytol.*, **169**, 525-536.
- Larson, T. R. and Rees, T. a. V. (1996) Changes in cell composition and lipid metabolism mediated by sodium and nitrogen availability in the marine diatom *Phaeodactylum tricoratum* (Bacillariophyceae). *J. Phycol.*, **32**, 388-393.

-
- Levasseur, M., Thompson, P. A. and Harrison, P. J. (1993) Physiological acclimation of marine-phytoplankton to different nitrogen-sources. *J. Phycol.*, **29**, 587-595.
- Li, Y. T., Han, D. X., Hu, G. R., Sommerfeld, M. and Hu, Q. A. (2010) Inhibition of starch synthesis results in overproduction of lipids in *Chlamydomonas reinhardtii*. *Biotechnol. Bioeng.*, **107**, 258-268.
- Li, Y. T., Han, D. X., Sommerfeld, M. and Hu, Q. A. (2011) Photosynthetic carbon partitioning and lipid production in the oleaginous microalga *Pseudochlorococcum* sp (Chlorophyceae) under nitrogen-limited conditions. *Bioresource Technol.*, **102**, 123-129.
- Lourenco, S. O., Marquez, U. M. L., Mancinifilho, J., Barbarino, E. and Aidar, E. (1997) Changes in biochemical profile of *Tetraselmis gracilis*. 1. Comparison of two culture media. *Aquaculture*, **148**, 153-168.
- Lynn, S. G., Kilham, S. S., Kreeger, D. A. and Interlandi, S. J. (2000) Effect of nutrient availability on the biochemical and elemental stoichiometry in the freshwater diatom *Stephanodiscus minutulus* (Bacillariophyceae). *J. Phycol.*, **36**, 510-522.
- Liang, Y., Beardall, J., Heraud, P. (2006) Changes in growth, chlorophyll fluorescence and fatty acid composition with culture age in batch cultures of *Phaeodactylum tricornerutum* and *Chaetoceros muelleri* (Bacillariophyceae). *Bot. Mar.* **49**, 165-173
- Lin, Q. and Lin, J. D. (2011) Effects of nitrogen source and concentration on biomass and oil production of a *Scenedesmus rubescens* like microalga *Bioresource Technol.* **102**, 1615-1621

-
- Laws, E. A. and Bannister T. T. (1980) Nutrient and light limited growth of *Thalassiosira fluviatilis* in continuous culture, with implications for phytoplankton growth in the ocean. *Limnol. Oceanogr.* **25**, 457-473
- Leonardos, N. and Geider, R. J. (2004) Responses of elemental and biochemical composition of *Chaetoceros mulleri* to growth under varying light and nitrate: phosphate supply ratios and their influence on critical N:P. *Limnol. Oceanogr.* **49**, 2105-2114
- Lourenco, S. O., Barbarino, E. Mancini-Filho, J. et al. (2002) Effects of different nitrogen sources on the growth and biochemical profile of 10 marine microalgae in batch culture: an evaluation for aquaculture. *Phycologia.* **41**, 158-168
- Livne, A. and Sukenik, A. (1992) Lipid synthesis and abundance of acetyl-coA carboxylase in *Isochrysis galbana* (Prymnesiophyceae) following nitrogen starvation. *Plant Cell l Physiol*, **33**, 1175-1181
- Lacour, T., Sciandra, A., Talec, A et al., (2012) Neutral lipid and carbohydrate productivity as a response to nitrogen status in *Isochrysis* sp. (T-ISO; Haptophyceae): starvation versus limitation. *J. Phycol.* **48**, 647-656
- Macintyre, H. L., Kana, T. M., Anning, T. & Geider, R. J. 2002 Photoacclimation of photosynthesis irradiance response curves and photosynthetic pigments in microalgae and cyanobacteria. *J. Phycol.* **38**, 17-38.
- Mairet, F., Bernard, O., Masci, P., et al., (2011) Modelling neutral lipid production by the microalga *Isochrysis galbana* under nitrogen limitation. *Biores. Technol.* **102**, 142-149
- Malzahn, A. M., Abele, N., Clemmesen, C., Boersma. M (2007) Nutrient limitation of primary producers affects planktivorous fish condition. *Limnol. Oceanogr.* **52**, 2062-2071

-
- Mata, M. T., Martins, A. A. and Caetano N. S. (2010) Microalgal for biodiesel production and other applications: A review. *Renew. Sust. Energ. Rev.* **14**, 217-232
- Markou, G. Angelidaki, I. and Georgakakis, D. (2012) Microalgal carbohydrates: an overview of the factors influencing carbohydrates production, and of main bioconversion technologies for production of biofuels. *Appl Microbiol Biotechnol.* **96**, 631–645
- Meiser, A., Schmid-Staiger, U. and Trosch, W. (2004) Optimization of eicosapentaenoic acid production by *Phaeodactylum tricornutum* in the flat panel airlift (FPA) reactor. *J. App.Phycol.* **16**, 215-225
- Melis, A. 2009 Solar energy conversion efficiencies in photosynthesis: Minimizing the chlorophyll antenna to maximize efficiency. *Plant Sci.* **177**, 272–280.
- Mitra, A. and Flynn, K. J. (2006) Promotion of harmful algal blooms by zooplankton predatory activity. *Biol. Lett.*, **2**, 194-197.
- Mizusawa, N. and Wada, H (2012) The role of lipids in photosystem II. *Biochim. Biophys. Acta.* **1817**, 194-208
- Montagnes, D. J. S., Berges, J. A., Harrison, P. J. et al., (1994) Estimating carbon, nitrogen, protein, and chlorophyll a from volume in marine phytoplankton. *Limnol. Oceanogr.* **39**, 1044-1060
- Muller-Navarra, D. C., Brett, M. T., Liston, A. M., et al (2000) A highly unsaturated fatty acid predicts carbon transfer between primary producers and consumers. *Nature* **403**, 74-77

-
- Murphy, T. E. and Berberoglu, H. (2011) Effect of algae pigmentation on photobioreactor productivity and scale-up: A light transfer perspective. *J. Quant. Spectrosc. Radiat. Transfer.* **112**, 2826–2834
- Olsen, L. M. Ozturk, M, Sakshaug, E. et al. (2006) Photosynthesis-induced phosphate precipitation in seawater: ecological implications for phytoplankton. *Mar Ecol Prog Ser.* **319**, 103-110
- Packer, A., Li, Y. T., Anderson, T. et al., (2011) Growth and neutral lipid synthesis in green microalgae: A mathematical model. *Biores Technol.* **102**, 111-117
- Page, S., Hipkin, C.R. and Flynn, K.J. (1999) Interactions between nitrate and ammonium in *Emiliana huxleyi*. *J. Exp. Mar. Biol. Ecol.* **236**, 307-319
- Park, S; Brett, M. T., Muller-Navarra, D. C., et al. (2002) Essential fatty acid content and the phosphorus to carbon ratio in cultured algae as indicators of food quality for *Daphnia*. *Freshwater Biol.* **47**, 1377-1390
- Radakovits, R. Jinkerson, R. E., Darzins, A. & Posewitz, M. C. 2010 Genetic engineering of algae for enhanced biofuel production. *Eukaryotic cell* **9**, 486-501.
- Ramos M. J., Fernandez, C. M., Casas, A. et al. (2009) Influence of fatty acid composition of raw materials on biodiesel properties. *Bioresource Technol.* **100**, 261-268
- Recht, L., Zarka, A. and Boussiba, S. (2012) Patterns of carbohydrate and fatty acid changes under nitrogen starvation in the microalgae *Haematococcus pluvialis* and *Nannochloropsis* sp. *Appl microbial Biotechnol.* **94**, 1495-1503
- Redfield, A. C. (1958) The biological control of chemical factors in the environment. *Am. Sci.*, **46**, 205-221.

-
- Reitan, K. I., Rainuzzo, J. R. and Olsen, Y. (1994) Effect of nutrient limitation on fatty-acid and lipid-content of marine microalgae. *J. Phycol.*, **30**, 972-979.
- Richardson, K., Beardall, J., Raven, J. R. (1983) Adaptation of unicellular algae to irradiance - an analysis of strategies. *New phytol.* **93**, 157-191
- Richmond A. (1992) Open systems for the mass production of photoautotrophic microalgae outdoors: physiological principles *J. Appl. Phycol.*, **4**, 281-286
- Richmond, A. and Cheng-Wu, Z. (2001) Optimization of a flat plate glass reactor for mass production of *Nannochloropsis* sp. Outdoors, *J. Biotechnol.*, **85**, 259–269.
- Richmond, A. (2004) Principles for attaining maximal microalgal productivity in photobioreactors: an overview, *Hydrobiologia*, **512**, 33–37
- Rodolfi, L., Zittelli, G. C., Bassi, N., et al. (2009) Microalgae for oil: strain selection, induction of lipid synthesis and outdoor mass cultivation in a low-cost photobioreactor. *Biotechnol. Bioeng.* **102**, 100-112
- Schneider, J. C. and Roessler, P. (1994) Radiolabeling studies of lipids and fatty-acids in *Nannochloropsis* (eustigmatophyceae), an oleaginous marine alga. *J. Phycol.* **30**, 594-598
- Schneider, J. C., Livne, A., Sukenik, A., et al. (1995) A mutant of *Nannochloropsis* deficient in eicosapentaenoic acid production. *Phytochem.* **40**, 807-814
- Shifrin, N. S. and Chisholm, S. W. (1981) Phytoplankton lipids - interspecific differences and effects of nitrate, silicate and light-dark cycles. *J. Phycol.*, **17**, 374-384.
- Slegers, P. M., Wijffels, R.H., van Straten, G., van Boxtel, A. J. B (2011) Design scenarios for flat panel photobioreactors. *Appl. Energ.*, **88**, 3342-3353

-
- Smith, E. L. (1936). Photosynthesis in relation to light and carbon dioxide. *Proc. Natl. Acad. Sci. USA.* **20**, 177-184.
- Solovchenko et al (2008). Effects of light intensity and nitrogen starvation on growth, total fatty acids and arachidonic acid in the green microalga *Parietochloris incisa*, *J. App. Phycol* **20**, 245-251
- Spolaore, P, Joannis-Cassan, C, Duran, E, Isambert, A (2006) Commercial applications of microalgae. *J. Biosci. Bioeng.* **101**. 87-96
- Stansell, G. R., Gray, V. M., Sym, S.D. (2012) Microalgal fatty acid composition: implications for biodiesel quality. *J. App. Phycol.* **24**, 791-801
- Sterner, R. W. & Elser, J. J. 2002 *Ecological Stoichiometry: the Biology of Elements from Molecules to the Biosphere*. Princeton University Press, Princeton, NJ, U.S.A.
- Su, C.H., Chien, L.J., Gomes, J. et al., (2011) Factors affecting lipid accumulation by *Nannochloropsis oculata* in a two-stage cultivation process. *J. Appl. Phycol.* **23**, 903-908
- Sukenik, A., Carmeli, Y., Berner, T. (1989) Regulation of fatty-acid composition by irradiance level in the eustigmatophyte *Nannochloropsis sp.* *J. Phycol.* **25**, 686-692
- Sukenik, A. and Carmeli, Y. (1990) Lipid-synthesis and fatty-acid composition in *Nannochloropsis sp.* (Eustigmatophyceae) grown in a light-dark cycle. *J. Phycol.*, **26**, 463-469.
- Sukenik, A. and Wahnou, R. (1991) Biochemical quality of marine unicellular algae with special emphasis on lipid-composition. 1. *Isochrysis galbana*. *Aquaculture*, **97**, 61-72.

-
- Sukenik, A., Levy, R.S., Levy, Y. et al., (1991) optimizing algal biomass production in an outdoor pond- A simulation model. *J. App. Phycol.* **3**, 191-201
- Sukenik, A., Zmora, O. and Carmeli, Y. (1993) Biochemical quality of marine unicellular algae with special emphasis on lipid-composition. 2. *Nannochloropsis* sp. *Aquaculture*, **117**, 313-326.
- Sverdrup, H.U. (1945) Oceanography for meteorologists. Georgel Allen and Unwin Ltd., London, 246 pp.
- Thompson, P. A., Levasseur, M. E. and Harrison, P. J. (1989) Light-limited growth on Ammonium vs Nitrate – What is the advantage for marine phytoplankton. *Limnol. Oceanogr.*, **34**, 1014-1024.
- Thompson, P. A., Harrison, P. J. and Whyte, J.N.C. (1990) Influence of irradiance on the fatty acid composition of phytoplankton. *J. Phycol.*, **26**, 278-288.
- Thompson, G. A. (1996) Lipids and membrane function in green algae. *Biochim. Biophys. Acta.* **1302**, 17-45
- Tonon, T; Harvey, D; Larson, T. R. et al. (2002) Long chain polyunsaturated fatty acid production and partitioning to triacylglycerols in four microalgae. *Phytochem.* **61**, 15-24
- Turpin, D. H. (1991) Effects of inorganic N availability on algal photosynthesis and carbon metabolism. *J. Phycol.*, **27**, 14-20.
- Ugwu, C. U., Aoyagi, H., Uchiyama, H.(2008) Photobioreactors for mass cultivation of algae. *Bioresour. Technol.* **99**, 4021-4028
- Volkman, J. K., Jeffrey, S. W., Nichols, P. D., et al. (1989) Fatty-acid and lipid-composition of 10 species of microalgae used in mariculture. *J. Exp. Mar. Biol. Ecol.* **128**, 219-240

-
- Volkman, J. K., Brown, M. R., Dunstan, G. A. et al. (1993) The biochemical composition of marine microalgae from the class eustigmatophyceae. *J. Phycol.* **29**, 69-78
- Vrede, T., Dobberfuhl, D. R., Kooijman, S. and Elser, J. J. (2004) Fundamental connections among organism C: N:P stoichiometry, macromolecular composition, and growth. *Ecology*, **85**, 1217-1229.
- Weers, P. M. M. and Gulati, R. D. (1997) Growth and reproduction of *Daphnia galeata* in response to changes in fatty acids, phosphorus, and nitrogen in *Chlamydomonas reinhardtii*. *Limnol. Oceanogr.* **42**, 1584-1589
- Wijffels, R. H. & Barbosa, M. J. 2010 An outlook on microalgal biofuels. *Science* **329**, 796-799.
- Williams, P. J. (2007) Biofuel: microalgae cut the social and ecological costs. *Nature* **450**, p478
- Williams, P. J. L. and Laurens, L. M. L. (2010) Microalgae as biodiesel & biomass feedstocks: Review & analysis of the biochemistry, energetics & economics. *Energy Environ. Sci.*, **3**, 554-590.
- Wood, G. J. and Flynn, K. J. (1995) Growth of *Heterosigma Carterae* (Raphidophyceae) on nitrate and ammonium at three photon flux density: evidence for N stress in nitrate-growing cells. *J. Phycol.*, **31**, 859-867.
- Xu, N.J., Zhang, X.C.Fan, X. et al. (2001) Effects of nitrogen source and concentration on growth rate and fatty acid composition of *Ellipsoidion sp* (eustigmatophyta). *J. App. Phycol.* **13**, 463-469

Yu, G., Li, Y. G. Shen, G. M. et al., (2009) A novel method using CFD to optimize the inner structure parameters of flat photobioreactors, *J. Appl. Phycol.* **21**, 719-727

Appendix A

Table A1. Constants in algal physiology model.

Constant	Definition	Value	Unit
KQN	quota control constant for N	10	dl
NCo	minimum NC	0.05	gNg-1C
NCm	maximum NC affecting growth	0.16	gNg-1C
Kxi	uptake feedback control constant	0.001	dl
NCabs	absolute maximum NC	0.2	gNg-1C
NKu	half saturation for N-source uptake	2e-3	g/m3
beta	constant for N and P uptake control	0.05	dl
Qh	uptake feedback control Hill number	2	dl
AKt	half saturation for ammonium transport	1e-3	g/m3
Apref	ammonium preference constant	20	dl
N2Kt	half saturation for second nitrite transport	0.2	g/m3
N2pref	second nitrate preference constant	10	dl
NKt	half saturation for first nitrate transport	1	g/m3
Npref	first nitrate transport preference constant	1	dl
PKu	half saturation of phosphorus uptake	2e-3	g/m3
KQP	quota control constant for P	0.1	dl
PCm	maximum PC affecting growth	0.02	gPg-1C
PCo	minimum PC	0.005	gPg-1C
PCabs	absolute maximum PC	0.04	gPg-1C
Fht	control of Fe transport	0.05	dl
FKt	half saturation for Fe transport	1e-6	g/m3
FCm	maximum FC	0.00025	gFeg-1C
FKq	quota control for Fe	8.867e-6	gFe g-1C
PSU	Photosynthetics Unit	900	dl
Beta_Si	constant for Si uptake control	0.4	dl
SCm	maximum SC affecting growth	0.1	gSi g-1C
SKu	half saturation of Si uptake	5e-3	g/m3
SCo	minimum SC	0.05	gSi g-1C
SCabs	absolute maximum SC	0.2	gSi g-1C
ChlCm	maximum ChlC	0.06	gChl g-1C
M	control for photoacclimation rate	3	dl
Um	maximum growth rate	1	d-1
redco	reduction cost for nitrate to ammonium	1.71	gCg-1N

Table A2. Auxiliaries description in algal physiology model

Auxiliary	Description	Units
NCu	N-quota quotient	dl
Nup	N-source uptake rate	gNg-1Cd-1
NC	NC-quota	dl
AVP	potential ammonium transport	dl
NV	relative nitrate transport	dl
frat	f-ratio	dl
AV	relative ammonium transport	dl
NVP	potential nitrate transport	dl
NO3		gNO3/m3
PCu	P-quota quotient	dl
Pup	phosphorus uptake rate	gPg-1Cd-1
PC	PC-quota	gP/gC
Fup	uptake rate of Fe	gFeg-1Cd-1
FC	FC-quota	gFe/gC
Fcon	Fe control quotient	dl
Ftot	total Fe accounted for	gFeg-1C
VS	potential silicon uptake rate	gSig-1Cd-1
SCu	Si-control quotient	dl
SC	SC-quota	gSi/gC
Sup	silicon uptake rate	gSi g-1C d-1
dChlC	change in ChlC	gChlg-1 Cd-1
NPSCu	threshold quotient	dl
Pqm	maximum gross PS	gCg-1Cd-1
basres	basal respiration	gCg-1Cd-1
Cu	C-growth rate	gC g-1C d-1

Table A3. Constants for physical–chemical setting in bioreactor

Constant	Definition	Value	Unit
Flow_B	Flow into PBR	1	m ³
React_V_Max	Maximum volume of PBR	1	m ³
Flow_L	Flow into Lake	5	m ³
SW_rain	Rain switch; 0 close; 1 open	1	dl
Rainfall	Rainfall	0.5	m/d
surface_area	Lake area	10	m ²
MAX_V	Maximum volume of Lake	100	m ³
SW_SC	System check switch 0 is dynamic; 1 if steady-state	0	dl
Rain_NO3	NO ₃ concentration in rainfall	14	gN/m ³
Rain_NH4	NH ₄ concentration in rainfall	14	gN/m ³
inco_B	Inoculation for PBR	1.2	gC
inco_L	Inoculation for Lake	12	G
Rain_P	Phosphate con in rainfall	30	gP/m ³
ex_Si_L	External silicate concentration	28	g/m ³

Table A4. Auxiliaries in bioreactor model

Auxiliary	Description and equation	Units
In_B	Flow_B	M3
out_B	Flow_B*SW_React_V*(SW_PBR=0)	M3
dil_B	In_B/Reactor_V*HV_CON	d-1
SW_React_V	Reactor_V>=React_V_Max	dl
IN_L	Flow_B*SW_React_V*(SW_PBR=1)	M3
dil_L	(IN_L+Rain+Flow_L)/Lake_V	d-1
Flow_out	Rain+Flow_B*SW_PBR+Flow_L	M3
ex_flow_L	Flow_L	M3
rainfall	Rain	M3/d
Rain	Rain_V*surface_area*SW_rain	m3/d
optical_dept	Lake_V/surface_area	m
h		
SW_OF	(Lake_V>=MAX_V)	dl
iN_NO3_B	(DINO3_B/reactNO3<1)*NO2*(SW_SC=0)	g/d
OUT_NO3_B	NO3_B*dil_B*(SW_PBR=0)	g/d
IN_NO3_L	dil_B*NO3_B*(SW_PBR=1)	g/d
OUT_NO3_L	NO3_L*dil_L*SW_OF*(SW_SC=0)	g/d
extNO3	Flow_L*ex_NO3_L*(SW_SC=0)	g
Rain_in	Rain*Rain_NO3*(SW_SC=0)	g
groNO3_L	Nup_L*frat_L*AlgC_L	g/d
groNO3_B	AlgC_B*frat*Nup_B	g/d
PBR_out	dil_B*AlgN_B*(SW_PBR=0)	g/d
AlgN	dil_B*AlgN_B*(SW_PBR=1)	g/d
Out_N_L	AlgN_L*dil_L*SW_OF*(SW_SC=0)	g/d
IN_NH4_B	AlgN_L*dil_L*SW_OF*(SW_SC=0)	g/d
OUT_NH4_B	NH4_B*dil_B*(SW_PBR=0)	g/d
groNH4_B	Nup_B*AlgC_B*(1-frat)	g/d
IN_NH4_L	NH4_B*dil_B*(SW_PBR=1)	g/d
OUT_NH4_L	NH4_L*dil_L*SW_OF*(SW_SC=0)	g/d
groNH4_L	AlgC_L*Nup_L*(1-frat_L)	g/d
extNH4	Flow_L*ex_NH4_L*(SW_SC=0)	g/d
Rate_44	Rain*Rain_NH4*(SW_SC=0)	g/d
IN_DIC_B	(DICC_B/reactDIC<1)*CO2_B*(SW_SC=0)	g/d
OUT_DIC_B	DIC_B*dil_B*(SW_PBR=0)	g/d
CO2_B	IF(NET_V_B=0, (reactDIC-DICC_B)*Reactor_V+(IN_DIC_L*(SW_PBR=1)+OUT_DIC_B*(SW_PBR=0))+groC_B, reactDIC*NET_V_B+(IN_DIC_L*(SW_PBR=1)+OUT_DIC_B*(SW_PBR=0))+ groC_B)	g
IN_DIC_L	DIC_B*dil_B*(SW_PBR=1)	g/d
OUT_DIC_L	DIC_L*dil_L*SW_OF*(SW_SC=0)	g/d
ext_C	((DICC_L/ex_DIC_L<=1)*CO2_L)*(SW_SC=0)	g/d

CO2_L	IF(NET_V_L=0, (ex_DIC_L-DICC_L)*Lake_V+OUT_DIC_L+groC_L, ex_DIC_L*NET_V_L+OUT_DIC_L+groC_L)	g
Rain_99	AlgC_B*dil_B*(SW_PBR=0)	g/d
groC_B	AlgC_B*Cu_B	g/d
AlgC	dil_B*AlgC_B*(SW_PBR=1)	g
groC_L	AlgC_L*Cu_L	g/d
Rate_87	AlgC_L*dil_L*SW_OF*(SW_SC=0)	g/d
IN_P_B	(reactP-P_B)*Phosphate_B*(SW_SC=0)	g/d
OUT_P_B	DIP_B*dil_B*(SW_PBR=0)	g/d
Phosphate_B	IF(NET_V_B=0, (reactP-P_B)*Reactor_V+(IN_P_L*(SW_PBR=1)+OUT_P_B*(SW_PBR=0))+groP_B, reactP*NET_V_B+(IN_P_L*(SW_PBR=1)+OUT_P_B*(SW_PBR=0))+groP_B)	g
groP_B	AlgC_B*Pup_B	g/d
IN_P_L	DIP_B*dil_B*(SW_PBR=1)	g/d
OUT_P_L	DIP_L*dil_L*SW_OF*(SW_SC=0)	g/d
groP_L	AlgC_L*Pup_L	g/d
Rate_47	Flow_L*ex_P_L*(SW_SC=0)	g/d
Rate_46	Rain*Rain_P*(SW_SC=0)	g/d
Rate_100	AlgP_B*dil_B*(SW_PBR=0)	g/d
AlgP	dil_B*AlgP_B*(SW_PBR=1)	g/d
Rate_88	AlgP_L*dil_L*SW_OF*(SW_SC=0)	g/d
IN_Fe_B	(Fe_B/reactFe<1)*iron_B*(SW_SC=0)	g/d
OUT_Fe_B	DIF_B*dil_B*(SW_PBR=0)	g/d
groFe_B	Fup_B*AlgC_B	g/d
IN_Fe_L	DIF_B*dil_B*(SW_PBR=1)	g/d
OUT_Fe_L	DIF_L*dil_L*SW_OF*(SW_SC=0)	g/d
groFe_L	AlgC_L*Fup_L	g/d
Rate_49	ex_F_L*Flow_L*(SW_SC=0)	g/d
Rate_101	dil_B*AlgF_B*(SW_PBR=0)	g/d
AlgFe	dil_B*AlgF_B*(SW_PBR=1)	g/d
Rate_89	AlgF_L*dil_L*SW_OF*(SW_SC=0)	g/d
IN_Si_B	(S_B/reactSi<1)*Silicate_B*(SW_SC=0)	g/d
OUT_Si_B	Si_B*dil_B*(SW_PBR=0)	g/d
groSi_B	AlgC_B*Sup_B	g/d
Silicate_B	IF(NET_V_B=0, (reactSi-S_B)*Reactor_V+(IN_Si_L*(SW_PBR=1)+OUT_Si_B*(SW_PBR=0))+groSi_B, reactSi*NET_V_B+(IN_Si_L*(SW_PBR=1)+OUT_Si_B*(SW_PBR=0))+groSi_B)	g/d
IN_Si_L	dil_B*Si_B*(SW_PBR=1)	g/d
OUT_Si_L	Si_L*dil_L*SW_OF*(SW_SC=0)	g/d
groSi_L	AlgC_L*Sup_L	g/d

Rate_80	$\text{Flow}_L * \text{ex}_{Si}_L * (\text{SW}_{SC}=0)$	g/d
Rate_102	$\text{AlgSi}_B * \text{dil}_B * (\text{SW}_{PBR}=0)$	g/d
AlgSi	$\text{dil}_B * \text{AlgSi}_B * (\text{SW}_{PBR}=1)$	g/d
Rate_90	$\text{AlgSi}_L * \text{dil}_L * \text{SW}_{OF} * (\text{SW}_{SC}=0)$	

Table A5. Default state variables for bioreactor model.

State variable	Initial value	Units
Reactor_V	1	m ³
Lake_V	100	m ³
NO3_B	reactNO3	gN of NO3
NO3_L	ex_NO3_L	gN
AlgN_B	AlgC_B*0.16	g
AlgN_L	AlgC_L*0.16	g
NH4_B	reactNH4	gN of NH4
NH4_L	ex_NH4_L	gN
DIC_B	reactDIC	kg
DICseq_B	0	g CO2
DIC_L	24	g
DICseq_L	0	g
AlgC_B	inoc_B	gC
AlgC_L	inoc_L	gC
DIP_B	reactP	gP
DIP_L	ex_P_L	gP
AlgP_B	AlgC_B*0.02	g
AlgP_L	AlgC_L*0.02	g
DIF_B	reactFe	gFe
DIF_L	ex_F_L	gFe
AlgF_B	AlgC_B*0.00025	g
AlgF_L	AlgC_L*0.00025	g
Si_B	reactSi	gSi
Si_L	ex_Si_L	g
AlgSi_B	AlgC_B*0.1*SW_diat	g
AlgSi_L	AlgC_L*0.1*SW_diat	g

Table A6 Auxiliaries for model

Auxiliary	Description	Units
totN_B	NH4_B+NO3_B	gN
DINO3_B	NO3_B/Reactor_V	g/m3
DINH4_B	NH4_B/Reactor_V	g/m3
N_B	totN_B/Reactor_V	gN/m3
totN_L	NH4_L+NO3_L	g/m3
N_L	totN_L/Lake_V	gN/m3
C_biomass_con_B	AlgC_B/Reactor_V	gC/m3
C_biomass_con_L	AlgC_L/Lake_V	g/m3
DICC_B	DIC_B/Reactor_V	gC/m3
DICC_L	DIC_L/Lake_V	g/m3
P_B	DIP_B/Reactor_V	g/m3
P_L	DIP_L/Lake_V	g/m3
Fe_B	DIF_B/Reactor_V	g/m3
F_L	DIF_L/Lake_V	g/m3
NET_V_B	$(In_B-IN_L)*(SW_PBR=1)+(In_B-out_B)*(SW_PBR=0)$	M3
NET_V_L	IN_L+ex_flow_L-OUT_L	M3
AP_B	VP_B*mix_depth	g/m2
AP_L	VP_L*optical_depth	g/m2
VP_B	Volumetric production for PBR	g/m3
VP_L	Volumetric production for Lake	g/m3
S_B	Si_B/Reactor_V	g/m3
S_L	Si_L/Lake_V	g/m3

Appendix B

ASCII form equation directly taken from model platform is given below.

```
init AlgC_B = inoc_B
flow AlgC_B = -dt*Rate_99
      +dt*Cup_B
      -dt*Auxiliary_62
doc AlgC_B = gC
init AlgC_L = inoc_L
flow AlgC_L = -dt*Rate_87
      +dt*Cup_L
      +dt*Auxiliary_62
doc AlgC_L = gC
init AlgN_B = AlgC_B*iniNC
flow AlgN_B = -dt*Rate_98
      -dt*Auxiliary_61
      +dt*Rate_56
doc AlgN_B = g
init AlgN_L = AlgC_L*NC_B
flow AlgN_L = -dt*Rate_86
      +dt*Auxiliary_61
      +dt*Rate_58
doc AlgN_L = g
init AlgP_B = AlgC_B*iniPC
flow AlgP_B = -dt*Rate_100
      -dt*Auxiliary_63
      +dt*groP_B
doc AlgP_B = g
init AlgP_L = AlgC_L*PC_B
flow AlgP_L = -dt*Rate_88
      +dt*Auxiliary_63
      +dt*Rate_62
doc AlgP_L = g
init avgCu = 0
flow avgCu = -dt*Rate_83
      +dt*Rate_82
init avgCu_L = 0
flow avgCu_L = -dt*Rate_85
      +dt*Rate_84
```

```
init ChlC_B = iniChlC
flow ChlC_B = +dt*dChlC
doc ChlC_B = chlorophyll quota; gChl g-1C
init ChlC_L = ChlC_B
flow ChlC_L = +dt*dChlC_1
doc ChlC_L = chlorophyll quota; gChl g-1C
init DIP_B = reactP
flow DIP_B = -dt*Rate_95
            -dt*groP_B
            +dt*Rate_61
            -dt*Rate_39
doc DIP_B = gP
init DIP_L = ex_P_L
flow DIP_L = -dt*Rate_38
            +dt*Rate_47
            -dt*Rate_62
            +dt*Rate_39
doc DIP_L = gP
init Harvest_C = 0
flow Harvest_C = +dt*Rate_87
init Harvest_V = 0
flow Harvest_V = +dt*OUT
init HV_VPLIP = 0
flow HV_VPLIP = -dt*Rate_105
            +dt*Rate_104
init Lake_V = MAX_V
flow Lake_V = -dt*OUT
            +dt*ex_flow
            +dt*IN_L
doc Lake_V = m3
1m3=1000L (m3)
init NO3_B = reactNO3
flow NO3_B = -dt*Rate_92
            +dt*Rate10
            -dt*Rate_56
            -dt*Rate_31
doc NO3_B = gN of NO3
init NO3_L = ex_NO3_L
flow NO3_L = -dt*Rate_33
            +dt*extNO3
            -dt*Rate_58
            +dt*Rate_31
doc NO3_L = gN
init Reactor_V = ini_V
```

```

flow Reactor_V = -dt*Rate_91
    -dt*IN_L
    +dt*In_B
doc Reactor_V = m3
init VP = 0
flow VP = +dt*VP1in
    -dt*P1out
doc VP = volumetric production averaged over the day (gC/m3/d)
init VP_L = 0
flow VP_L = -dt*P1out_1
    +dt*VP1in_1
doc VP_L = volumetric production averaged over the day (gC/m3/d)
init VPlipid = 0
flow VPlipid = -dt*VPLout
    +dt*VPlin
doc VPlipid = day-averaged volumetric production of lipid (gC/m3/d)
init VPlipid_L = 0
flow VPlipid_L = +dt*VPlin_1
    -dt*VPLout_1
doc VPlipid_L = day-averaged volumetric production of lipid (gC/m3/d)
aux Auxiliary_61 = dil_B*AlgN_B*(SW_PBR=1)
aux Auxiliary_62 = dil_B*AlgC_B*(SW_PBR=1)
aux Auxiliary_63 = dil_B*AlgP_B*(SW_PBR=1)
aux Cup_B = AlgC_B*Cu_B
aux Cup_L = AlgC_L*Cu_L
aux dChlC =
Um*ChlCm*M*NPSCu*(1-(PS_B/Pqm_B)*(ChlC_B>0.003))*(1-ChlC_B/ChlCm)/(1-ChlC_B/ChlCm
+0.05)-ChlC_B*(Cu_B+(1-NCu)*Um)
doc dChlC = change in ChlC gChlg-1 Cd-1
aux dChlC_1 =
Um*ChlCm*M*NPSCu_L*(1-(PS_L/Pqm_L)*(ChlC_L>0.003))*(1-ChlC_L/ChlCm)/(1-ChlC_L/ChlCm
+0.05)-ChlC_L*(Cu_L+(1-NCu_L)*Um)
doc dChlC_1 = change in ChlC gChlg-1 Cd-1
aux ex_flow = Flow_L*(SW_PBR=1)
aux extNO3 = Flow_L*ex_NO3_L*(SW_SC=0)
aux groP_B = AlgC_B*Pup_B
aux In_B = Flow_B*(SW_SC=0)
aux IN_L = Flow_B*React_switch*(SW_PBR=1)
doc IN_L = m3/d
aux OUT = OF_swicth*Flow_out
doc OUT = l/d
aux P1out = DELAYPPL(VP1in,1,0)
doc P1out = output growth rate
aux P1out_1 = DELAYPPL(VP1in_1,1,0)

```

```
doc P1out_1 = output growth rate
aux Rate_100 = AlgP_B*dil_B*(SW_PBR=0)
aux Rate_104 = Rate_87*XSC_1/Lake_V
aux Rate_105 = DELAYPPL(Rate_104,1,0)
aux Rate_31 = dil_B*NO3_B*(SW_PBR=1)
aux Rate_33 = NO3_L*dil_L*(SW_SC=0)*OF_swicth
aux Rate_38 = DIP_L*dil_L*(SW_SC=0)*OF_swicth
aux Rate_39 = DIP_B*dil_B*(SW_PBR=1)
aux Rate_47 = Flow_L*ex_P_L*(SW_SC=0)
aux Rate_56 = AlgC_B*Nup_B
aux Rate_58 = Nup_L*AlgC_L
aux Rate_61 = reactP*dil_B*Reactor_V
aux Rate_62 = AlgC_L*Pup_L
aux Rate_82 = Cu_B
aux Rate_83 = DELAYPPL(Rate_82,1,0)
aux Rate_84 = Cu_L
aux Rate_85 = DELAYPPL(Rate_84, 1,0)
aux Rate_86 = AlgN_L*dil_L*(SW_SC=0)*OF_swicth
aux Rate_87 = AlgC_L*dil_L*(SW_SC=0)*OF_swicth
aux Rate_88 = AlgP_L*dil_L*(SW_SC=0)*OF_swicth
aux Rate_91 = Flow_B*React_switch*(SW_PBR=0)
aux Rate_92 = NO3_B*dil_B*(SW_PBR=0)
aux Rate_95 = DIP_B*dil_B*(SW_PBR=0)
aux Rate_98 = dil_B*AlgN_B*(SW_PBR=0)
aux Rate_99 = AlgC_B*dil_B*(SW_SC=0)*(SW_PBR=0)
aux Rate10 = reactNO3*dil_B*Reactor_V
doc Rate10 = gN
aux VP1in = Cup_B/Reactor_V
doc VP1in = input growth rate
aux VP1in_1 = Cup_L/Lake_V
doc VP1in_1 = input growth rate
aux VPlin = Cup_B*XSC/Reactor_V
doc VPlin = volumetric lipid production input
aux VPlin_1 = Cup_L*XSC_1/Lake_V
doc VPlin_1 = volumetric lipid production input
aux VPLout = DELAYPPL(VPlin,1,0)
doc VPLout = volumetric lipid production ouput
aux VPLout_1 = DELAYPPL(VPlin_1,1,0)
doc VPLout_1 = volumetric lipid production ouput
aux A_C = C_biomass_con_B*mix_depth
doc A_C = areal biomass (gC/m2)
aux A_C_1 = C_biomass_con_L*optical_depth
doc A_C_1 = areal biomass (gC/m2)
aux AmemC = VmemC*mix_depth
```

```

doc AmemC = areal membranous C (gC/m2)
aux AmemC_1 = VmemC_1*optical_depth
doc AmemC_1 = areal membranous C (gC/m2)
aux AnonN_C = VnonN_C*mix_depth
doc AnonN_C = areal lipid C (gC/m2)
aux AnonN_C_1 = VnonN_C_1*optical_depth
doc AnonN_C_1 = areal lipid C (gC/m2)
aux AP = VP*mix_depth
doc AP = areal production averaged over the day (gC/m2/d)
aux AP_L = VP_L*optical_depth
doc AP_L = areal production averaged over the day (gC/m2/d)
aux APlipid = VPlipid*mix_depth
doc APlipid = day-average areal production of lipid (gC/m2/d)
aux APlipid_L = VPlipid_L*optical_depth
doc APlipid_L = day-average areal production of lipid (gC/m2/d)
aux attenuation_B = mix_depth*(water_atten+Chl_B*P_atten)
doc attenuation_B = attenuation of light by water and by phytoplankton; dl
m*(W+g/m3*P)=m*(W+gChl/m3*m2/mgChl)=m*(W+1e+3/m)
aux attenuation_L = optical_depth*(water_atten_L+Chl_L*P_atten_L)
doc attenuation_L = attenuation of light by water and by phytoplankton; dl

m*(W+gchl/m3*m2/gchl)
aux AXSC = VXSC*mix_depth
doc AXSC = areal XSC (gC/m2)
aux AXSC_1 = VXSC_1*optical_depth
doc AXSC_1 = areal XSC (gC/m2)
aux basres =
Um*0.05*1.01*((NCabs-NC_B)/(NCabs-NCo))/((NCabs-NC_B)/(NCabs-NCo)+0.01)*(NC_B<NCabs
)
doc basres = basral respiration kgCkg-1Cd-1
Um*0.05*(1+Kb)*((NCm-NC)/(NCm-NCo))/((NCm-NC)/(NCm-NCo)+Kb)*(NC<NCm)
aux basres_L =
Um*0.05*1.01*((NCabs-NC_L)/(NCabs-NCo))/((NCabs-NC_L)/(NCabs-NCo)+0.01)*(NC_L<NCabs)
doc basres_L = basral respiration gCg-1Cd-1
Um*0.05*(1+Kb)*((NCm-NC)/(NCm-NCo))/((NCm-NC)/(NCm-NCo)+Kb)*(NC<NCm)
aux C_biomass_con_B = AlgC_B/Reactor_V
doc C_biomass_con_B = gC/m3
aux C_biomass_con_L = AlgC_L/Lake_V
doc C_biomass_con_L = g/m3
aux Chl_B = C_biomass_con_B*ChlC_B
doc Chl_B = total Chl; g/m3

aux Chl_L = C_biomass_con_L*ChlC_L
doc Chl_L = gChl /m3

```

```

aux CN_B = 1/NC_B
doc CN_B = CN ratio (i.e. reciprocal of Q) (ugC/ugN)
aux CN_L = 1/NC_L
doc CN_L = CN ratio (i.e. reciprocal of Q) (ugC/ugN)
aux CNcore = 1/NCcore
aux CNcore_1 = 1/NCcore_1
aux coszen = MAX(SIN(latrad)*SIN(sdeca)+COS(latrad)*COS(sdeca)*COS(hrr),0)
doc coszen = cosine of zenith angle

aux Cu_B = (PS_B-(redco*Nup_B+Nup_B*1.5+basres))
doc Cu_B = C-growth rate; gC g-1C d-1
aux Cu_L = (PS_L-(redco_L*Nup_L+Nup_L*1.5+basres_L))
doc Cu_L = C-growth rate; gC g-1C d-1
aux daycal1 = -1*TAN(latrad)*TAN(sdeca)
aux daycal2 = daycal1*(daycal1>-1)*(daycal1<=1)+-1*(daycal1<=-1)+1*(daycal1>1)
aux daylen = (2*ARCCOS(daycal2)*12/PI)
doc daylen = day length at the specific day of the year; hr
aux dil_B = ln_B/Reactor_V
aux dil_L = (IN_L+Flow_L)/Lake_V
doc dil_L = d-1
aux DIN = N_B/14
doc DIN = mmol/L
aux exat = EXP(-attenuation_B)
doc exat = -ve exponent of attenuation      e(1/attenuation)
aux exat_L = EXP(-attenuation_L)
doc exat_L = -ve exponent of attenuation      e(1/attenuation)
aux Flow_out = Flow_B*SW_PBR+Flow_L
aux hr = ABS(12-t24)*15
doc hr = degrees of hour angle away from noon (default 12:00)
aux hrr = hr*PI/180
doc hrr = hour angle radians
aux HV_APlip = HV_VPLIP*optical_depth
aux irr = sun/rvector/rvector*coszen*(coszen>0)
doc irr = noon irradiance; umol photons
aux latrad = lat*PI/180
aux LD_cycle_B = (FRAC(TIME)>0.5)=0
doc LD_cycle_B = value of fraction of timestep BIGGER than 0.5 gives the value as 0
12:12hr LD operation.
aux LD_cycle_L = (FRAC(TIME)>0.5)=0
doc LD_cycle_L = value of fraction of timestep BIGGER than 0.75 gives the value as 0
18:6hr LD operation.
aux memC = NC_B*memCN
doc memC = g membrane C per g cell C

```

```

aux memC_1 = NC_L*memCN_1
doc memC_1 = g membrane C per g cell C
aux memCN = (1/NCabs)-CNcore
doc memCN = amount of membrane lipid at NCabs, as g lipid C / g total N
aux memCN_1 = (1/NCabs)-CNcore_1
doc memCN_1 = amount of membrane lipid at NCabs, as g lipid C / g total N
aux N_B = NO3_B/Reactor_V
doc N_B = gN/m3
aux N_L = NO3_L/Lake_V
doc N_L = gN/m3
aux NC_B = AlgN_B/AlgC_B
doc NC_B = kgNkgC-1
aux NC_L = AlgN_L/(AlgC_L+(AlgC_L=0))
aux NCu = (NC_B<NCm)*(1+KQN)*(NC_B-NCo)/((NC_B-NCo)+KQN*(NCm-NCo))+(NC_B>=NCm)
doc NCu = N-quota quotient; dl
aux NCu_L = (NC_L<NCm)*(1+KQN)*(NC_L-NCo)/((NC_L-NCo)+KQN*(NCm-NCo))+(NC_L>=NCm)
doc NCu_L = N-quota quotient; dl
aux nonN_C = (CN_B-CNcore)/CN_B
doc nonN_C = total non-N material, assumed here as lipid (C/C)
aux nonN_C_L = (CN_L-CNcore_1)/CN_L
doc nonN_C_L = total non-N material, assumed here as lipid (C/C)
aux NPSCu = MIN(NCu,PCu)
doc NPSCu = threshold quotient; dl
aux NPSCu_L = MIN(NCu_L,PCu_L)
doc NPSCu_L = threshold quotient; dl
aux Nup_B =
(N_B>0)*Um*NCm*((NCu>NPSCu)*NPSCu^beta+(NCu=NPSCu))*(NC_B<NCabs)*N_B/(N_B+NKu
)*(1-NC_B/NCabs)^Qh/((1-NC_B/NCabs)^Qh+Kxi)
doc Nup_B = N-source uptake rate; gNg-1Cd-1
aux Nup_L =
(N_L>0)*Um*NCm*((NCu_L>NPSCu_L)*NPSCu_L^beta_L+(NCu_L=NPSCu_L))*(NC_L<NCabs)*N
_L/(N_L+NKu)*(1-NC_L/NCabs)^Qh_L/((1-NC_L/NCabs)^Qh_L+Kxi_L)
doc Nup_L = N-source uptake rate; gNg-1Cd-1
aux OF_swicth = (Lake_V>=MAX_V)
aux optical_depth = Lake_V/surface_area
aux P_B = DIP_B/Reactor_V
doc P_B = g/m3
aux P_L = DIP_L/Lake_V
aux PAR_B = irr*(SW_LD_B=1)+PFD_B*(SW_LD_B=0)
doc PAR_B = PAR light density per surface
aux PAR_L = irr*(SW_LD_L=1)+PFD_L*(SW_LD_L=0)
doc PAR_L = PAR light density per surface
aux PC_B = AlgP_B/AlgC_B
doc PC_B = kgP/kgC

```

```

aux PC_L = AlgP_L/(AlgC_L+(AlgC_L=0))
aux PCu =
(PC_B<PCm)*(1+KQP)*(PC_B-PCo)/((PC_B-PCo)+KQP*(PCm-PCo))*(PCo<PC_B)+(PC_B>=PCm)
doc PCu = P-quota quotient; dl
aux PCu_L =
(PC_L<PCm)*(1+KQP)*(PC_L-PCo)/((PC_L-PCo)+KQP*(PCm-PCo))*(PCo<PC_L)+(PC_L>=PCm)
doc PCu_L = P-quota quotient; dl
aux Pqm_B = (Um+basres+NCm*Um*(redco+1.5))*NPSCu+1e-6
doc Pqm_B = maximum gross PS; kgCkg-1Cd-1
aux Pqm_L = (Um+basres_L+NCm*Um*(redco_L+1.5))*NPSCu_L+1e-6
doc Pqm_L = maximum gross PS kgCkg-1Cd-1
aux PS_B =
Pqm_B*(LN(Pyt+SQRT(1+Pyt^2))-LN(Pyt*exat+SQRT(1+(Pyt*exat)^2)))/attenuation_B
doc PS_B = depth integrated photosynthesis at a given instant in time taking into account
mixing depth and attenuations
LN=loge
SQRT=square root
d-1*g/l/m2/d*1e+6/(W+1e+6)
aux PS_L =
Pqm_L*(LN(Pyt_L+SQRT(1+Pyt_L^2))-LN(Pyt_L*exat_L+SQRT(1+(Pyt_L*exat_L)^2)))/attenuation
_L
doc PS_L = depth integrated photosynthesis at a given instant in time taking into account mixing
depth and attenuations
LN=loge
SQRT=square root
aux Pup_B =
(P_B>0)*Um*PCm*((PCu>NPSCu)*NPSCu^beta+(PCu=NPSCu))*(PC_B<PCabs)*P_B/(P_B+PKu)*{
1-PC_B/PCabs)^Qh/((1-PC_B/PCabs)^Qh+Kxi)
doc Pup_B = phosphorus uptake rate; gPg-1Cd-1
aux Pup_L =
(P_L>0)*Um*PCm*((PCu_L>NPSCu_L)*NPSCu_L^beta_L+(PCu_L=NPSCu_L))*(PC_L<PCabs)*P_L/
(P_L+PKu)*(1-PC_L/PCabs)^Qh_L/((1-PC_L/PCabs)^Qh_L+Kxi_L)
doc Pup_L = phosphorus uptake rate; gPg-1Cd-1
aux Pyt = (alpha*ChlC_B*PAR_B*24*60*60)/Pqm_B*1e+3
doc Pyt = photosynthesis according to the Smith equation
(kgC/kgChl/d*kgChl/kgC*umol photon/m2/d)/ kgC/kgC/d=umol/m2/d=
mol/m2/d/1000=ug/L/m2/d
aux Pyt_L = (alpha*ChlC_L*PAR_L*24*60*60)/Pqm_L*1e+3
doc Pyt_L = photosynthesis according to the Smith equation

(gCgChl-1d-1*gChlG-1*umolPhoton/m2/s*24*60*60)/gCgC-1d-1 = umolPhoton/m2/d/gCgC-1
aux React_switch = Reactor_V>=React_V_Max
aux reactNO3 = f2N*AMP*14/1000
doc reactNO3 = g/m3=mg/L

```

mgN/m³ = ugN/L; 14g/L = 1M, 14e-6g = 14ug/L = 1uM, 100uM = 1400ugN/L
 typical max N in media would be ca. 10mM, 1mM = 14mg/L, 10= 140mgN/L = 140gN/m³
 aux reactP = f2P*AMP*31/1000
 doc reactP = g/m³=mg/L
 2mM= 30mg/l= 0.03g/l
 10mM= 150mg/l= 0.15g/l
 aux relPS = PS_B/Pqm_B
 aux relPS_L = PS_L/Pqm_L
 aux rvector = 1/(1+0.033*COS(2*PI*t365*0.00274))^0.5
 doc rvector = earth radius vector
 aux sdeca = 23.45*SIN(2*PI*(284+t365)*0.00274)*PI/180
 doc sdeca = solar declination angle

aux SysN = SysN_B+SysN_L
 aux SysN_B = AlgN_B+NO3_B
 aux SysN_L = AlgN_L+NO3_L
 aux SysP = SysP_L+SysP_B
 aux SysP_B = AlgP_B+DIP_B
 aux SysP_L = AlgP_L+DIP_L
 aux t = FRAC(TIME)
 aux t24 = 24*t
 doc t24 = time of the day, hr

change between 1-24
 aux t365 = TIME
 doc t365 = day of the year
 aux VmemC = C_biomass_con_B*memC
 doc VmemC = concentration of membranous C (gC/m³)
 aux VmemC_1 = C_biomass_con_L*memC_1
 doc VmemC_1 = concentration of membranous C (gC/m³)
 aux VnonN_C = C_biomass_con_B*nonN_C
 doc VnonN_C = concentration of lipid C (gC/m³)
 aux VnonN_C_1 = C_biomass_con_L*nonN_C_L
 doc VnonN_C_1 = concentration of lipid C (gC/m³)
 aux VXSC = C_biomass_con_B*XSC
 doc VXSC = concentration of XSC (gC/m³)
 aux VXSC_1 = C_biomass_con_L*XSC_1
 doc VXSC_1 = concentration of XSC (gC/m³)
 aux water_atten = .032323*SW_W
 doc water_atten = attenuation of light by water (certain water)
 aux water_atten_L = .032323*SW_W
 doc water_atten_L = attenuation of light by water (certain water) m-1
 aux XSC = nonN_C-memC

```
doc XSC = storage (excess) C (g storage-C / g cell-C)
aux XSC_1 = nonN_C_L-memC_1
doc XSC_1 = storage (excess) C (g storage-C / g cell-C)
const alpha = 7e-6
doc alpha = initial slope of Chl-specific PE curve; gCg-1Chl d-1
const AMP = 5
doc AMP = amplifier
const beta = 0.05
doc beta = constant for N and P uptake control; dl
const beta_L = 0.05
doc beta_L = constant for N and P uptake control; dl
const ChlCm = 0.06
doc ChlCm = maximum ChlC; gChl g-1C
const ex_NO3_L = 28
doc ex_NO3_L = gN/m3
const ex_P_L = 150
doc ex_P_L = g/m3
const f2N = 882
doc f2N = umol/L
const f2P = 36.2
const Flow_B = 0.693
doc Flow_B = m3
1m3 = 1000L
const Flow_L = 5
doc Flow_L = m3
const ini_V = 1
const iniChlC = 0.01
const iniNC = 0.16
const iniPC = 0.02
const inoc_B = 1.2
doc inoc_B = gC
const inoc_L = 1e-12
doc inoc_L = g
const KQN = 10
doc KQN = quota control constant for N; dl
const KQP = 0.1
doc KQP = quota control constant for P; dl
const Kxi = 0.001
doc Kxi = uptake feedback control constant; dl
const Kxi_L = 0.001
doc Kxi_L = uptake feedback control constant; dl
const lat = 0
doc lat = latitude
const M = 3
```

```
doc M = control for photoacclimation rate;dl
const MAX_V = 10
doc MAX_V = m3
RESERVA MAXVOL (1000L=1m3)
const mix_depth = 0.03
doc mix_depth = mixed layer depth (m)
const NCabs = 0.2
doc NCabs = absolute maximum NC; gNg-1C
const NCcore = 0.311
doc NCcore = N:C of core N-containing material (protein and NA) (g/g)
const NCcore_1 = 0.311
doc NCcore_1 = N:C of core N-containing material (protein and NA) (g/g)
const NCm = 0.16
doc NCm = maximum NC affecting growth; kgNkg-1C
const NCo = 0.035
doc NCo = minimum NC; gNg-1C
const NKu = 28e-3
doc NKu = half saturation for N-source uptake; 2uM = 2*14ug/l = 28e-3g/m3
const P_atten = 0.02*1e+3
doc P_atten = attenuation of light by Chl 0.02 m2/mgChl =0.02*1e+3 m2/gChl

const P_atten_L = 0.02*1e+3
doc P_atten_L = attenuation of light by Chl; 0.02m2/mgchl
0.02 m2/mgChl = 0.02*1000 m2/gChl
const PCabs = 0.04
doc PCabs = absolute maximum PC; gPg-1C
const PCm = 0.02
doc PCm = maximum PC affecting growth; gPg-1C
const PCo = 0.005
doc PCo = minimum PC; gPg-1C
const PFD_B = 250
doc PFD_B = umol photon/m2/s no more than 2000
const PFD_L = 2000
doc PFD_L = umol photon/m2/s
const PKu = 2e-3*31
doc PKu = half saturation of phosphorus uptake; 2uM = 2*31ug/L = 2e-3 *31g/m3
const Qh = 2
doc Qh = uptake feedback control Hill number; dl
const Qh_L = 2
doc Qh_L = uptake feedback control Hill number; dl
const React_V_Max = 1
doc React_V_Max = m3
const redco = 1.71
doc redco = reduction cost for nitrate to ammonium; kgCkg-1N
```

```
const redco_L = 1.71
doc redco_L = reduction cost for nitrate to ammonium; gCg-1N
const sun = 2000
doc sun = umol/m2/s
```

```
1368Wm-2=Js-1
```

```
const surface_area = 10
doc surface_area = m2
const SW_LD_B = 0
const SW_LD_L = 0
const SW_PBR = 0
doc SW_PBR = if 1 open, 0 is close
const SW_SC = 0
doc SW_SC = 0 STEADY-STATE; 1 DYNAMIC
const SW_W = 1
const Um = 0.693*2
doc Um = maximum growth rate; d-1
```

Appendix C

Numerical deduction of depth integrated photosynthesis is initialled by Fasham 2006 and mathematically deducted by Phil Kenny. His work is cited below.

The expression for depth integrated photosynthesis in the Powersim model can be derived from Smith's original empirical formula describing the the photosynthesis curve [1]. Talling [2] and Vollenweider [3] show how this can be done. I've added some extra details.

Smith's original description of the curve may be written in our language as

$$PS = P_{qm} \frac{\beta I}{\sqrt{1 + (\beta I)^2}}$$

where we define

$$\beta = \frac{\alpha \text{ChlC}}{P_{qm}}$$

and I is the irradiance. We then integrate over the water column from the surface to the optical depth D :

$$\int_0^D PS dz = P_{qm} \int_0^D \frac{\beta I}{\sqrt{1 + (\beta I)^2}} dz$$

We can then use the Beer-Lambert law to make a change of variable:

$$\frac{dI}{dz} = -att \times I \implies dz = \frac{dI}{-att \times I}$$

and substituting in:

$$\int_0^D PS dz = \frac{P_{qm}}{att} \beta \int_{I_0}^{I_D} \frac{dI}{\sqrt{1 + (\beta I)^2}}$$

as $\int_{I_D}^{I_0} = - \int_{I_0}^{I_D}$.

Now we do a second change of variable to perform the integration. Set $I = \tan \theta / \beta$ so that

$$dI = \frac{\sec^2 \theta}{\beta} d\theta$$

and now our integral looks like this:

$$\int_0^D PS dz = \frac{P_{qm}}{att} \int_{\theta(I_D)}^{\theta(I_0)} \frac{\sec^2 \theta}{\sqrt{1 + \tan^2 \theta}} d\theta.$$

Using the identity $\tan^2 \theta + 1 = \sec^2 \theta$, we now have

$$\begin{aligned} \int_0^D PSdz &= \frac{Pqm}{att} \int_{\theta(I_D)}^{\theta(I_0)} \sec \theta d\theta \\ &= \frac{Pqm}{att} [\ln(\tan \theta + \sec \theta)]_{\theta(I_D)}^{\theta(I_0)} \\ &= \frac{Pqm}{att} \left[\ln(\tan \theta + \sqrt{1 + \tan^2 \theta}) \right]_{\theta(I_D)}^{\theta(I_0)} \end{aligned}$$

We remember that $\theta(I_0) = \tan^{-1}(\beta I_0)$ and $\theta(I_D) = \tan^{-1}(\beta I_D)$ and subbing back in we get

$$\int_0^D PSdz = \frac{Pqm}{att} \left[\ln \left(\beta I_0 + \sqrt{1 + (\beta I_0)^2} \right) - \ln \left(\beta I_D + \sqrt{1 + (\beta I_D)^2} \right) \right]$$

As $\beta I_0 = P_{yt}$ and $\beta I_D = P_{yt} \times \exp(-att) = P_{yt} \times e_{rat}$ we finally have the expression in the Carbon Trust model:

$$\int_0^D PSdz = \frac{Pqm}{att} \left[\ln \left(P_{yt} + \sqrt{1 + P_{yt}^2} \right) - \left(P_{yt} \times e_{rat} + \sqrt{1 + (P_{yt} \times e_{rat})^2} \right) \right].$$

The Smith equation is the only suitable form of the varied equations governing the PS curve that can be integrated analytically [1], which is handy for using in Powersim but doesn't relate to the other equations in the model. If the exponential version of the PS equation is to be used, the integration must be done using some numerical technique.

References

- [1] Smith, Emil L., Photosynthesis in Relation to Light and Carbon Dioxide, 1936
- [2] Talling, J. F., The Phytoplankton Population As A Compound Photosynthetic System, 1957
- [3] Goldman, C.R., Primary Productivity in Aquatic Environments, p.425, 1980
- [4] Jassby, A.D and Platt, T., Mathematical formulation of the relationship between photosynthesis and light for phytoplankton, 1976

Appendix D

Day irradiance is calculated according to the solar position. Change of input variables including sun irradiance in a clear sky (sun), latitude (lat), day of the year (N) and time of the day (t) will alter the day irradiance and day length (i.e. light dark cycle). Parameters and ASCII form equation are listed in Table D1

Table D1

Parameters	Description	Numerical description
Irr	Light irradiance; $\mu\text{mol photons m}^{-2} \text{s}^{-1}$	$\text{sun}/\text{rvector}/\text{rvector}*\text{coszen}*(\text{coszen}>0)$
rvector	earth radius vector	$1/(1+0.033*\text{COS}(2*\text{PI}*N*0.00274))^{0.5}$
coszen	cosine of zenith angle	$\text{MAX}(\text{SIN}(\text{latrad})*\text{SIN}(\text{sdeca})+$ $\text{COS}(\text{latrad})*\text{COS}(\text{sdeca})*\text{COS}(\text{hrr}),0)$
sdeca	solar declination angle	$23.45*\text{SIN}(2*\text{PI}*(284+N)*0.00274)*\text{PI}/180$
latrad	Latitude radius	$\text{lat}*\text{PI}/180$
hrr	hour angle radians	$\text{ABS}(12-t)*15*\text{PI}/180$
daycal1	Day length calculation	$-1*\text{TAN}(\text{latrad})*\text{TAN}(\text{sdeca})$
daycal2	See above	$\text{daycal1}*(\text{daycal1}>-1)*(\text{daycal1}\leq 1)+$ $-1*(\text{daycal1}\leq -1)+1*(\text{daycal1}>1)$

daylength	Day length	$(2 * \text{ARCCOS}(\text{daylcal2}) * 12 / \text{PI})$
-----------	------------	---

Daylight simulation in scenarios 5.2.2.2 and 5.2.2.3 are setting to a condition mimicking summer time in equator. Clear sky irradiance (sun) set at $2000 \mu\text{mol photons m}^{-2} \text{s}^{-1}$, location latitude set at 0 degree and culture starts at Jun.

Figure D1 shows the simulated light condition. X axis is time of the year, Y axis is irradiance.

